LIPID MEMBRANES FOR THE FABRICATION OF FUNCTIONAL MICRO-AND NANO-STRUCTURES

THÈSE N° 3566 (2006)

PRÉSENTÉE LE 21 JUILLET 2006

À LA FACULTÉ SCIENCES DE BASE

Laboratoire de chimie physique des polymères et membranes

SECTION DE CHIMIE ET GÉNIE CHIMIQUE

ÉCOLE POLYTECHNIQUE FÉDÉRALE DE LAUSANNE

POUR L'OBTENTION DU GRADE DE DOCTEUR ÈS SCIENCES

PAR

Gopakumar GOPALAKRISHNAN

M.Sc. in Chemistry, Mahathma Gandhi University, Kottayam, Inde
et de nationalité indienne

acceptée sur proposition du jury:

Prof. K. Johnsson, président du jury
Prof. H. Vogel, directeur de thèse
Prof. H. Hofmann, rapporteur
Dr M. Liley, rapporteur
Prof. G. Schmid, rapporteur

ÉCOLE POLYTECHNIQUE
FÉDÉRALE DE LAUSANNE

Lausanne, EPFL
2006

To My Parents and Teachers....

The work presented here was conducted between February 2003 and April 2006 in the Laboratory of Physical Chemistry of Polymers and Membranes (LCPPM) at the Swiss Federal Institute of Technology Lausanne (EPFL) under the supervision of Prof. Horst Vogel. This work was supported by a grant (No: 4047-057562) from the NRP-47 program of the Swiss National Science Foundation and by internal grants of EPFL.

Parts of the work contained in this thesis are published and/ or in preparation for publication:

Publications:

Gopakumar Gopalakrishnan, Jean-Manuel Segura, Dimitrios Stamou, Cedric Gaillard, Marinela Gjoni, Ruud Hovius, Kurt J. Schenk, Pierre A. Stadelmann, and Horst Vogel, Synthesis of nanoscopic optical fibers using lipid membranes as templates. *Angew. Chem. Int. Ed., 44, 2005, 4957-4960*

Gopakumar Gopalakrishnan, Christophe Danelon, Paulina Izewska, Michael Prummer, Pierre-Yves Bolinger, Isabelle Geissbühler, Davide Demurtas, Jacques Dubochet, and Horst Vogel, Multifunctional Lipid/Quantum-Dot Hybrid Nanocontainers for Controlled Targeting Live Cells. *Angew. Chem. Int. Ed. 2006 (in press)*

Gopakumar Gopalakrishnan, and Horst Vogel, "Lipid Chemistry"- Based Organization of Quantum Dots *manuscript in preparation*

Content

Abstract

The central goal of this thesis work is to fabricate novel, functional fluorescent nanostructures in confined systems offered by phospholipid membranes, which are known to have highly ordered, thermotropic and lyotropic structures. In separate approaches, we have used three different lipid systems: multilamellar planar lipid membranes, unilamellar vesicular membranes as well as lipid monolayers for the development of functional fluorescent nano-, micro- and meso-scopic structures. Techniques like fluorescence microscopy, single particle imaging, electron microscopy, electron diffraction were used to achieve fundamental understanding of the resulting structures.

Multilayer stacks of phospholipid membranes have been used as an effective template for the growth of high aspect ratio fluorescent nanowires. The room temperature synthesis was achieved in the confined nanometer-sized interlamellar water space of lipid multilayers where supersaturating $CdCl_2$ concentrations were induced by acidification leading to controlled unidirectional growth of nanowires. The possibility to render the nanowires fluorescent by doping with CdS quantum dots (QDs) and the light waveguiding along hundreds of micrometers together with the possibility of lateral manipulation make these nanowires attractive candidates for future optoelectronic applications.

Novel organic-inorganic functional nanocontainers have been designed and tested by making use of vesicle forming lipid bilayers in combination with semiconductor QDs. Hydrophobic QDs can be integrated into bilayers of lipid vesicles and such lipid/QD hybrid vesicles are capable to fuse with live cells, thereby stain the cell's plasma membrane selectively with fluorescent QDs and transfer the vesicle's cargo into the cell. Modification of the membrane of such hybrid vesicles on the other hand, made them capable to enter the cytoplasm of live cells. Additionally, these hybrid vesicles were found extremely useful for long-term model membrane imaging studies. The results described in this thesis imply that cell and lipid membranes can integrate any kind of hydrophobic nanoparticle whose size matches the membrane thickness, opening novel possibilities to manipulate them as individuals or in ensemble with wide-ranging applications for nanobiotechnology.

In a further step, the ability of phospholipid molecules to exhibit lamellar to non-lamellar transition using external stimuli enabled a directed self-assembly of QDs into mesoscale fluorescent structures. An easy and versatile method for the surface modification of TOPO coated CdSe QDs using 1,2-dipalmitoyl-sn-glycero-3-phosphatidic acid (DPPA) have been achieved. DPPA predominantly form non-lamellar phases when dispersed in water, for example, upon addition of Ca^{2+} or at a pH below 6 are known to form hexagonal II phases. This particular property of DPPA has been exploited to form mesoscale self-assemblies of QD based structures both in solution and in confined systems. Potential applications include the detection or removal of Ca^{2+} ions in attoliter volumes, the construction of functional devices where QDs are reversibly organized in different forms as well as use of fluorescently labeled DPPA molecules for cellular studies using fluorescence microscopy.

Keywords: Nanotechnology · Nanoparticles · Quantum dots · Lipid membranes · Self-assembly · Vesicles · Cell targeting · Membrane staining · Hybrid materials · Template synthesis · Nanostructures

Version abrégée

Le but principal de cette thèse était la fabrication de nouvelles nanostructures fluorescentes et fonctionnelles en système confiné. Les membranes de phospholipides ont été choisies come matrices en vertu du haut niveau de leur organisation et de leurs propriétés thermotropiques et lyotropiques. Nous avons utilisé trois différents arrangements de molécules lipidiques, à savoir des membranes lipidiques planes multilamellaires, des membranes de vésicules unilamellaires et des monocouches lipidiques pour le développement de structures nano- micro- et mesoscopiques fluorescentes et fonctionnelles. Des méthodes comme la microscopie de fluorescence, l'imagerie de molécules uniques, la microscopie électronique et la diffraction électronique ont été utilisées pour obtenir une compréhension à un niveau fondamental des structures obtenues.

L'empilement de couches lipidiques constitue un "template" efficace pour la croissance de fils (fibres) nanoscopiques ayant un rapport longueur/ diamètre particulièrement élevé. Les parties aqueuses entre les couches lipidiques définissent un espace confiné d'épaisseur nanométrique qui permet la croissance contrôlée des fils nanoscopiques dans une direction. Cette synthèse s'effectue à temperature ambiante en provoquant des concentrations supersaturées de $CdCl_2$ par acidification. Les structures obtenues peuvent être manipulées latéralement et sont particulièrement intéressantes pour des applications en optoélectronique du fait de propriétés telles que la fluorescence après un dopage avec des points quantiques CdS ou le guidage d'onde sur des centaines de micromètres.

Des nouveaux nanocontainers fonctionnels composés d'éléments organiques et minéraux ont été réalisés à partir de bicouches lipidiques et de points quantiques. Des points quantiques hydrophobes peuvent être intégrés dans des bicouches lipidiques. Les vésicules hybrides (HV) ainsi formées peuvent fusionner avec des cellules vivantes, marquer les membranes cellulaires de manière sélective (avec des points quantiques fluorescents) et transférer le contenu des vésicules à l'intérieur des cellules. Une modification de la membrane des HV les rend capables de pénétrer dans le cytoplasme des cellules vivantes. De plus, ces HV se sont révélées extrêmement utiles pour l'imagerie à long terme de membranes modèles. Les résultats décrits dans

cette thèse montrent que les membranes lipidiques d'une cellule ou d'une vésicule sont à même d'intégrer les nanoparticules hydrophobes dont la taille correspond à l'épaisseur de la membrane. Cette localisation permet la manipulation individuelle ou collective des nanoparticules et ouvre de nouvelles voies en biotechnologie et en nanotechnologie.
De plus, la possibilité d'induire, par stimulation externe, la transition d'un arrangement phospholipidique de phase lamellaire en phase non-lamellaire permet l'autoassemblage dirigé des points quantiques dans des structures fluorescentes de taille mésoscopique. Une méthode élégante et versatile de modification de points quantiques CdS recouverts de TOPO a été établie en utilisant le phospholipide DPPA. Ce phospholipide forme principalement des phases non lamellaires dans l'eau qui peuvent se transformer en présence de Ca^{2+} ou à des pH inférieurs à 6 en phases hexagonales de type II. Cette propriété particulière du DPPA a été exploitée dans la formation d'autoassemblages de structures contenant des points quantiques à la fois en solution et dans des systèmes confinés. Les applications potentielles englobent la détection ou la suppression de ions Ca^{2+} dans des volumes de l'ordre de l'attolitre, la construction de dispositifs fonctionnels où les points quantiques sont organisés de manière réversible dans des formes différentes ainsi que l'utilisation de molécules marquées de DPPA pour des analyses cellulaires.

Mots clés: Nanotechnologie · Nanoparticules · Quantum dots · Membranes lipidiques · Auto-assemblage · Vésicules · Ciblage cellulaire · Marquage membranaire · Matériaux hybrides · Synthèse guidée · Nanostructures

Chapter 1

Introduction

1.1 Nanotechnology

> "A biological system can be exceedingly small. Many of the cells are very tiny, but they are very active; they manufacture various substances; they walk around; they wiggle; and they do all kinds of marvelous things - all on a very small scale. Also, they store information. Consider the possibility that we too can make a thing very small which does what we want - that we can manufacture an object that maneuvers at that level." *[1]

Nanotechnology is the branch of modern science, which deals with the fabrication and/or the use of physical, chemical, and biological systems at nanoscales (1 nm=10^{-9}m or in other words about one eighty thousandth the width of a human hair) i.e., scales ranging from individual atoms or molecules to submicron dimensions, as well as the integration of the resulting nanostructures into larger systems (Fig. 1.1). Areas such as electronics, healthcare, biotechnology, information technology, and materials science are believed to gain from the technological output of nanotechnology. Nanotechnology is also considered as next industrial revolution after information technology [1].

There are two main approaches to obtain nanostructured materials. The so-called "bottom-up" approach that deals with the chemical route of fabrication as well as the "top-down" approach, which the microtechnology has been dealing with, in order to make tiny, smart microelectronic device parts. In the bottom-up strategy, nanofabrication is performed at molecular level through the interactions and assembly of chemical and/or biological entities (Fig. 1.2) resulting nanostructures ranging from

[1] From the talk "There's Plenty of Room at the Bottom", delivered by Richard P. Feynman at the Annual Meeting of the American Physical Society at the California Institute of Technology on December 29, 1959. *taken without modification from [1]

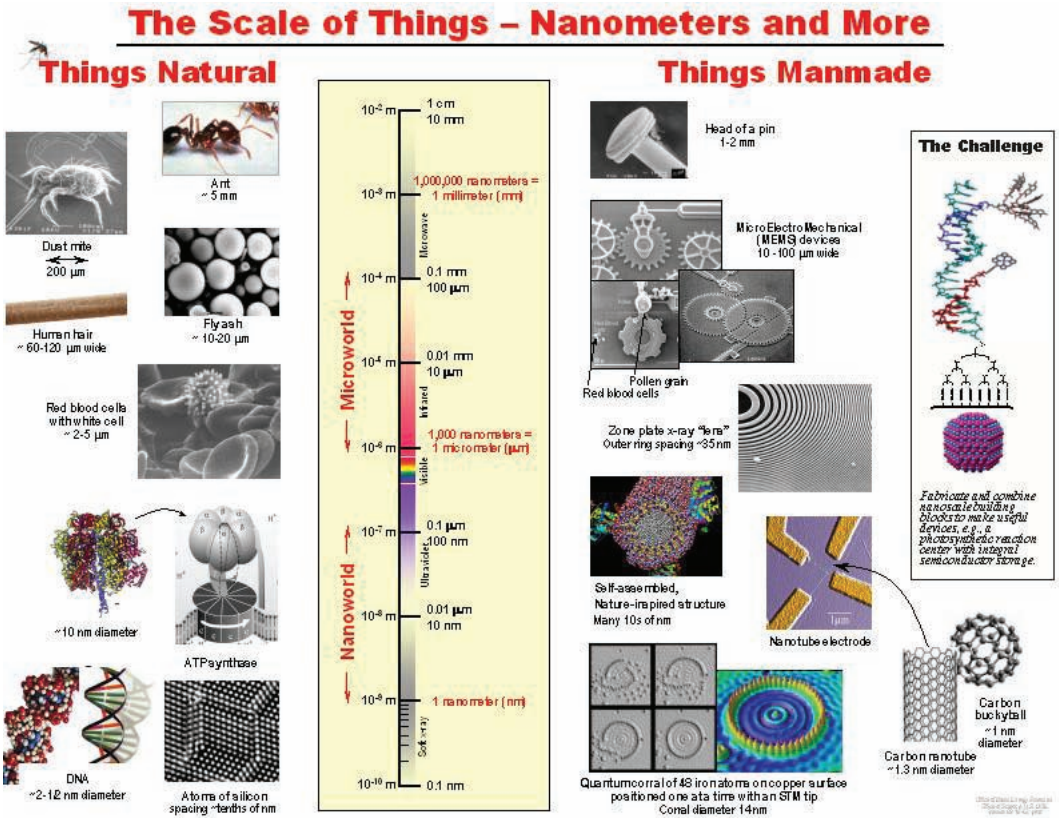

Figure 1.1: Scheme of scale of things. *Illustration of the size of matter that nanotechnology deals with. The natural systems (left) and the manmade systems (right) correlates the dimensions at the nano/microscales (middle) (taken from [1]).*

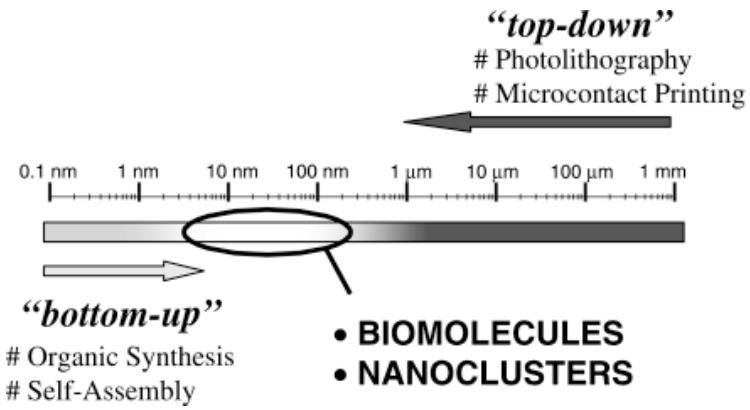

Figure 1.2: Bottom-up meets top-down. *Conventional top-down approach can go down to a maximum of only 100 nm whereas the bottom-up can create materials in the range of few Å to lower nm regime. The gap between the two (ie., 10-100 nm) can be addressed by biomolecules as well as colloids (taken from [2]).*

few Å to few nm. The top-down strategy, on the other hand, through photolithography and microcontact printing, can address micro/nanoscopic materials from few mm down to 100 nm (Fig. 1.2) [2]. Irrespective of the strategy of fabrication, these materials show extremely novel and interesting properties at smaller length scales. Such unique properties are mainly due to the high surface/volume ratio as well as the quantum confinement effects at lower nm scale regime that include optical, magnetic as well as electronic materials for applications in nanotechnology.

Though Feynman has envisioned the importance of an interdisciplinary research to create functional devices at tiny length scales already in 1959, until late 1980s the scientific research have been conducted under clear-cut separate branches of science such as chemistry, physics, biology etc. In the early nineties though, when nanomaterials attracted the attention of researchers working in diverse fields of science and technology, the importance of an interdisciplinary research activity has came-up.

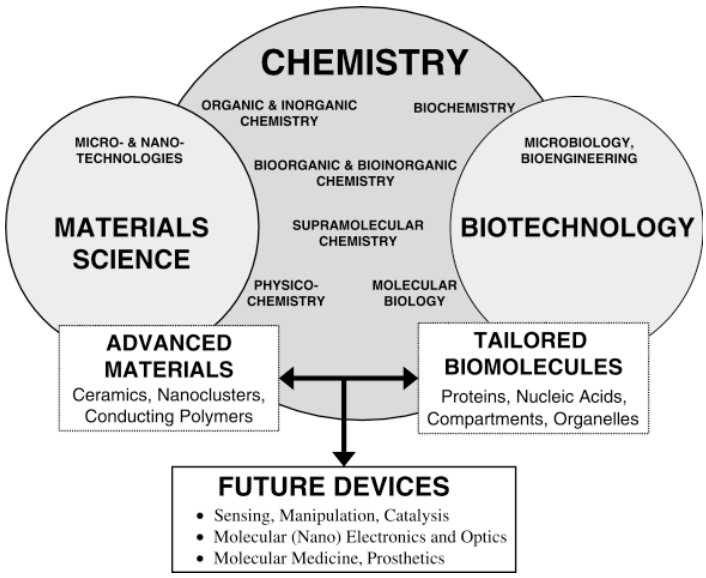

Figure 1.3: Interdisciplinary nature of nanotechnology. *The importance and contributions of main branches of nanotechnology is illustrated here. Both materials science and biotechnology keeps chemistry as the key discipline as when it comes to the molecular level, it ties one way or other to chemistry (taken from [2]).*

Thus, what we see today in modern nanotechnology is an assembly of different disciplines under one umbrella. Fig. 1.3 illustrates the major disciplines that nanotechnology deals with. Despite the three important branches of science shown, many other disciplines such as physics, electronics, computational science etc have profited each other through the inevitable contribution in the development of mod-

ern nanotechnology, which eventually will result in smart, functional nano devices of the future.

1.2 Nano-biotechnology

Nano-biotechnology is, as the name implies, the application of nanotechnology in life sciences and has shown already its impact on diagnostics and drug delivery applications. Nano-biotechnology enables the diagnosis at molecular level and some of the nano components has been incorporated in the current molecular diagnostic tools such as nanobiosensors and biochips. Although there are some safety concerns about the in vivo use of nanoparticles, studies are currently in place to determine the nature and extent of adverse effects. Future prospects for the application of nano-biotechnology in healthcare and for the development of personalized medicine appear to be excellent as it will extend the limits of current molecular diagnostics and may potentially enable point-of-care diagnosis. Although the potential diagnostic applications are unlimited, most important current applications are foreseen in the areas of biomarker research, cancer diagnosis and detection of infectious microorganisms. Fig. 1.4 shows the rapid developments that have achieved in the last few years in the field of nano-biotechnology.

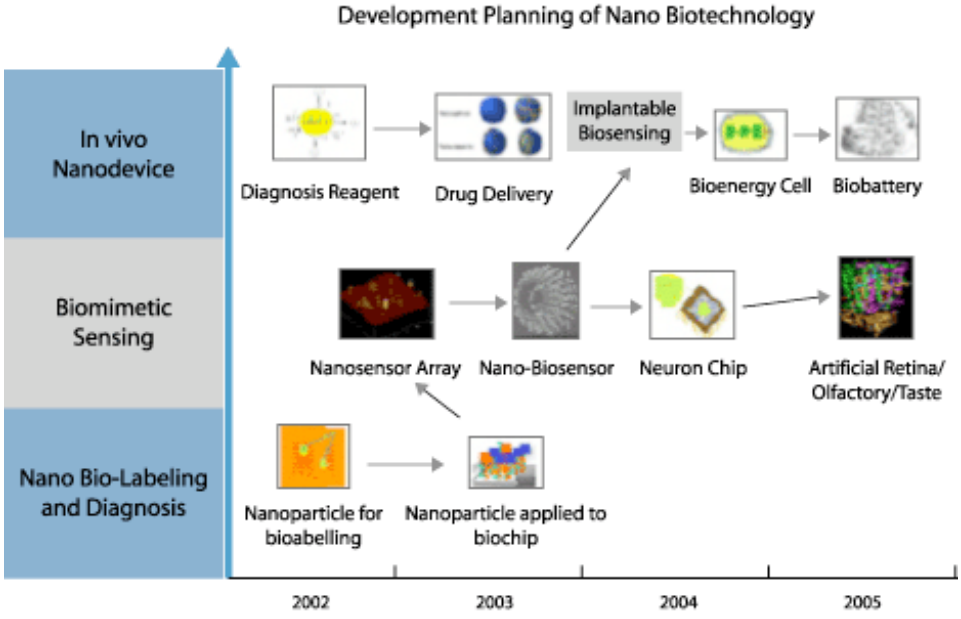

Figure 1.4: Evolution of nano-biotechnology. *From 2002 onwards, the nano-biotechnology has evolved in an incredible momentum. Indeed, the first successful applications were the use of QDs for labeling of biomolecules in-vitro, which as of now has developed to a stage where scientists have developed biobatteries as well as artificial retina that can be used in-vivo.*

1.3 Materials in nano-biotechnology

Nanoparticles (NPs), such as metallic and magnetic NPs and semiconductor quantum dots (QDs) (broadly classified as nanocrystals; see 1.4) are the most widely used inorganic components in nano-biotechnology. It has been shown recently that carbon nanotubes (CNTs) can be used as an effective drug-delivery vehicle. This, as a supplement to the already developed liposomal as well as polymeric vesicle drug delivery systems, will increase the potential role of nanomaterials in advanced medical applications. The organic components in nano-biotechnology, i.e., the biomolecules, are inherently "nano" with respect to their dimension. Oligonucleotides (3 nm), proteins (1-10 nm range), retrovirus (100 nm), open plasmid DNA (>100 nm range), etc have already been found useful in nano-device construction that may find potential biomedical applications. In most cases, the biomolecules were used either as a template (removable) or as one of the components (hybrid) for the production of high-quality functional nanomaterials. Section 3.2.1 of this thesis explains more about the template synthesis whereas the preceding section (1.3.1) outlines the state-of-the art in the organic-inorganic hybrid materials research.

1.3.1 Organic-inorganic hybrid materials

Organic-inorganic hybrid materials represent a new class of functional composite materials derived from crystalline nanomaterials in combination with soft organic/bio molecules [3]. Several approaches have been put in place including biomineralized growth of hybrid materials [4], [5], [6], [7], [8], polymer based organic-inorganic hybrids [9], [10], photosensitive polyimide/silica hybrid optical materials [11] as well as organized colloidal NPs using organic molecules [9], [12]. These methods result hybrid inorganic-organic materials with unique and optimized properties and hierarchical order over extended length scales [13]. Insertion of double-stranded DNA (ds-DNA) alternating copolymers into the inner space of a multi-walled carbon nanotube (MWNT) with a sufficiently large diameter has been reported by Iijima et al. clearly reveal the DNA-encapsulation through an open-end of a tube and also the DNA-wrapping on the outside-surface of a tube [14] thus making it biocompatible. I. Willner and co-workers have reported the DNA modification of CNTs, which enables the use of such hybrid systems as biosensor devices (enzymes electrodes, immunosensors or DNA sensors) [15]. Other applications of such hybrid materials include fabrication of bone implants, as scaffolds for tissue engineering, as potential drug delivery vehicles, and as effective surface coating agents. [10], [16].

1.4 Nanocrystals

Nanocrystals are aggregates of a few hundreds to tens of thousands of atoms resulting a crystalline matter. Nanocrystals of different composition, size and shapes have been studied well in more than two decades [17]. Typically around ten nanometers in diameter, nanocrystals are larger than molecules but smaller than bulk solids and therefore usually exhibit physical and chemical properties somewhere in between. A nanocrystal is virtually only surface and no interior, its properties can vary with the crystal size [18] and precise tuning of which would result with dramatic changes in the physical properties. It has been shown that just by controlling the kinetics of crystal growth in a typical synthetic method, scientists were able to vary the shapes of resulting nanocrystals [17], [19]. Irrespective of the shape and physical properties of the nanocrystals, their surface can be modified. In the context of this thesis work, more interesting are biomodified nanocrystals [20], which can find important biological applications in-vitro and in-vivo [20]. More about the (bio)chemical modification of QDs is described in detail in 4.2.1.

1.4.1 0D and 1D nanocrystals

The classification of 3, 2, 1 and 0D systems is based on the quantum confinement effects exerted in crystals at small dimensions [21], [22]: confinement in one dimension is observed in quantum wells, two dimension in quantum wires and three dimension in quantum dots (Fig. 1.5). The relation between the dimensionality of the crystal and the quantum confinement is as follows.

$$q = 3 - d$$

Where q is the quantum confinement and d is the dimension of the crystal, which can take the values 0, 1, 2 and 3. Thus, bulk 3D crystals possess no confinement of electrons whereas small, dimensionless nanoparticles possess confinement of electrons in all three directions. Since this thesis mainly deals with the fabrication of nanocrystal based functional structures and our interest has been limited to 0D (nanoparticles) and 1D (nanowires) nanocrystals. Consequently, here the discussion is limited to the synthesis (colloidal synthesis), characterization and applications of only 0D and 1D nanocrystals.

Synthesis and Applications — Historically, Alexandria, Egypt was believed to have been the original founding place for the use of gold in medicine by a group of experts known as Alchemists. The alchemists developed an “elixir” made of liquid gold

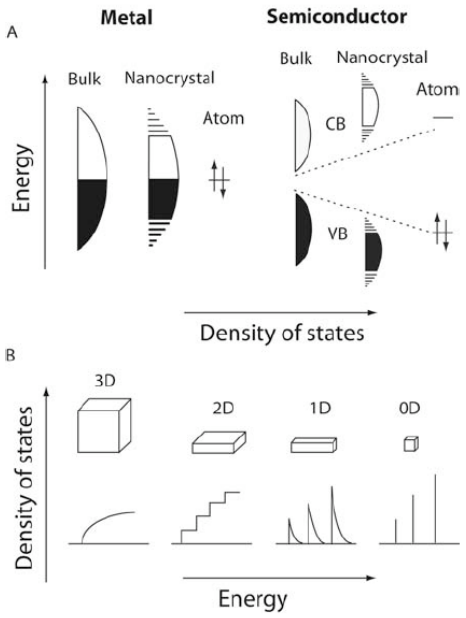

Figure 1.5: Schematic illustration of density of states. *(A) In metals, nanocrystals show discrete state (indicated using lines) band gaps in comparison to their bulk counterparts, which show a continuum of states. The shaded region indicates valence band (VB) whereas non-shaded region indicates conduction band (CB). For semiconductors, the dashed lines show the increasing band gap between VB and CB while going from bulk towards atom. (B) Density of states in one band of a semiconductor as a function of the dimensional freedom. 3-D represents the bulk, 2D quantum wells, 1D quantum wires and 0D the quantum dots.*

which apparently had the ability to restore youth and perfect health. Paracelsus, one of the greatest known alchemist, developed medicines from metallic minerals including gold, to cure the diseases. Later, alchemy spread to Arabia then throughout the Middle East to India and China and eventually to Europe. Though the scientific background still remains unclear, many tribal doctors in India use fine metal powders, which they claim can cure certain diseases. Small gold particles have been used to color stained glasses for over a century and to treat arthritis continuously since 1927. However, serious research in colloidal gold did not begin until Michael Faraday's discovery in mid-ninetieth century [23] that metal particle colloids showed color variations through surface charge variations.

The most common method to obtain colloidal gold (gold nanocrystals) in modern chemistry is by reducing $HAuCl_4$ in a suitable solvent. In order to prevent the aggregation of thus produced NPs, a suitable stabilizer is usually employed in the reaction mixture during the reduction process. There had been several publications

showing different protocols to achieve uniformly sized Au, Ag and other metallic NPs, in protic as well as in non-protic solvents, using wide variety of stabilizer molecules [24], [25] that allow further surface modification for eventual use in electronic as well as biological applications [26], [27].

Semiconductor colloids and clusters had been used in the study of photochemical reactions since 1970s [28], [29] though the increased potential of such materials in modern nanotechnology was not realized until 1990s when Murray et al. first published size tunable synthesis of CdSe QDs using TOPO [30]. Many studies on their photophysical properties have been carried out in the following years [31], [32] but still restricted their use in biological applications due to their insolubility in protic solvents. Five years later, Alivisatos and co-workers showed that such TOPO coated CdSe QDs can be made water soluble via coating with ZnS shell for using them as fluorescent labels in biological applications [33]. In the same issue of Science, Warren et al. showed a QD-bioconjugate for ultrasensitive detection in living cells [34]. It thus flourished the research on semiconductor QDs for the use in biological applications [20]. It is important to mention here that H.Weller, in parallel, has pioneered in developing systematic methods for the synthesis of QDs in water [35], [36] using water soluble thiols as stabilizers.

Magnetic NPs [37] also have synthesized first in the form of ultrasmall colloids [38], [39]. Later, magnetic NPs have been synthesized inside phospholipid vesicles [40], [41]. The use of such particles in biology started with their use in cell-sorting experiments [42], [43] already in 1980s. Numerous biological applications for magnetic NPs have then been framed-up [44], [45], [46] and more than 60% out of 1000 selected publications has came out in the 2000s indicating the enormous growth achieved in recent years in this field. The use of magnetic NPs as effective MRI contrast agents [45], [47] in hyperthermia [45], [47] and in cancer research [48], [49] shows the impact magnetic nanocrystals has generated in the biomedical research field.

Synthetic routes to 1D nanocrystals of both metals and semiconductors have also been established well in these years and the important findings include the colloidal route through kinetic control [17], [19], template route such as porous alumina [50], [51], polymers [52], DNA [53], and virus molecules [54], sol-gel route [55], electrochemical deposition [56], NP catalysed growth [57] etc. More interesting in the context of present thesis is the template directed synthesis of 1D nanocrystals, which will be discussed in 3.2.1 in detail.

The applications of nanocrystals range from nanoelectronics that can be used to build computer memory, using individual molecules or nanotubes to store bits of

information, as well as molecular switches, molecular or nanotube transistors, nanotube flat-panel displays, nanoscopic lasers, and nanotubes as electrodes in fuel cells. Biomodification of nanocrystals might be extremely interesting in applications such as biological detection, controlled drug delivery, point-to-care diagnostic, (bio)chemical sensors, new printing technologies etc. Being considered next industrial revolution, the prospects of nanomaterials in modern human life is enormous!

1.4.2 Synthesis of nanocrystals in confined systems

As discussed in 1.4.1, the synthesis of colloidal nanocrystals requires a growth-arresting agent to get the nanocrystals in the smallest possible dimension. Failure of which will lead to coagulation and eventual precipitation of the particles. There are several organic as well as biomolecules that had been successfully used for this purpose. Alongside with it, there progressed another approach to synthesize nanocrystals with uniform size-distribution using confined reaction systems. The main inspiration to such an approach is actually nature, which, as always, has the far superior ability to construct nanostructured materials in a controlled, specific morphological way. Magnetotactic bacterium is the best example to illustrate it. As depicted in Fig. 1.6, it is capable of producing 40 - 100 nm sized, spherical, single-domain Fe_3O_4 (magnetite) particles fixed on the inner leaflet of the plasma membrane, which are nicely aligned along its body [58].

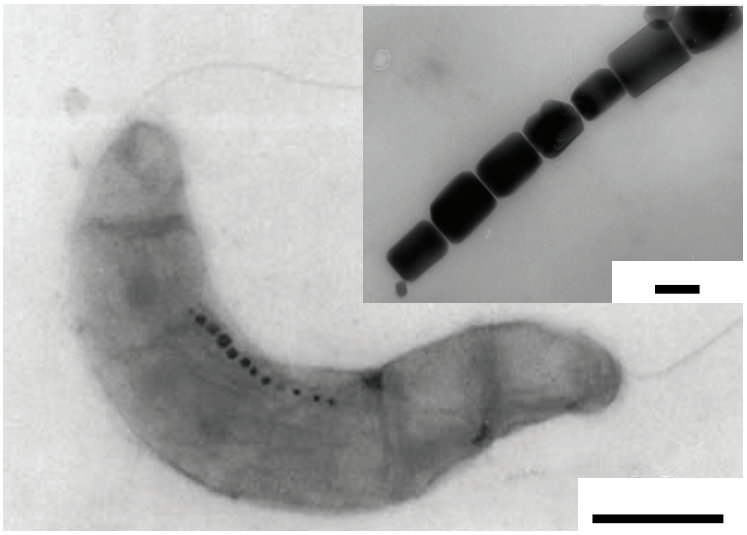

Figure 1.6: Electron micrograph of magnetotactic bacteria. *The particle chain is visible as dark spherical spots (scale bar = 0.5 μm). The inset shows a closer view of the Fe_3O_4 particle chain (scale bar= 100 nm).*

The field known as "biomineralization or biomimetic materials chemistry" has thus

evolved by mimicing nature's tactics in the laboratory to produce high quality, functional nanostructures [59], [4], [8], [7]. The protein assembly of collagen, for example, provides an organized matrix in which apatite crystals can grow, in the spaces provided, resulting a functional composite material: 'bone' [60].

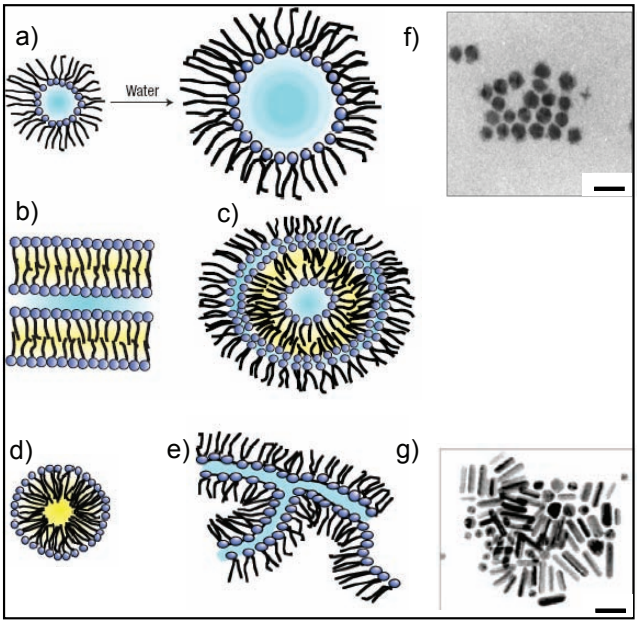

Figure 1.7: Shape of different confined membrane structures. *(a) Reverse micelles with control of their size by the water content, (b) planar lamellar phase, (c) onion-like lamellar phase, (d) normal micelles, and e) interconnected cylinders. The corresponding nanostructures obtained; (f) is produced using (a) and (g) is obtained from (e): scale bars = 21 nm [61].*

Materials constrained in 1, 2 or 3 dimensions have been used for obtaining spatially confined reaction vessels. Micelles [61], [62], [63], vesicles [64], zeolites [65], protein cages [66], polymers [67] and Langmuir-Blodgette films [68], [39], [69] are some of the many confined systems already exploited. Compartmentalization provided by membranes and cells is considered to be responsible for the inflow of ionic precursors and for the imposition of shape and size control over the incipient crystal growth in biomineralization. Fig. 1.7 illustrates the common detergent and lipid based structures that has been used in the fabrication of nanocrystals. The in-vitro and in-vivo studies on biomembranes has been very useful for understanding their properties such as phase transition, phase separation, fluidity, permeability, fusion and substrate mobility into and out of the membranes. The afore mentioned parameters are very important to understand and control in order to use membrane mimetic compartments as confined reaction vessels. As a mostly studied system, phospholipids

are considered as an ideal system to pursue such confined reactions [64]. Particularly interesting in the context of this thesis are phospholipid vesicles and multilayers, which through its closed (in the case of vesicles), aqueous interior, can act as a reaction vessel. The size of such vesicles can be tuned from about 10 nm to few tens of micrometers thereby control the amount of individual reactants inside such vessels precisely [70]. The structure, chemical and physical properties, biological function as well as thermodynamic properties of phospholipid membranes will thus be discussed in the preceding section, which stands as a common platform on which this thesis work is built on.

1.5 Phospholipid bilayers

Lipids are considered as one of the most essential biomolecules in the structure and function of living matter. The interest in phospholipid bilayers arises as they are one of the major structural elements in biological membranes. Phospholipids have the ability to form bilayer vesicles spontaneously when dispersed in water. This peculiar property of bilayer formation is due to the amphiphilic structure of phospholipids. Hydrophobic effects along with geometric constrains result bilayers as favored structure for most two-chain phospholipids [71]. At higher lipid concentrations, these bilayers form lamellar liquid crystalline phases where two-dimensional planar lipid bilayers are separated by distinct water layers, whereas upon dilution they become unstable, curved and thus form lipid vesicles [72]. One of the key features of phospholipid bilayers is their thermotropic phase behavior, in which lipid chains reversibly take either an ordered (gel) state below phase transition or a disordered (fluid) state above phase transition. The important parameters of phospholipids, in the context of this thesis, such as chemical structure, lipid shapes and phase behavior will be discussed here. A seperate section dedicated for lipid vesicles is included in chapter 4.

1.5.1 Chemical structure and shapes of phospholipids

There are two main classes of diacyl phospholipids that are naturally occurring: glycerophospholipids and sphingophospholipids. The predominant phospholipids in biological membrane is glycerophospholipids (Fig. 1.8) and hence from hereon, wherever used the word phospholipids, is strictly for glycerophospholipids. In biological membranes the glycerophospholipids are all derivatives of *sn*-glycero-3-phosphatidic acid. A typical phospholipid is phosphatidylcholine, which has many different species and properties depending on the alkyl chain length (12:0; lauric, 14:0; myristic, 16:0;

palmitic, 18:0; stearic, 20:0; arachidic etc) and degree of unsaturation in the alkyl chain (16:1(9); palmitoleic, 18:1(9); oleic, 18:2(9,12): linoleic etc). variations in the headgroup (PA and PS- negative, PC and PE- neutral etc) result in different lipid types [72].

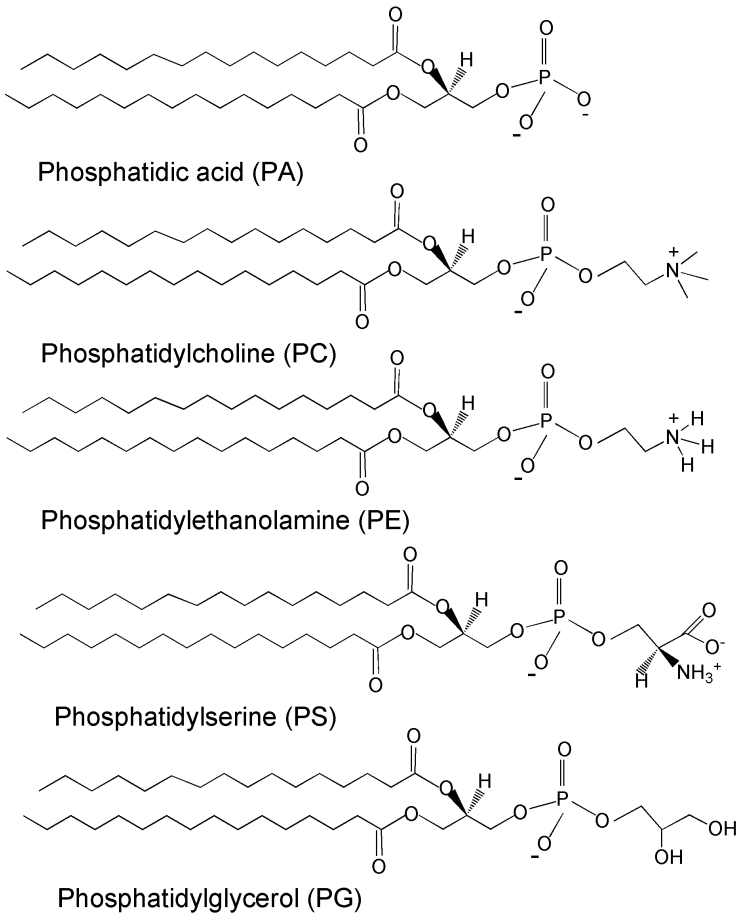

Figure 1.8: Common phospholipids. *The glycerophospholipid types depend on the organic base, amino acid, or alcohol with which the phosphate is esterified. The figure shows different headgroups bearing dimyristoyl alkyl chain.*

The lipid molecules form supramolecular structures, which depend on the particular shape of the lipid molecules, such as cones, cylinders, or inverted cones depending on the relative size of the polar headgroup with respect to the alkyl chains as illustrated in Fig. 1.9.

1.5.2 Lipid phases and phase transitions

Hydrated bilayers of phospholpids perform well-defined thermotropic phase transitions. The lamellar fluid phase (L_α), which is thought to be the form representing lipids in the biological membrane and lamellar gel phase (L_β). L_β phase is formed

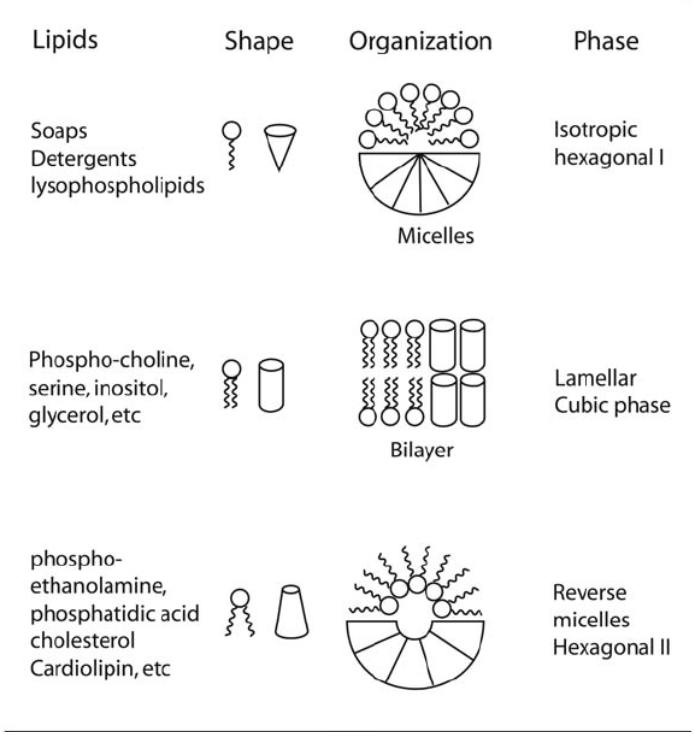

Figure 1.9: Shapes and corresponding supramolecular asssemblies of different phospholipids *[72].*

at low temperatures in those lipids that form lamellar structure. In this phase the molecules are packed more tightly and the acyl chains form a two-dimensional crystal [73]. There are a number of lipids that form nonbilayer structures. Such nonbilayer forming lipids usually show two distinct phases:

(i) hexagonal I phase (H_I) in which the lipids are organized in the form of cylinders with the polar headgroups facing outside, in contact with water. The cylinders are packed in a hexagonal pattern.

(ii) hexagonal II phase (H_{II}) in which the lipids are organized in the form of cylinders with the polar headgroups facing inside, where there is a pool of water. In this case too, the cylinders are packed in a hexagonal fashion (Fig. 1.10).

In the case of bilayer forming lipids that undergo thermotropic phase transitions, the phase transition temperatures T_t and phase behavior differ between various lipid types, but all depend very strongly on water content. The phase transition temperatures decrease as water is taken up by the bilayer. Water molecules bind to the phospholipid headgroups and depress the T_t by approximately 4^oC per water molecule. The gel phase achieves maximum hydration at approximately 30% water, at which point there is no further decrease in T_t. Above this water content,, free water separates out. Hydration continues further in the fluid phase, a free water

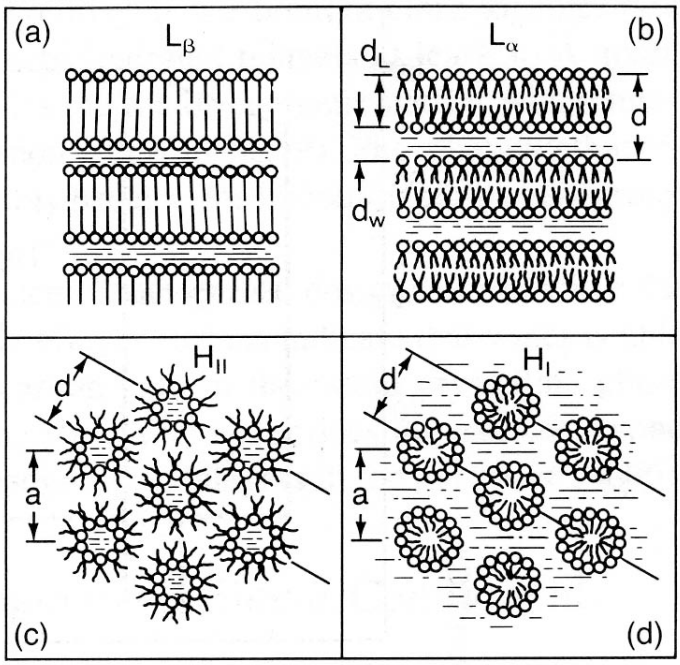

Figure 1.10: Schematic representations of lipid-water phases. *(a) lamellar gel phase, (b) lamellar fluid, (c) hexagonal II and (d) hexagonal I (taken from [73]).*

phase not appearing until above 40% water. This increased hydration has little or no effect on the thermodynamics of the phase transition [71]. The T_t of different PCs and PEs can be seen as a table in Fig. 1.11. The T_ts are systematically higher for PEs compared to PCs of the same chain length.

Thus by choosing appropriate hydration effects as well as the headgroup functionalities of phospholipids, many controllable, confined structures (spherical, tubular, planar etc) can be obtained.

1.6 Thesis in the context of current nano-biotech research

Though nano-biotechnology is still in its emerging stage, its future prospects in biomedical as well as nano-electronics are limitless. Several biomolecules such as proteins, DNA, virus molecules etc have already been used as components in such functional nanodevices. As discussed above, the possibilities of phospholipid membranes in terms of controllability, flexibility, bio-compatibility as well as functionality are enormous. This thesis work focuses mainly on the following issues:

	T_t (°C)
di C_{12}−PC	−1.0
di C_{14}−PC	24.0
di C_{16}−PC	41.4
di C_{18}−PC	55
di C_{12}−PE	30.5
di C_{14}−PE	49.5
di C_{16}−PE	64
di C_{18}−PE	74
di C_{20}−PE	82.5

Figure 1.11: Change of T_t for various phospholipid types. *Phosphatidylcholines (PC) and phosphatidylethanolamines (PE) of chain length C_n (taken from [71]).*

- ▷ Can one use lamellar phospholipid membranes as a template for the fabrication of functional nanostructures?
- ▷ How tunable is the thermotropic phase behavior of phospholipid membranes as confined membrane compartments?
- ▷ Despite the well-studied drug delivery applications of lipid vesicles, can one fabricate highly controllable, multi-stimulus responsive cargo systems by combining the properties of lipid molecules with inorganic nanocrystals? Is it possible to target such hybrid vesicles in a controlled way to live cells?
- ▷ How important is the use of known lipid-chemistry in the future development of nano-biotechnology?

Several specific aspects related to these issues have been elaborated in this thesis. The synthesis of novel nanoscopic optical fibers by making use of phospholipid membranes as a template is the subject of chapter 3. Fabrication of lipid/QD hybrid vesicles and their targeting to specific cellular locations as well as potential use of such nanocontainers in delivery applications are the content of chapter 4. It also describes a novel single particle study showing the controlled diffusion of fluorescent nanocrystals in a supported planar bilayer system. Finally, while discussing mainly the use of known basic lipid chemistry for organization of fluorescent nanocrystals in chapter 5, the importance of type, concentration and method of formation of lipid structures in the development of lipid based nanocrystal arrangement too takes the centre of discussion.

Chapter 2

Methods

2.1 Confocal fluorescence microscopy

Confocal microscopy is an optical sectioning technique producing images free from out-of-focus blur. It is a light microscopy technique and commonly employs visible wavelength lasers as light sources and confocal apertures or 'pinholes' in the excitation and detection paths. The technique is frequently described as CLSM (Confocal Laser Scanning Microscopy).
The main advantages of confocal microscopy are: (i) Generation of completely in-focus 3D images of microscope samples, (ii) localisation of multiple fluorescent labels in 3D space within a single sample, (iii) accurate measurements between features in 2D and 3D space, and (iv) offering superior spatial resolution compared to wide-field light microscopy (Fig. 2.1a&b).

How does it work?
Optical sectioning is achieved by including an additional optical element - a confocal aperture - into the light collection path (see Fig. 2.2). 'Confocal' means that both the illumination focal volume and the detection focal volume are coincident (Fig. 2.1d). This optical constraint ensures that light from outside the focal region does not reach the detector. In a confocal imaging system the basic rule is - 'in-focus bright, out-of-focus black'. The apparently simple optical principle of the laser scanning confocal microscope has very great flexibility in practice. By making the confocal aperture variable in size, the optical section thickness can be optimised for the chosen objective and wavelength of light. The smallest optical section thickness, obtained with a high NA lens, is ∼0.5 micron. The freedom to increase the size of the confocal aperture can also be important when imaging very faint fluorescence where it allows a trade off between optical section quality and image brightness.
The confocal data presented in this thesis are recorded using the ConfoCor-2 and

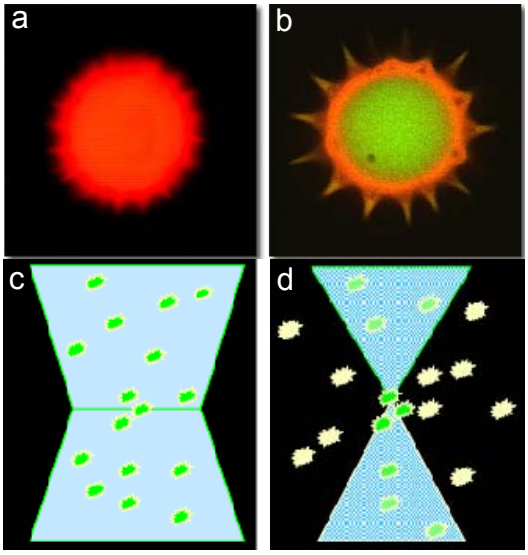

Figure 2.1: Comparison between wide-field and confocal microscopies. *The specimen of pollen grain when viewed through widefield illumination in a classical fluorescence microscope (a), while (b) presents a thin optical section from the confocal microscope at the same focal plane on the microscope z-axis. Illustration of a typical illumination volume in a wide-field microscope (c) in comparison to a confocal microscope (d).*

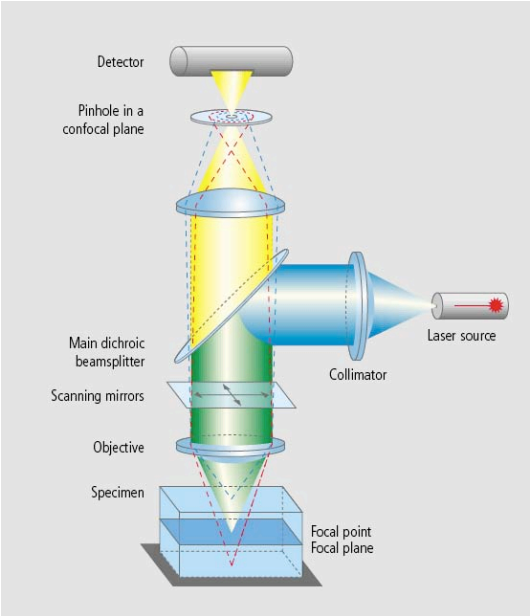

Figure 2.2: Scheme illustrating the set-up in a typical CLSM. *Taken from www.zeiss.de.*

ConfoCor-3 laser scanning confocal microscope (LSM 510, Zeiss) equipped with excitation wavelengths of 454 nm, 488 m, 543 nm and 633 nm and free choice of the emission wavelengths selected using various combinations of emission filters. Fig. 2.2 shows the instrumental set-up of a typical CLSM microscope from Zeiss.

2.2 Single molecule fluorescence micro/spectroscopy

Fluorescent single-molecule studies at room temperature have recently become possible and have opened a wide field of biological applications [74], [75]. The observation of single molecules requires the use of excellent fluorophores with high quantum yields and high photostability, which emit light at a wavelength where background auto-fluorescence of the biological sample is low and where the detection efficiency of the recording system is high. Dyes that emit in the far red, like Cy5 and Alexa647 are best suited. Alternatively, fluorescent semiconductor QDs have been used because of their high photostability [76], [77], [78]. To discriminate single molecules, their average distance has to be larger than the resolution of the observation system. Using microscope optics the diffraction limit is around 350 nm at the emission wavelength of ∼650 nm.

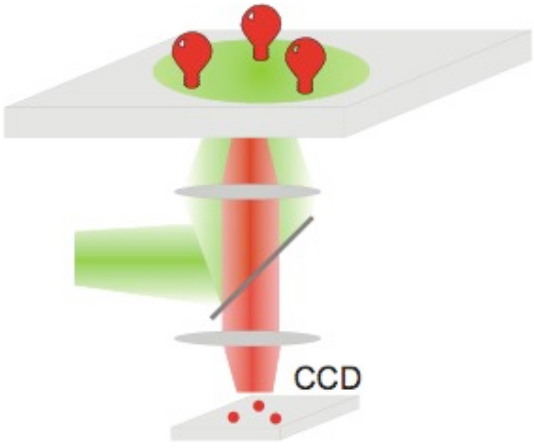

Figure 2.3: Principle of single molecule imaging. *A ca 35 µm spot is illuminated with laser light and the fluorescence of single molecules is recorded with a high sensitivity CCD camera.*

In contrast to other techniques, the evaluation of single molecule experiments resembles the pure behavior of a certain molecule and can deliver precious information that is averaged or hidden otherwise in ensemble experiments; i.e. there is no time averaging, no population averaging and there might be also access to new experimental observables. Typical applications for single molecule studies are (i) single

molecule tracking experiments, different populations of diffusing molecules can be distinguished even if their diffusion constants are similar, kinetics of biochemical reactions or single ligand binding events can be observed resulting in a higher time resolution than possible with ensemble measurements.

How does it work?

The principle of single molecule imaging is illustrated in Fig. 2.3. The wide-field epi-illumination together with the CCD camera detection allows the observation and the localization of several single molecules in parallel. To prove the observation of single molecules several criteria must be fulfilled: First, light emitted from a point source like a single fluorophore will be imaged as a diffraction limited spot of a characteristic size on the CCD camera. Second, the intensity of the emitted light and the saturation excitation intensity are characteristic for each fluorophore and only depend on its photophysical properties. Third, blinking and single-step photobleaching are unique signatures of single fluorophores. Typical fluorescence image of single QDs is shown in Fig. 3.14d & Fig. 4.15a. After usually 2 - 50 images the QDs go to the "off" state resulting in a one-step decrease of fluorescence intensity. The statistical processes of blinking and photobleaching occur randomly but always in the same manner.

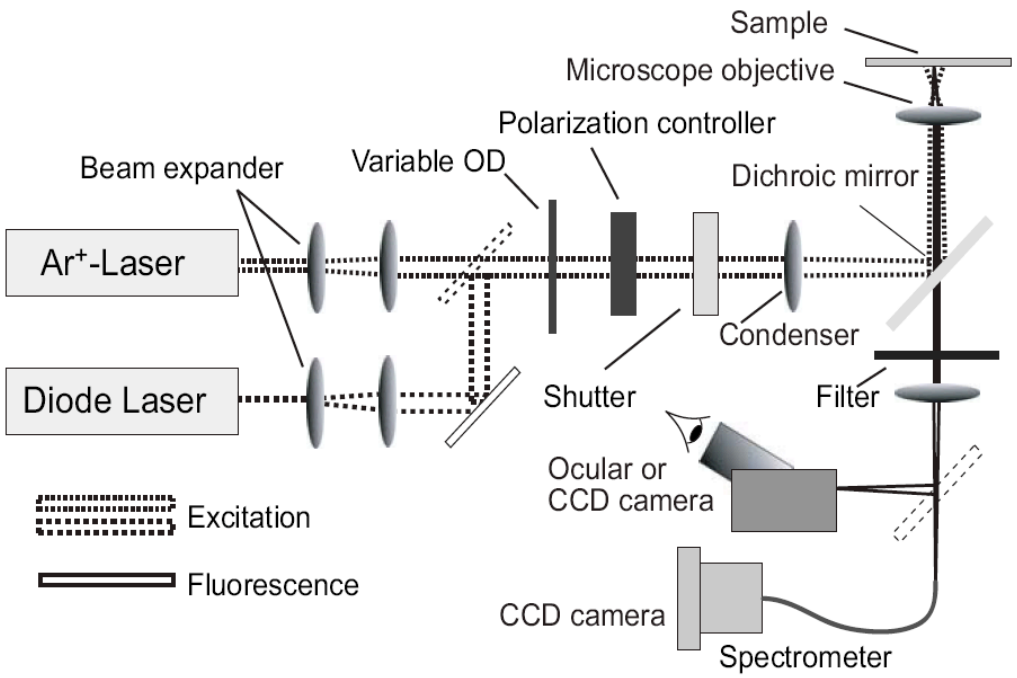

Figure 2.4: Schematic of the single molecule fluorescence imaging set-up.

The single molecule microscopy data presented in this thesis were recorded on a modified epiluminescence wide-field microscope (Axiovert 100 TV, Zeiss). A scheme of the set-up is shown in Fig. 2.4. Circularly polarized light of 488 nm of an Ar^+ laser (Innova Sabre, Coherent) was directed by a dichroic mirror (Q495LP, Chroma) into a microscope objective (C-Apochromat 63x, 1.2 NA, W Korr, Zeiss) to illuminate a 35 μm diameter region of the sample. The sample temperature was controlled, where necessary, using a thermostat attached to the sample stage. Fluorescence was collected by the same objective, passed through a filter (515 LP, Zeiss) and was imaged (ISP, INW) on an Electron Multiplying CCD camera (IXon DV887AC-FI, Andor Technology Ltd). To avoid photobleaching, the samples were only illuminated for 50 ms per image using a shutter (LS3T2, Vincent Associates, Rochester, USA). Sampling frequencies ranged from 0.2-12 Hz.
The single molecule fluorescence spectrum of samples were spectrally resolved using an attached monochromator (CP-140, Spectroscopy Instruments GmbH) coupled to a CCD camera (LN/CCD-576 EUV, Spectroscopy Instruments GmbH). Circularly polarized light of 457 nm of an Ar^+ laser (Innova Sabre, Coherent) was directed by a dichroic mirror (LP480 HQ, Chroma) into a microscope objective (Chroma) to record the emission spectra.

2.3 Fluorescence correlation spectroscopy

The concept of fluorescence correlation spectroscopy (FCS) was introduced in the early 1970s [79]. Since then, the technique has been developed into a powerful tool in analytical chemistry and biological research. The elegance of FCS lies in its ability to extract a wealth of molecular and environmental information from a weak fluorescence signal using correlation analysis of the fluorescence fluctuations of very small samples at nanomolar concentrations. Fluorescence fluctuations due to concentration fluctuations via molecular diffusion, chemical reactions, and physical processes of a few fluorescent molecules in a an optically restricted sub-micron observation volume ($\sim$1 fL=10^{-15} L) can be studied with temporal resolution typically from 1 ms to >10 s.
The FCS results presented in this thesis are obtained using a commercial ConfoCor-2 LSM 510 microscope (Carl Zeiss). This is the same microscope used for confocal data acquisition which enable to combine the two techniques for precise localization of the FCS detection volume in a sample. Using pinhole diaphragms the detection volume can go down to few hundreds of nanometers in diameter corresponding typically to $\sim 3 \cdot 10^{-16}$L $\Leftrightarrow$ 0.3 femto liters. The Fig. 2.5 illustrates the shape of the detection

volume and the principles of the FCS technique.

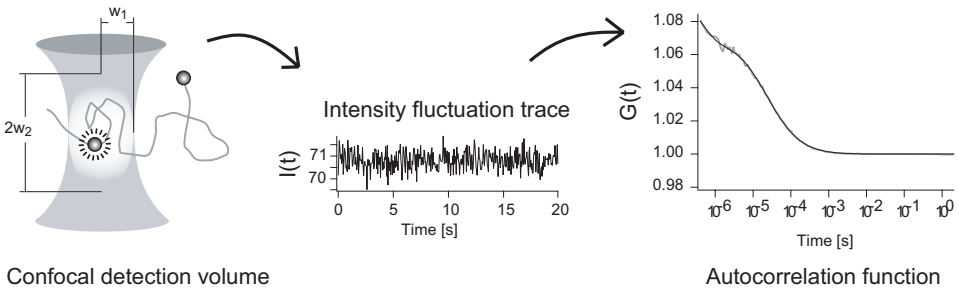

Figure 2.5: Illustration of the principle of FCS technique. *The fluorescent particle is only excited when present in the confocal detection volume. The fluorescent intensity is recorded with time and gives the intensity fluctuation trace I(t). From this trace, the autocorrelation curve G(τ) is calculated.*

How does it work?

The confocal detection volume is characterized by its radius w_1 and its height w_2. Diffusing fluorescent particles are excited only when they are present in this tiny volume. In order to obtain valuable data, the particles analyzed should fit inside this volume, thus only particles below $w_1 \simeq 200$nm can be characterized with this technique. The fluorescence intensity is recorded as function of time that gives fluctuation trace I(t) which shows characteristic fluctuation δI(t) around the average fluorescence signal $\langle$I$\rangle$. The fluctuations might be due to change in fluorescent quantum yield or can be produced by particle motions which induce fluctuations in the number of fluorescent particles per detection volume and thus the fluorescence intensity. In order to get experimental parameters, the normalized autocorrelation function (ACF) G(τ) is automatically calculated from I(t) by the instrument software.

$$G(\tau) = 1 + \frac{\langle I(t) \cdot I(t+\tau) \rangle}{\langle I \rangle^2} \tag{2.1}$$

The autocorrelation function compares the value of the signal at any arbitrary time t with the value of a short time interval τ later. The definition of the ACF is written for one particular interval τ and the complete ACF function specifies G(τ) for every τ where the angular brackets $\langle\rangle$ indicate a time average. In the situation where the fluorescence decay is much shorter than the translational diffusion, the ACF can be fitted and gives experimental parameters following this equation.

$$G(\tau) = 1 + \frac{1}{N} \cdot \frac{1}{1 + 4D\tau/w_1^2} \left(\frac{1}{1 + 4D\tau/w_2^2} \right)^{\frac{1}{2}} \tag{2.2}$$

with the fitting parameters:

D; the diffusion coefficient is $D = w_1^2/4\tau_D$

w_1; the radius of the detection volume as in Fig. 2.5

w_2; the half height of the detection volume as in Fig. 2.5

and the experimental parameters extracted from the fitted ACF:

▷ N; the number of molecules in the detection volume

▷ τ_D; the translational diffusion time of the detected particle

2.4 Laser tweezers

Optical Tweezers use light to manipulate microscopic objects as small as a single atom. The radiation pressure from a focused laser beam is able to trap small particles. In the biological sciences, these instruments have been used to apply forces in the pN-range and to measure displacements in the nm range of objects ranging in size from 10 nm to over 100 mm.

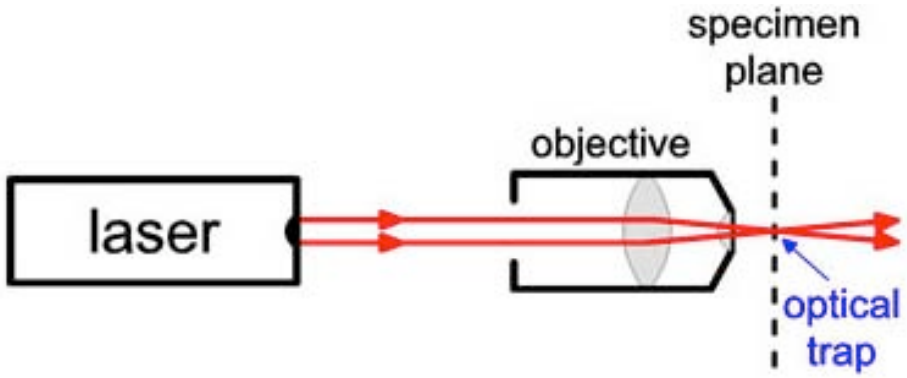

Figure 2.6: Schematic of the simplest form of an optical tweezers.

The most basic form of an optical trap is illustrated in Fig. 2.6. A laser beam is focused by a microscope objective to a spot in the specimen plane. This spot creates an "optical trap" which is able to hold a small particle at its center. The forces felt by this particle consist of the light scattering and gradient forces due to the interaction of the particle with the light. Most frequently, optical tweezers are built by modifying a standard optical microscope. These instruments have evolved from simple tools to manipulate micron-sized objects to sophisticated devices under computer-control that can measure displacements and forces with high precision and accuracy.

How does it work?

The basic principle behind optical tweezers is the momentum transfer associated with bending light. Light carries momentum that is proportional to its energy and in the direction of propagation. Any change in the direction of light, by reflection or refraction, will result in a change of the momentum of the light. If an object bends the light, changing its momentum, conservation of momentum requires that the object must undergo an equal and opposite momentum change. This gives rise to a force acting on the object [80] that creates an optical trap.

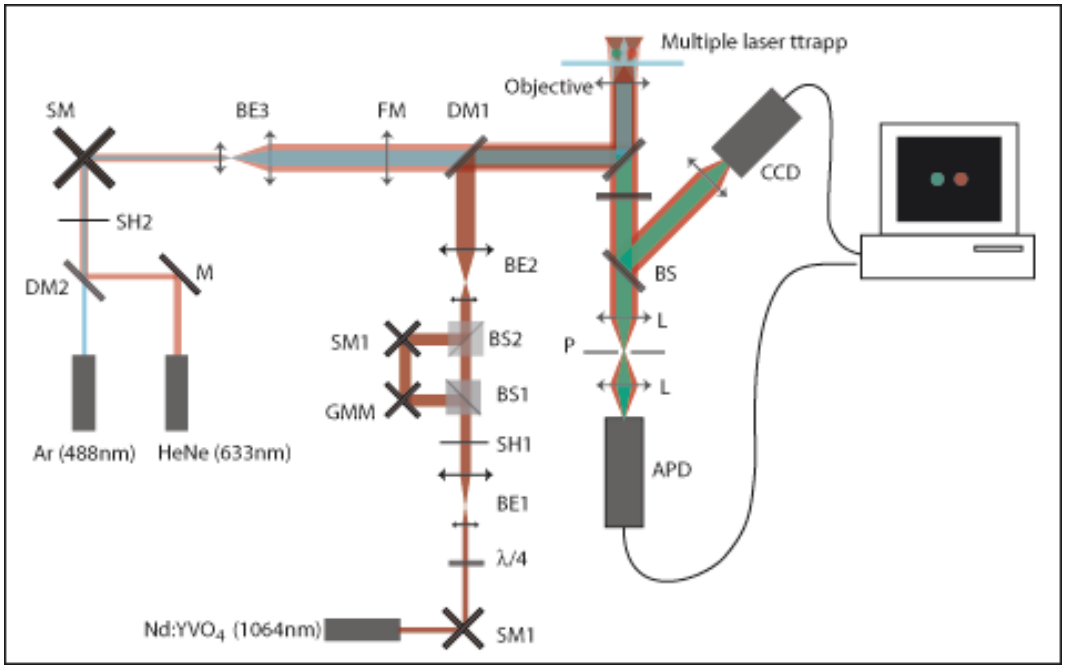

Figure 2.7: Illustration of the optical tweezers set-up. *It is a custom-built set-up in LCPPM, EPFL.*

Modern optical tweezers: In practice, optical tweezers are very expensive, custom-built instruments. These instruments usually start with a commercial optical microscope but add extensive modifications. In addition, the capability to couple multiple lasers into the microscope poses another challenge. High power infrared laser beams are often used to achieve high trapping stiffness with minimal photo-damage to biological samples. Precise steering of the optical trap is accomplished with lenses, mirrors, and acousto/electro-optical devices that can be controlled via computer. Fig. 2.7 gives an idea of the number of elements in such a system. In short, these are very complicated instruments that require a working knowledge of microscopy, optics, and laser techniques.

2.5 Electron microscopy

In contrast to optical microscopes, electron microscopes (EMs) use a beam of highly energetic electrons to examine objects on a very fine scale that can yield the information about topography, morphology, chemical composition as well as crystallographic information about a specimen (Fig. 2.8). The two most common types of EMs are scanning electron microscopy (SEM) and transmission electron microscopy (TEM).

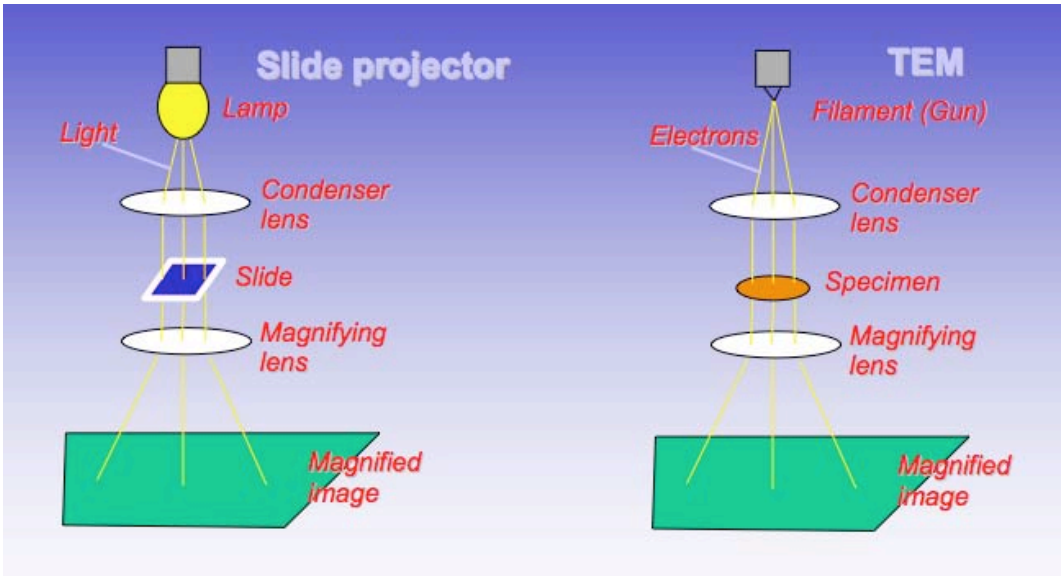

Figure 2.8: Scheme of the analogy between optical microscopy and electron microscopy. *(Taken from EM course material, CIME, EPFL)*

How does it work?

A stream of electrons is formed (by the electron source) and accelerated toward the specimen using a positive electrical potential. This stream is confined and focused using metal apertures and magnetic lenses into a thin, focused, monochromatic beam, which then focused onto the sample using a magnetic lens. Interactions occur inside the irradiated sample, due the electron beam. These interactions and effects are detected and transformed into an image (the same for all types of EMs regardless of type). The main interactions of electrons with matter is illustrated in Fig. 2.9. Such enormous effects has been utilized well in the past years, which led to the development of several accessory techniques coupled with EMs. For instance, the X-rays emitted by the specimen is able to address the chemical composition of the specimen and thus the technique called energy dispersive spectroscopy (EDS). Analyzing auger electrons also would give a wealth of information about the chemical composition through the technique called electron energy loss spectroscopy (EELS). Scattered electrons (both elastically and inelastically) also used for imaging purposes

that gives additional information on topography and morphology, which normal imaging modes might not produce.

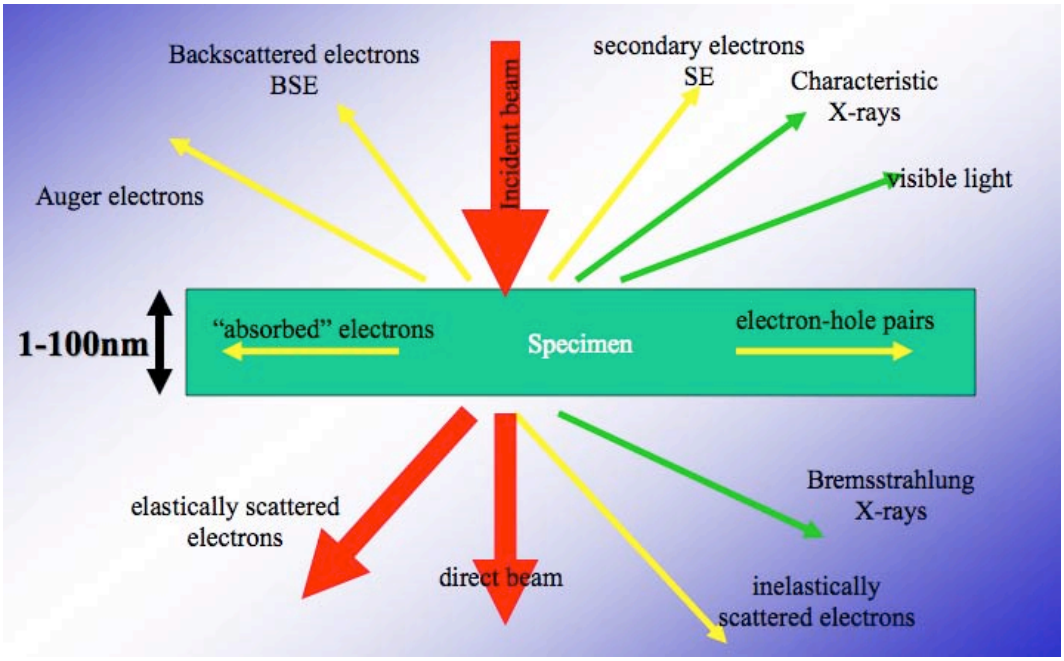

Figure 2.9: Schematic of the interactions of electron beam with matter.
(Taken from EM course material, CIME, EPFL)

Fig. 2.10 outlines two important modes used in TEM. Nowadays, electron diffraction technique equipped in TEMs are vital in studying the crystal structure such as growth direction, monocrystallinity and other important crystal parameters.

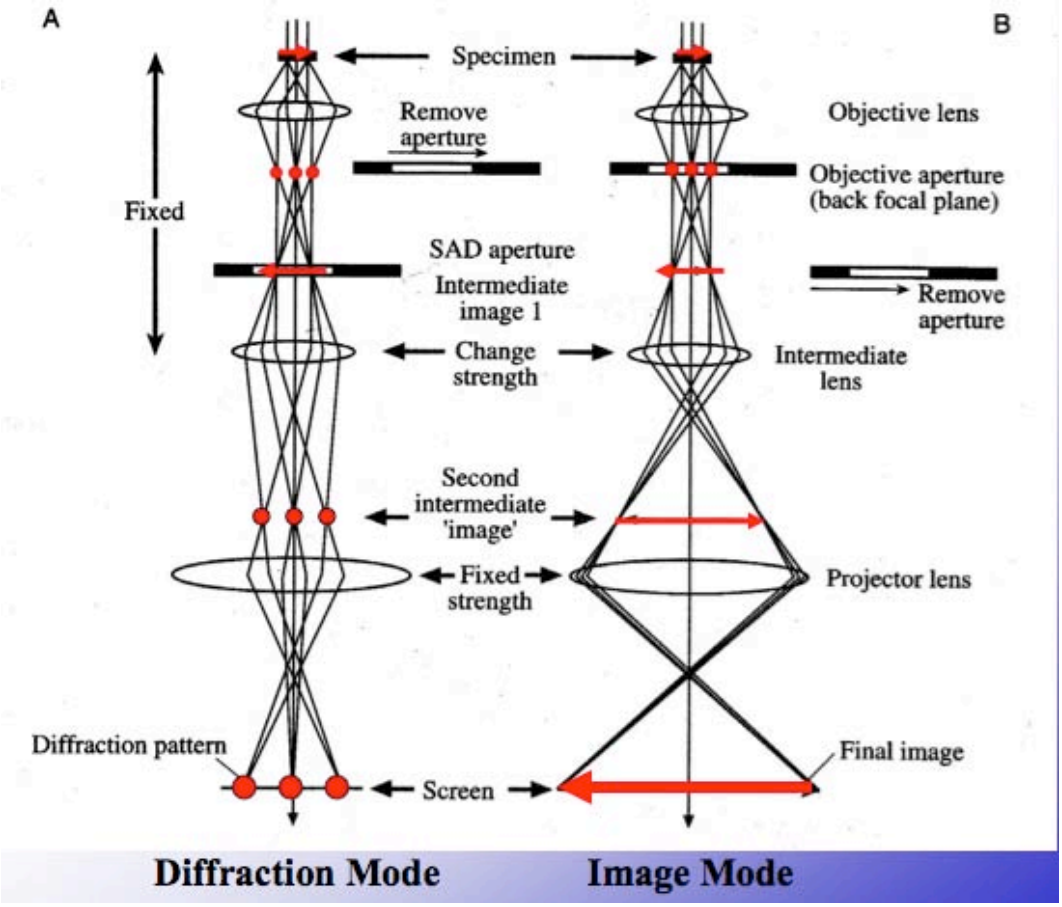

Figure 2.10: Schematic of the diffraction and image modes in EMS. *(Taken from EM course material, CIME, EPFL)*

Chapter 3

Synthesis of Nanoscopic Optical Fibers

3.1 Introduction

Nanostructures of various materials with different sizes and shapes have been synthesized and studied in the last years due to their high impact for optoelectronic applications. In particular, one-dimensional (1D) nano structures (nanowires, nanorods, nanotubes, etc) show optical and electronic properties [81], [17], [82] which are of importance to downsize opto-electronic components to the nanometer scale [83], [84]. Development and integration of such 1D nanostructures rely on suitable synthetic procedures. Several methods have been designed such as template-directed synthesis [50], [85], [9], [53], [54], [86], solvothermal synthesis [55], microfabrication [87], [88], metal nanocluster catalyzed growth [81], and surfactant-mediated self-assembly [89]. In particular, template-directed synthesis offers significant advantages: Ease of performance, the possibility to work at mild reaction conditions and above all the control over unique, well-defined morphologies of the resulting nanostructures. Various templates have reportedly been used for the fabrication of 1D nanostructures (see 3.2.1). Though simple to implement, the main limitations in many template-directed syntheses are poor yield and the polycrystallinity of the resulting nanomaterial [90].

This chapter discusses the use of lipid bilayers as templates for the synthesis of asymmetric, monocrystalline nanowires (NWs) [78] as they are well known self-organized nanostructures [73]. The following section briefs the state-of-the art in the fabrication and application of NWs.

3.2 Nanowires

1D systems are the structures of lowest dimension that can be used for efficient transport of electrons and optical excitations and hence their high potential in the function and integration of nanodevices. In other words, as discussed in 1.4, NWs (and other types of 1D nanostructures) possess 2D quantum confinement leaving one unconfined direction for electron conduction.

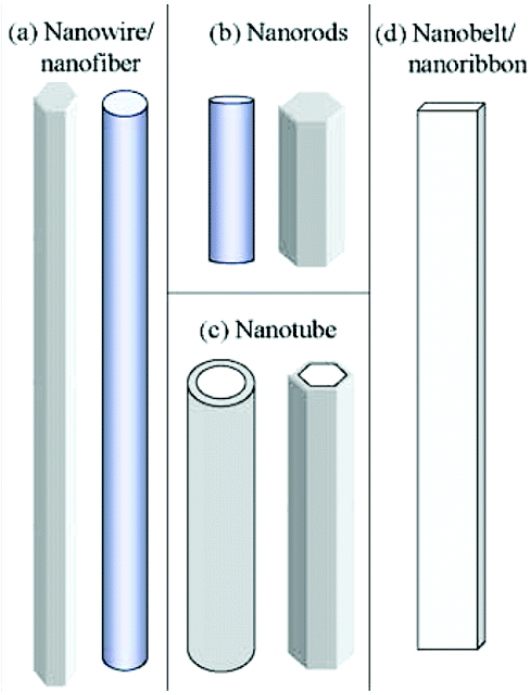

Figure 3.1: Morphology of 1D nanostructures. *a) A NW typically comprises a linear structure that has a specific growth direction; (b) a nanorod is a nanowire with a shorter length. (c) A nanotube is a 1D nanostructure with a hollow interior channel. (d) 1D nanostructures with well-defined side facets are called as nanobelts/nanoribbons [91].*

Because of their unique density of electronic states, NWs in the limit of small diameters are expected to exhibit significantly different optical, electrical, and magnetic properties from their 0D and bulk 3D crystalline counterparts. By morphological definition (Fig. 3.2), it has been widely accepted that NWs typically comprise a linear structure that has specific growth direction, but its side surfaces and shape of cross-section may not be well defined or uniform (Fig. 3.2a). But for achieving property control, it is important to clearly define the side surfaces of a nanowire. A nanorod is a nanowire with a shorter length (Fig. 3.2b). A nanotube is a 1D nanostructure with a hollow interior channel (Fig. 3.2c). Nanobelts/nanoribbons

are 1D nanostructures with well-defined side facets (Fig. 3.2d), and they have more restrictive shape and uniformity than the NWs [91].
Obtaining atomic building blocks rationally assembled into anisotropic structures with diameters in the nm regime but possessing longer length scales is the key goal to be achieved in the fabrication of NWs. It has been shown that the essence of 1D nanocrystal growth is the crystallization process that had been studied well for more than centuries. The two fundamental steps of crystallization are the nucleation and growth. Different synthetic methodologies have been widely used for the fabrication of such nanomaterials. Fig. 3.2 illustrates six different strategies that have been demonstrated for achieving 1D growth [92]. Special emphasis will be given to the template directed synthesis (Fig. 3.2C) as that is more relevant to the discussion of this chapter.

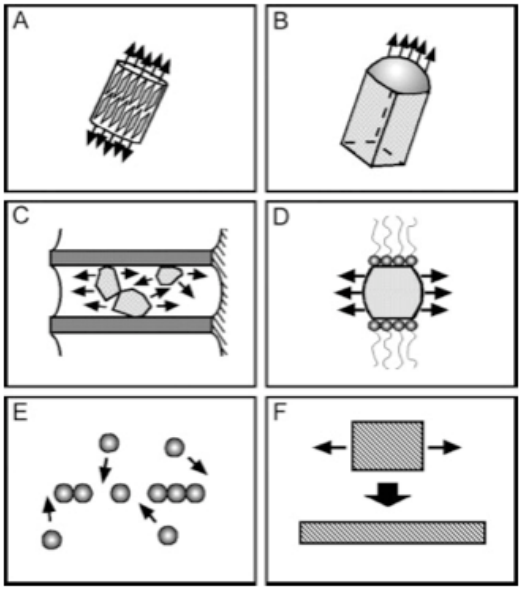

Figure 3.2: Different strategies for the 1D growth of nanostructures. *A) Dictation by the intrinsic anisotropic crystallographic structure of a solid; B) confinement by a liquid droplet; C) template directed growth; D) kinetic controlled growth using capping molecules; E) self-assembly of 0D nanoparticles; and F) size reduction (top-down approach) of a 1D nanostructure [92].*

3.2.1 Template-directed synthesis

Template-directed synthesis is considered as a straightforward route to obtain NWs, in which the template acts as a host matrix or scaffold within or around which the guest molecules find a pore or binding pocket. The nucleation and growth of different crystals thus occur in-situ with a morphology dictated by the template. Various

kinds of templates such as porous alumina [50], [51], molecular sieves [93], [85], soft-templates such as polymers [52], DNA [53], viruses [54], micelles [94] etc, and self-assembled monolayers [86] have been reported to guide the synthesis of 1D nanostructures. Here, the discussion is limited to the reports on the soft-template directed synthesis of NWs.

Polymer templates — A polymer-controlled growth method for fabricating high aspect ratio CdS NWs (Fig. 3.3) has been reported by Zhan et al. [52]. The polymer used in their approach is polyacrylamide, which has been extensively used in the separation of proteins, as a molecular sieve and as a protecting agent for NPs. In a typical synthetic method, Cd^{2+} ions were well distributed in the polyacrylamide matrix and then treated with thiourea solvothermally in ethylenediamine at 170^oC that resulted an yellow gel of CdS crystallites having wurtzite structure.

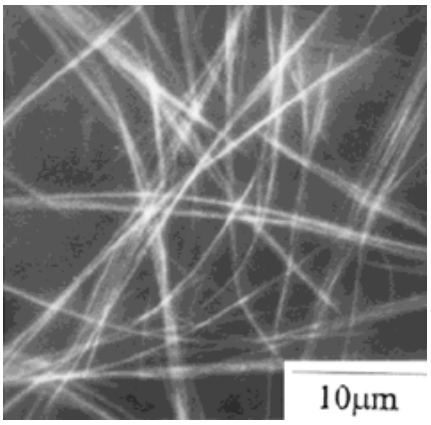

Figure 3.3: SEM image of CdS NWs. *High aspect ratio NWs of CdS obtained through polymer template directed synthesis. The diameters are in the range of 40 nm with lengths extending up to 100 μm [52].*

DNA templates — Liang et al. showed that crystallographic control of an inorganic nanostructure is possible using synthetic biomolecular templates comprised of anionic DNA and cationic lipid membranes, which self-assemble into a multilamellar structure where a periodic 1D lattice of parallel DNA chains is confined between stacked 2D lipid sheets. They have organized Cd^{2+} ions within the interhelical pores between DNA strands, which upon subsequent reaction with H_2S formed CdS nanorods of controllable widths and crystallographic orientation (Fig. 3.4). The strong electrostatic interactions align the templated CdS (002) polar planes parallel to the negatively charged sugar-phosphate DNA backbone, which indicates that molecular details of the DNA molecule are imprinted onto the inorganic crystal

structure. The resultant nanorods have (002) planes tilted by 60^o with respect to the rod axis, in contrast to all known II-VI semiconductor nanorods [53].

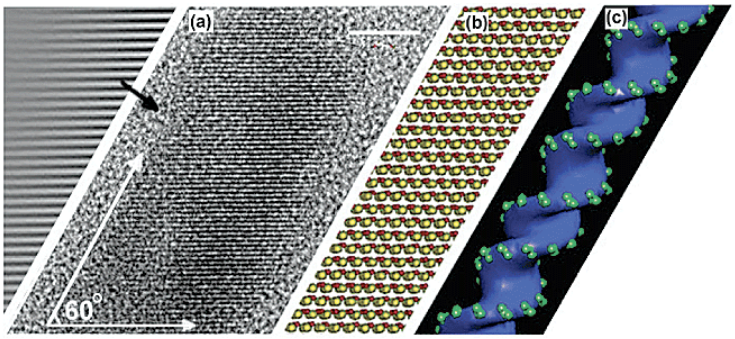

Figure 3.4: DNA templated growth of 1D CdS nanorods. *a) TEM image of a typical DNA templated CdS nanorod (scale bar = 5 nm): The tilt of (002) planes relative to rod axis is indicated. b) Schematic representation of crystal structure within nanorod (Cd, red; S, yellow) showing (002) planes. c) Schematic representation of B-form DNA, showing the negatively charged phosphate groups (green) on the backbone, which organize the Cd^{2+} ions and guide the nucleation of CdS [53].*

Virus templates — A virus-based scaffold for the synthesis of single-crystal magnetic and semiconducting NWs had been reported by Mao et al. [54]. The means of modifying substrate specificity through standard biological methods make the approach more extendable. Peptides that exhibit control over composition, size, and phase during nanoparticle nucleation have been expressed on the highly ordered filamentous capsid of the M13 bacteriophage. The incorporation of specific, nucleating peptides into the generic scaffold of the M13 coat structure provides a viable template for the directed synthesis of semiconducting and magnetic materials. Removal of the viral template by means of annealing promoted oriented aggregation-based crystal growth, forming individual crystalline nanowires (Fig. 3.5). The unique ability to interchange substrate-specific peptides into the linear self-assembled filamentous construct of the M13 virus introduces a material tunability and thus it provides a genetic toolkit for growing and organizing NWs from semiconducting and magnetic materials.

Micelle templates — Micelles formed from surfactant molecules have been widely used for the synthesis of different kinds of nanostructures (see section 1.4.2). In a typical approach, Huang et al. have demonstrated production of arrayed Ag NWs having high aspect ratio. The crystalline Ag NWs were prepared using cylindrical

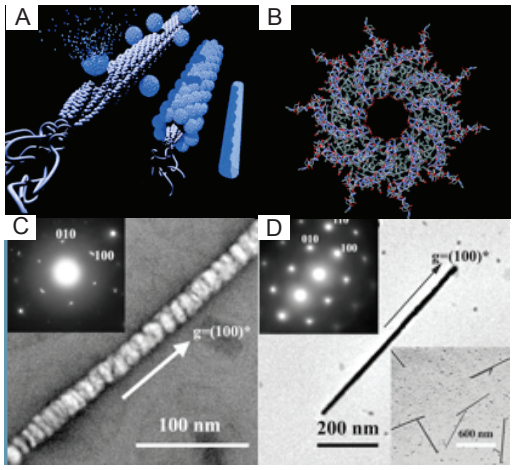

Figure 3.5: Virus templated growth of 1D ZnS NWs. *A) The NW synthesis scheme is visualized for the nucleation, ordering, and annealing of virus-particle assemblies. B) The symmetry of the virus allows for ordering of the nucleated particles along the x, y, and z directions, fulfilling the requirements for aggregation-based annealing. C) Dark-field diffraction-contrast imaging of the pre-annealed ZnS system. Inset shows electron diffraction pattern of the polycrystalline pre-annealed wire. D) Bright-field TEM image of (C) after annealing. Inset showing electron diffraction pattern of the monocrystalline annealed NW. (Inset, lower right) TEM image showing the monodisperse, isolated single-crystal NWs [54].*

micelles composed of sodium bis(2-ethylhexyl)sulfosuccinate (AOT), *p*-xylene, and water [94].

The water phase was substituted by an aqueous 0.1 M $AgNO_3$ solution. The electrodeposition was then conducted using a potentiostat in a two-electrode configuration with the two electrodes narrowly spaced (0.5±1.0 mm) and the reverse micellar phase as electrolyte. The NW were deposited on the cathode substrate (polished stainless steel). The figure (Fig. 3.6) outlines the general scheme of using micelles as templates.

3.2.2 Properties and applications

As discussed already in section 1.4 the properties of low-dimensional materials are usually explained on the basis of their high surface/volume ratio as well as possible quantum confinement effects. Important and noticeable properties of 1D nanostructures are: **(1) Their thermal stability:** It has been reported by several research groups that the melting points observed in NWs are reduced compared to their bulk [95], [96]. This effect is very remarkable when considering NWs as building blocks of nanoelectronic devices. For example, wherever a connection is needed, one can cut,

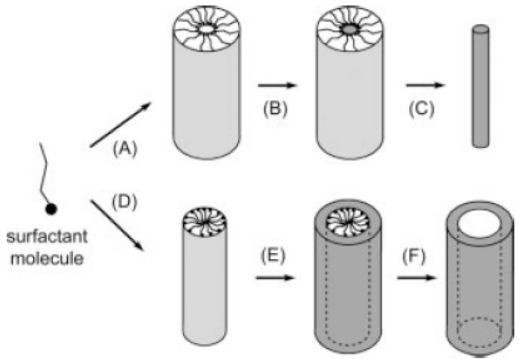

Figure 3.6: Illustration of the micellar strategy for the 1D growth of nanostructures. *A) Formation of a cylindrical micelle from surfactant molecules; B) formation of the desired material in the aqueous phase of the micelle; C) removal of the template yielding pure NWs; D-F) similar process as in (A-C) except that the NWs are formed at the exterior surface of the template [92].*

interconnect and weld NWs at milder temperatures, which is vital in device construction. **(2) The mechanical stability of NWs:** This is an important parameter to consider for an interconnecting part in nanoelectronic devices. As reported by Rubio-Bollinger et al. [97], in their STM investigation of the mechanical property studies on Au NWs. They found that the bond-strength of the NW is two times stronger than that of bulk Au. **(3) Electron transport properties:** Nanoelectronic device fabrication needs miniaturized electronic components. The presently using "top-down" approach has some fundamental limitations that is expected to affect the computing speed. Consequently, chemically synthesized ("bottom-up" approach) NWs are found more attractive in terms of computing capability as well as fabrication cost, in nanodevice fabrication through self-assembly. Another important aspects of such a "bottom-up" approach is the possibility of making high density device on a single chip as well as the enormous flexibility in choosing the right material for a specific application. It has been reported that arrays of single crystalline Bi NWs showed a metal-to-semiconductor transition at ~ 52 nm [98]. Studies on individual Bi NWs showed similar effects at ~ 40 nm [99]. These effects have been explained based on the quantum confinement effects. The electron-transport properties of Au also have been studied [100]. A prototype p-n junctions made from the assembly of semiconducting NWs have been reported by Lieber and his co-workers, which has been used to create integrated field-effect transistors [101]. **(4) Optical properties:** As in 0D nanocrystals, NWs also exhibit size-dependent quantum confinement effects [102]. It is well-known that semiconductor QDs exhibit size-dependent blue/red-shift in their emission wavelengths. On the other hand with

Si NWs, it has been reported that variation in the growth direction resulted different optical behavior [103]. Another important aspect is that the photoluminescence from NWs is highly polarized. Emission from catalytically grown CdS NWs have been reported by Duan et al.. in 2003 [81], which they have used for the construction of an electrically driven laser. ZnO NWs also have been found showing lasing, waveguide as well as NLO properties [104], [105], [106]. **(5) Optical switching:** Kind et al. have shown that highly sensitive NW switches can be created using ZnO NWs [84]. The light-induced conductivity increases, which is extremely sensitive to UV light and thus allows the reversible switching of the NWs between the "OFF" and "ON" states. **(6) Sensing applications:** Last but not least, the potential sensor applications of 1D nanostructures. They can be highly useful in medical and environmental applications have to be considered. NWs might be a useful material for sensing purposes due to their high surface/volume ratio so that the sensitivity to adsorbed species on their surface is increased due to the high surface area. Penner and co-workers fabricated Pd NWs that can be used in hydrogen sensing [56]. Surface modified semiconducting NWs have been found useful as highly sensitive, real time sensors biological samples [107].

3.3 Lipid membranes as templates

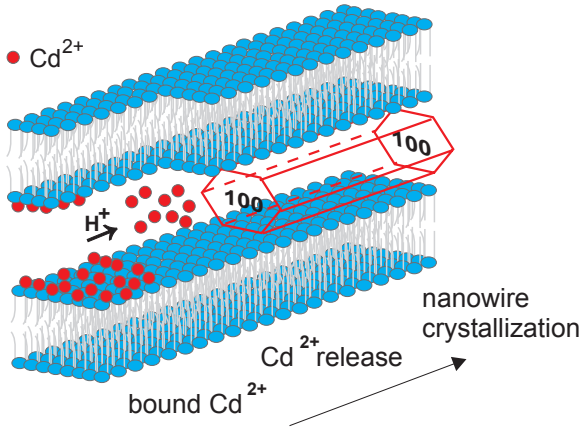

Figure 3.7: Strategy of using lipid membranes as templates for the 1D growth of nanostructures. *High-aspect-ratio, monocrystalline, cadmium chloride NWs doped with fluorescent CdS nanoparticles have been synthesized using planar lipid membranes as templates. Cd^{2+} ions bound to the lipid bilayers are released at low pH to the nanometer-sized, interlamellar water films where the sudden increase in concentration leads to the formation of NWs [78].*

The closed compartments of single phospholipid vesicles have already been used as nanoreactors to perform simple chemical reactions [70], [108]. Upon drying from aqueous dispersions many phospholipids spontaneously form well-organized periodic multilayers of lipid membranes separated by distinct nanometer-thick water films [71]. The rich variability of the lipid hydrocarbon chains and lipid polar headgroups results in numerous lyotropic and thermotropic phases and phase transitions [71]. Of particular interest in the present context are lipid polar headgroups which bind selectively and reversibly certain cations. This opens the possibility to modulate the concentration of precursor ions, e.g. when a second reactant is added, and thus control the synthesis of nanomaterials in the confined, nanometer sized water films of multilamellar lipid phases (Fig. 3.7). Here we applied this strategy to synthesize high-aspect ratio (∼1000) cadmium chloride NWs, which exhibit interesting optical properties if doped in situ with fluorescent CdS quantum dots.

3.3.1 Synthesis of $CdCl_2{\cdot}4H_2O$ nanowires

This part of the thesis deals with the results and discussion on the synthesis and properties of novel high aspect ratio (>1000) NWs of $CdCl_2{\cdot}4H_2O$. The room temperature synthesis was achieved in the confined nanometer-sized interlamellar water space of lipid multilayers where supersaturating $CdCl_2$ concentrations were induced by acidification leading to controlled unidirectional growth of NWs.

Experimental Part: Lipids used:

- ▷ 1,2-Dimyristoyl-sn-glycero-3-phosphatidylcholine (DMPC)
- ▷ 1,2-dilauroyl-sn-glycero-3-phosphothioethanol (DLPSH)
  (DMPC was purchased from Fluka and DLPSH from Avanti Polar Lipids)

Solutions in chloroform of 100 μL of 4mM DMPC and 10 μL of 16 mM DLPSH were mixed, dried in vacuum and the resulting lipid film was hydrated in 110 μL deionized water (room temperature, 10 minutes). After adding 30 μL of an aqueous solution of 10mM $CdCl_2$ (Fluka) the mixture was dispersed for 5 minutes in a bath sonifier. 15 μL of the obtained clear vesicle solution was transferred onto a microscope glass coverslip and dried in vacuum. The resulting transparent lipid film was rehydrated at 100% humid atmosphere in a closed desiccator at 60^{o}C for 3 hours. Then, a recipient containing 32% hydrochloric acid (Merck) was inserted in the desiccator, the lipid film was incubated for another 2 hours with preserved humidity while the temperature slowly decreased from 60^{o}C to room temperature.

To produce fluorescent NWs, the procedure was identical, except that HCl was mixed with a small flake of FeS (Riedel- de Haen, Germany) to produce H_2S while the dessicator was kept under vacuum (400 mbar) to enhance H_2S production. A typical synthesis yielded around 1,000,000 NWs of which 10-20% showed lengths exceeding 20 μm (Fig. 3.13). The yield of NWs in a single synthesis has been estimated as follows: The number of NWs from several confocal images of similar preparations were counted. This was possible because (1) the typical size of lipid film in each preparation was always constant and (2) the density of NWs were always homogeneous. The yield with an error of an order of magnitude was thus calculated. Changing the ratio of DLPSH to DMPC reduced the yield and delivered shorter NWs. For example, when 50 μL of 1.6 mM DLPSH was added to 100 μL of 10 mM DMPC, the synthesis produced shorter NWs with yield comparable to the optimized lipid ratio. Whereas, addition of 10 μL of 1.6 mM DLPSH into 100 μL of 10 mM DMPC, resulted with high aspect ratio NWs with very poor yield. Lipids could be removed from the produced NWs by washing (several times if necessary) with toluene (Fluka). Washing was performed by gentle rinsing of the sample using 300 μL toluene in each washing steps.

To observe colocalization of lipids and NWs, 1% rhodamine-labelled lipids (TRITC-DHPE, Molecular Probes) was added.

3.3.2 Characterization

Scanning Electron Microscopy (SEM):

The NWs obtained have high aspect ratios with a narrow distribution of diameters ranging from 80 to 200 nm and lengths extending up to 170 μm. Fig. 3.8 shows a typical SEM image of such $CdCl_2{\cdot}4H_2O$ NWs on a glass substrate. The as prepared NW sample on a microscopic glass cover slip has been washed twice using toluene and directly used for imaging. SEM were recorded on a high resolution/low accelerating voltage SEM (XL-30 SFEG, Philips). The Fig. 3.9 shows a magnified view of the same sample and was the maximum resolution we could achieve. As the substrate was glass, severe charging-up of electrons made the imaging difficult beyond certain focal length.

SEM images were also recorded on samples prepared on silicon (Si) coated glass substrates. These NWs were gown little more wider than usual NWs grown on glass substrates. The Fig. 3.9 shows representative SEM images and are interestingly looking faceted. The faceted structure of NWs were further confirmed by AFM imaging (image not shown) that has been used for the angle measurement in the

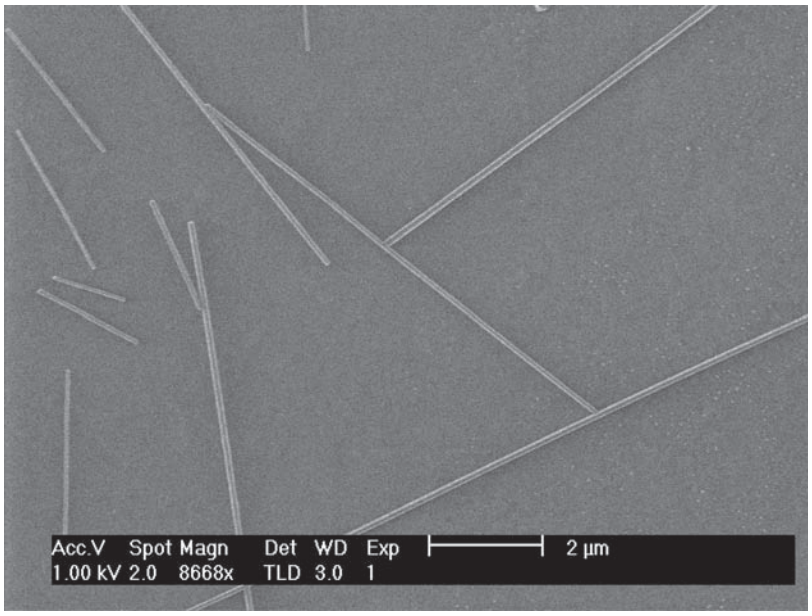

Figure 3.8: Scanning Electron Microscopy. *Scanning electron micrograph of typical $CdCl_2{\cdot}4H_2O$ NWs, illustrating the high aspect ratios. In this particular image, diameters of the NWs are around 100 nm and lengths range from 1.5 μm up to more than 20 μm (scale bar = 2 μm). The lengths of the NWs could be tuned by varying the duration of HCl exposure while the diameters showed little variation.*

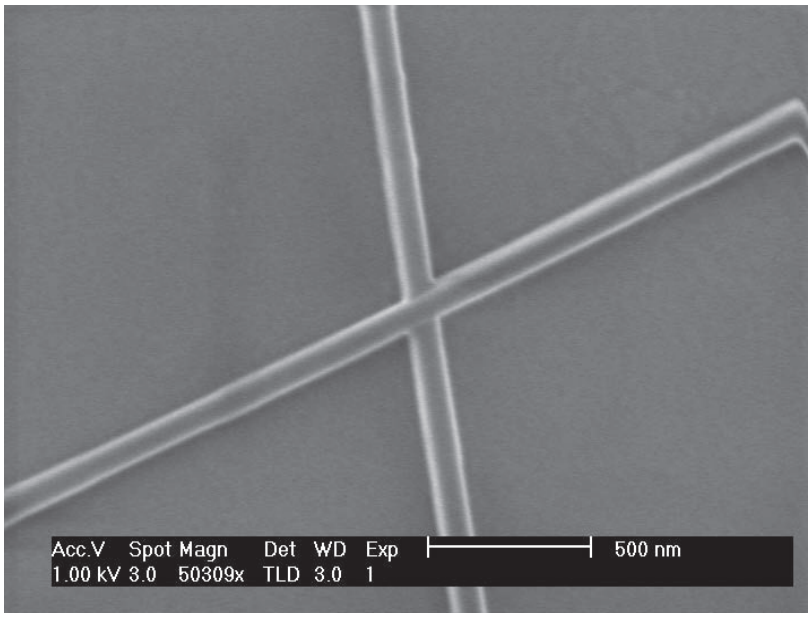

Figure 3.9: Scanning Electron Microscopy. *Magnified view of a part of Fig. 3.8 (scale bar = 200 nm). Though it looks like a junction between two NWs, from careful evaluation of many SEM images, we conclude that they are just crossing each other one over the other.*

crystal re-construction of $CdCl_2{\cdot}4H_2O$ NWs.

Transmission Electron Microscopy (TEM):
TEM measurements were performed using an analytical-holographic TEM (HF-2000, Hitachi) equipped with an energy dispersive x-ray spectrometer (EDS) (HP Ge diode, Voyager, Noran) except for the main image in Fig. 3.14c, which was recorded on a Philips CM300- UT. For TEM, the NWs were first washed with and then dispersed in toluene and transferred onto a carbon coated holy Cu-grid. To record the Selected area electron diffraction patterns (SAED) pattern, samples were mounted on a Gatan double-tilt/cooling sample holder and cooled to liquid N_2 temperature. Transmission electron microscopy (Fig. 3.11) shows bright-field (a) and dark-field (b) images of representative NWs. HRTEM showed that the NWs are monocrystalline along the entire lengths (Fig. 3.12a). Proper fitting of SAED pattern revealed that the NWs are made of orthorhombic $CdCl_2{\cdot}4H_2O$ crystals grown along the [100] direction (Fig. 3.12b).

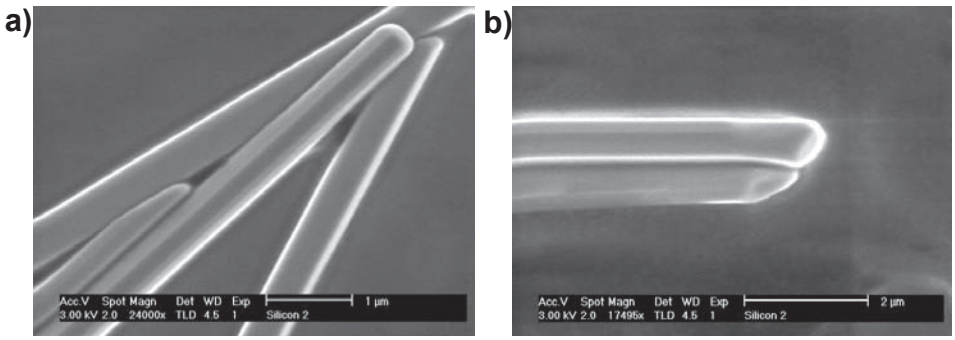

Figure 3.10: Scanning Electron Microscopy. *Scanning electron micrograph of typical $CdCl_2{\cdot}4H_2O$ NWs, grown on Si/glass substrate. In this particular image (a), diameters of the NWs are around 500 nm and are found faceted (scale bar = 1 μm). (b) The ends of the NWs showing open ends indicating the incomplete growth (scale bar = 2 μm). Similar incompletely grown NWs are also visible in (a), which are terminated their growth due to the obstacle generated by neighboring NWs.*

3.3.3 Optical properties

While $CdCl_2{\cdot}4H_2O$ crystals are non-fluorescent, CdS compounds, in particular nanocrystals, show size-dependent fluorescence. In order to endow the NWs with fluorescent properties, HCl vapor was supplemented with H_2S during the growth. As a result, the NWs became intensely fluorescent with high photostability.

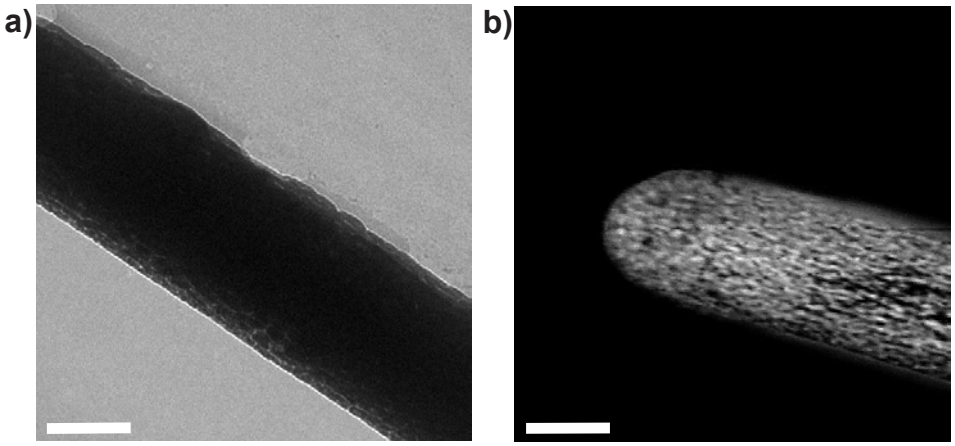

Figure 3.11: Transmission Electron Microscopy. *(a) Bright field transmission electron micrograph of middle of a NW showing the 1D crystal (scale bar = 100 nm). (b) Dark field transmission electron micrograph of the end of the same NW. Extended e-beam irradiation creates some damage to the NW (scale bar = 100 nm).*

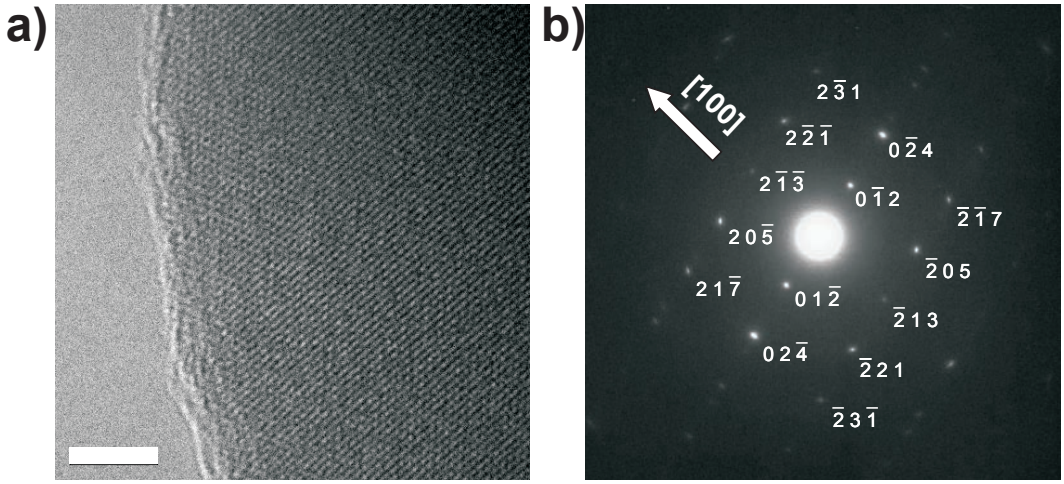

Figure 3.12: Transmission Electron Microscopy. *(a) High-resolution transmission electron micrograph of the edge of a NW showing the regular atomic arrangement in the crystal lattice (scale bar = 5 nm). (b) Selected area electron diffraction (SAED) pattern on a NW with indexation corresponding to orthorhombic $CdCl_2 \cdot 4H_2O$. The arrow indicates the [100] direction, which is the long axis as well as the growth direction of the NW.*

Confocal Fluorescence Microscopy images shown (Fig. 3.13 and Fig. 3.14a) were recorded on a ConfoCor-2 laser scanning confocal microscope (LSM 510, Zeiss; excitation = 488 nm, emission = 505 - 550 nm). In the confocal images a weak diffuse background fluorescence was observed within the lipid bilayer stacks (Fig. 3.14a). The background fluorescence has considerably reduced by multiple washing with toluene.

Single Particle Spectroscopy/ Microscopy (SMS):
Spectra of single NWs (SSN) and images of single particles (ISP) and of nano-waveguides (INW) were recorded on a modified epiluminescence wide-field microscope (Axiovert 100 TV, Zeiss). Circularly polarized light of either 457.9 nm (SSN, ISP) or 488 nm (INW) of an Ar^+ laser (Innova Sabre, Coherent) was directed by a dichroic mirror (z458rdc (SSN) or Q495LP (ISP, INW), Chroma) into a microscope objective (C-Apochromat 63x, 1.2 NA, W Korr., Zeiss) to illuminate either a 35 μm diameter region of the sample (ISP) or a diffraction-limited spot centered on a NW (SSN, INW). Fluorescence was collected by the same objective, passed through a filter (LP480 HQ (SSN), Chroma, or 515 LP (ISP, INW), Zeiss) and was either spectrally resolved (SSN) by a monochromator (CP-140, Spectroscopy Instruments GmbH) coupled to a CCD camera (LN/CCD-576 EUV, Spectroscopy Instruments GmbH) or imaged (ISP, INW) on an Electron Multiplying CCD camera (IXon DV887AC-FI, Andor Technology Ltd).

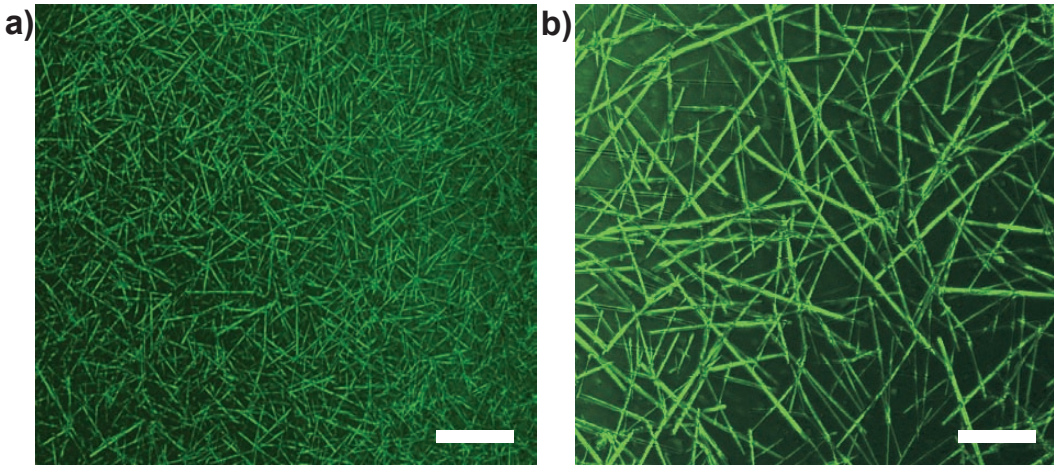

Figure 3.13: Confocal fluorescence microscopy. *Confocal images (false-color) showing (a) a high population of NWs in a typical preparation (scale bar = 20 μm). (b) Magnified view of (a) (scale bar = 5μm). The fluorescence from the NWs shows very high photostability (hours)*

The diffuse fluorescence in the lipid stacks (Fig. 3.14a) and the NWs featured a

similar, broad emission band upon excitation at 458 nm with a maximum at 522 nm typical for CdS nanoparticles (Fig. 3.14b). The full-width at half-maximum (FWHM) is larger than 100 nm and are much wider than the reported band-edge emission spectra of bulk CdS that exhibit an emission maximum at 512 nm with a FWHM of 24 nm [81], while deep-level emission is usually observed around 600 nm [109]. In contrast, emission spectra similar in width and spectral position have been observed for large CdS nanoparticles (>35 Å) [110], [111], which can be excited at 457.9 nm [112], and have been attributed to emission from deep-surface traps [113]. TEM images reveal a heterogeneous mixture of crystallites of CdS nanoparticles (Fig. 3.14c). Single nanoparticles were also detected by optical microscopy at high excitation intensities as diffraction-limited spots [77] in the middle of a fluorescent background (Fig. 3.14d). The single quantum dots featured the characteristic single-step photobleaching as seen in the inset of Fig. 3.14d, and in some cases blinking as well. The most stringent requirement for single-nanoparticle detection is high fluorescence quantum yields, which is fulfilled only for nanoparticles whose surface is effectively passivated. It is probable that the fluorescent background in Fig. 3.14d is due to the remaining nanoparticles that do not fulfill this requirement. The NWs exhibited spectra identical to the diffuse background in the lipid stacks showing that their fluorescence is due to associated CdS nanoparticles. Rough estimations from the fluorescence intensities indicate that CdS nanocrystals are only present as traces (below 1/1000 in volume) inside the NWs. This is further confirmed by the fact that sulfur was not detected by EDS analysis (Fig. 3.15), which has a detection limit of about 1%.

Optical waveguiding in the NWs:

The NWs' extended length and their diameter in the order of 100 nm make them attractive candidates for optical waveguiding [81], [105]. When fluorescent NWs were locally excited, fluorescence emission was detected not only at the excitation spot, but also from the ends of the NWs (Fig. 3.16a), i.e., NWs waveguide light over tens of micrometers, thus acting as effective nanoscopic optical fibers. The ability to waveguide light is connected with the high refractive index of the NWs, n_{NW}, which is expected to lie between the refractive index of pure $CdCl_2 \cdot 2.5H_2O$ (n =1.65) and CdS (n = 2.5). The corresponding minimal diameters D needed for the NW to act as a single-mode optical waveguide at the emission maximum at $\lambda = 520$ nm are thus between 80 and 190 nm using the relation,

$$D = \frac{\lambda}{\pi}(n_{NW}^2 - n_{medium}^2)^{-0.5}$$

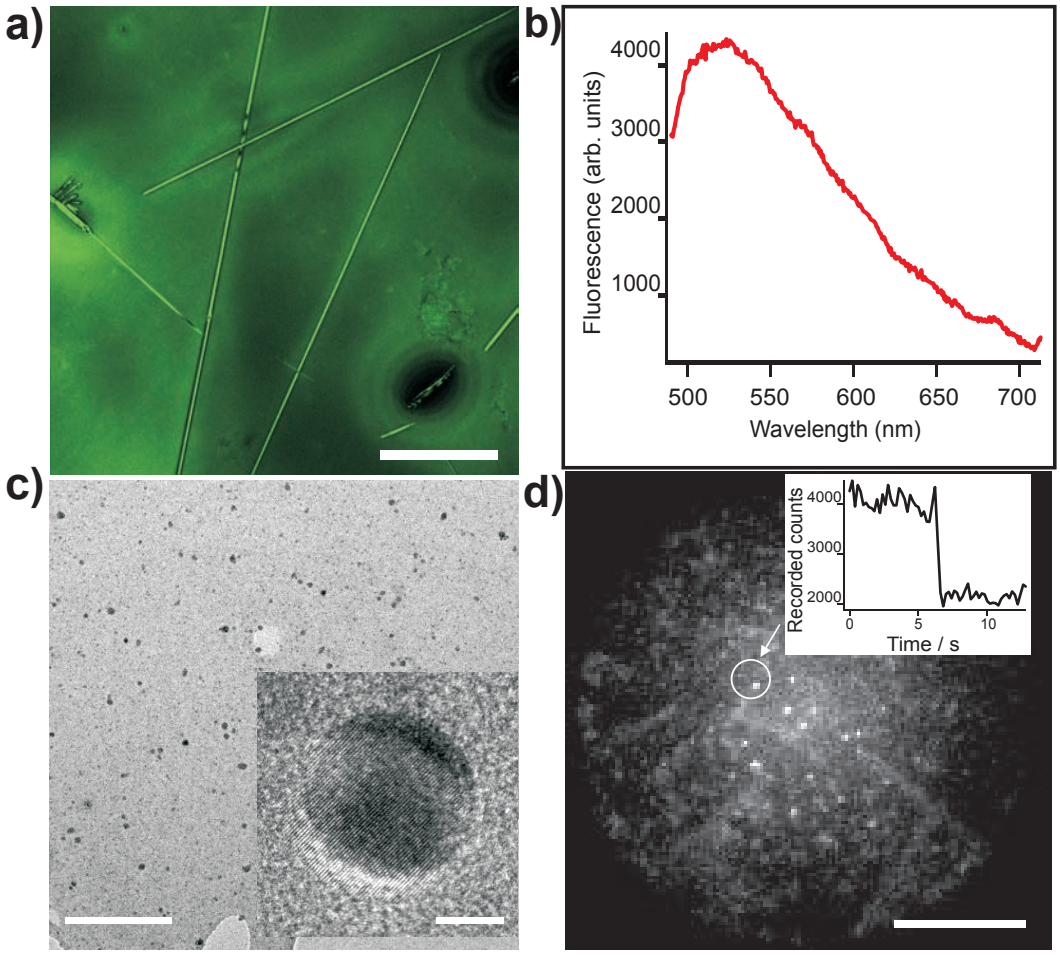

Figure 3.14: Fluorescence property of the NWs. *(a) Fluorescence confocal image (false-color) of NWs grown in the presence of H_2S showing that the thus prepared 100 μm long NWs are intensely fluorescent (scale bar = 20 μm, excitation = 488 nm, emission = 505-550 nm). (b) Fluorescence emission spectrum of a single washed NW upon excitation at 457.9 nm. The emission maximum is at 522 nm with a FWHM larger than 100 nm. The spectrum of the fluorescent background is identical. (c) Transmission electron micrograph of the background lipid multilayers showing the presence of a heterogeneous mixture of nanometer sized CdS crystallites (scale bar = 200 nm). Inset: HRTEM of a CdS nanoparticle (scale bar = 5 nm). (d) Wide-field image showing single QDs, recognized as diffraction-limited spots, which appear in a structureless fluorescent background. Only a small fraction of the QDs is observed at the single-QD level due to the stringent requirements for such observations, while the major fraction is contributing to the structureless fluorescent background. Inset shows a time trace of the emission from the encircled QD featuring the characteristic single-step photobleaching (scale bar = 10 μm, excitation = 457.9 nm, integration time = 100 μs, measurement frequency = 5 Hz).*

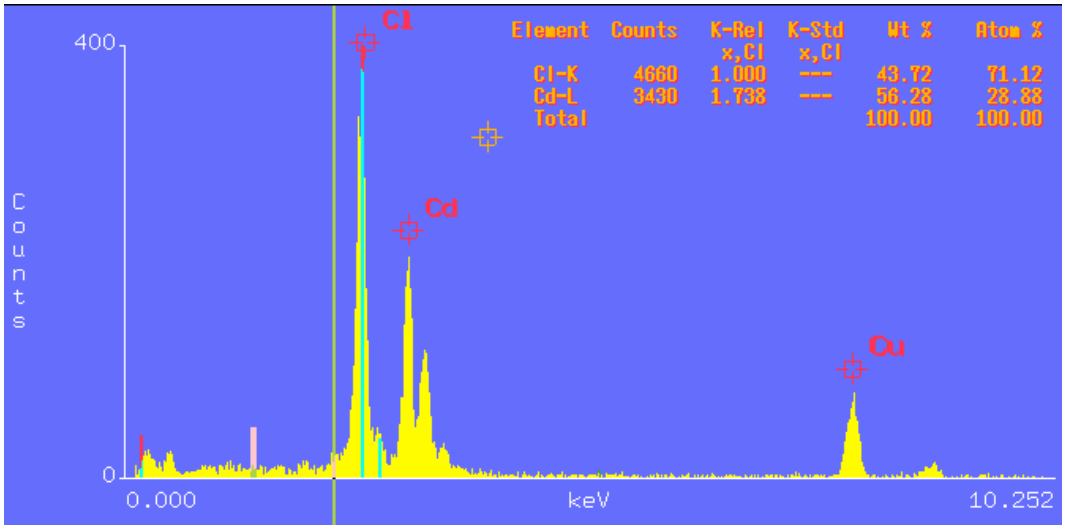

Figure 3.15: EDS analysis of NWs. *The EDS analysis of NWs clearly showed that the crystal composed of Cd and Cl atoms, which was further confirmed by the SAED as shown in Fig. 3.12b*

where n_{medium} is the refractive index of the medium, and is equal to 1.4 [81]. The range of diameters found for the NWs fall well within the theoretical sizes of the optical waveguides.

Optical trapping of the NWs:

Manipulation of a NW in the plane of the image and perpendicular to it by laser tweezers [114]. The 1064 nm focused cw beam of a Nd^{3+}:YVO_4 laser (Spectra-Physics, US) was used to rotate (Fig. 3.17a-h) and levitate (Fig. 3.17i-l) the NWs suspended in toluene. The images shown in Fig. 3.17 are snapshots from the rotation and levitation movie files.

3.3.4 Discussion

Role of Individual lipids in the design of template:

The synthesis of NWs was achieved in hydrated, multilamellar stacks of lipid bilayers comprising lipid-bound Cd^{2+} ions (Fig. 3.7). Proper design of the lipid template was crucial for the formation of NWs. The lipid bilayers comprised 70 mol% of DMPC, acting as a stable matrix, and 30 mol% of a thiolipid, DLPSH, added for its strong ability to bind Cd^{2+} ions via the -SH groups. Differential Scanning Calorimetric experiments showed a strong binding profile of Cd^{2+} ions onto unilamellar thiolipid vesicles in water. Addition of aq. $CdCl_2$ to a pure thiolipid vesicle solution led to the formation of a precipitate, which could be dissolved upon subsequent treatment

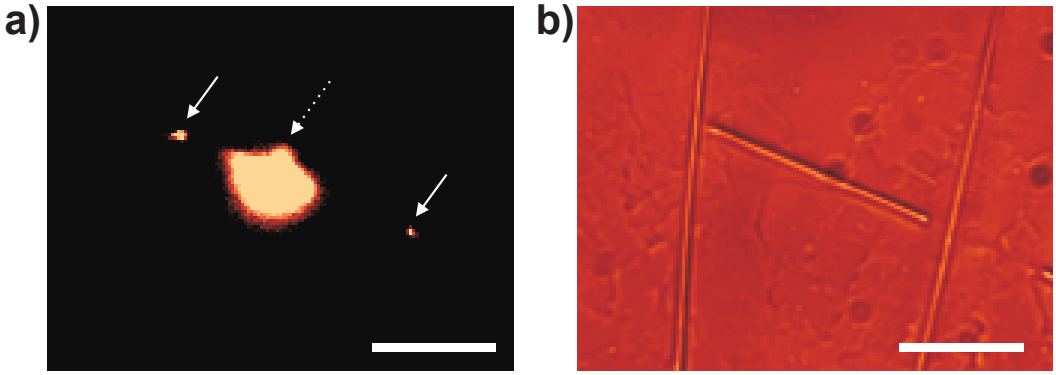

Figure 3.16: Optical waveguiding in the NWs. *False-color photoluminescence image of a NW (a) upon local excitation at the middle (dotted arrow) with excitation at 488 nm. Luminescence is observed at the excitation location (dotted arrow) and from both ends (solid arrows) due to optical waveguiding along the NW and (b) the corresponding false-color white-light transmission image of the NW.*

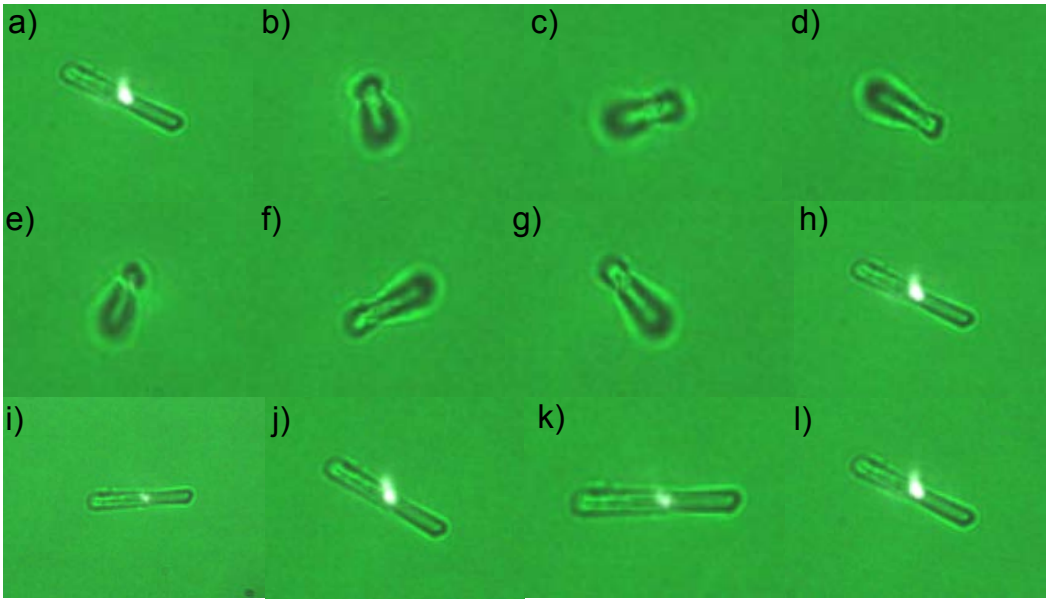

Figure 3.17: Optical manipulation of the NWs. *False-color fluorescent images of a rotating (a-h) and levitating (i-l) NWs in an optical trapping experiment.The excitation wavelength used was 488 nm. The bright spots on NW crystals are the laser points that act as optical tweezers.*

with HCl indicating reversible binding between Cd^{2+} and thiolipids. On the other hand, incorporation of 30 mol% of thiolipid in a DMPC vesicle solution prevented this precipitation under similar conditions, which in turn yielded NWs and the former did not, showing the respective roles of each lipid fractions in the controlled growth of NWs.

Role of critical reactant concentration:
With a molar ratio of lipid/Cd^{2+} of about 2, large quantities of Cd^{2+} ions were complexed by the lipid headgroups. Upon exposure to HCl vapour, Cd^{2+} ions were released as a result of competitive binding of protons to the polar lipid headgroups [115] leading to supersaturating concentration of Cd^{2+} in the nanometer-sized water film, and finally to the initiation of NW growth (Fig. 3.7). When either the Cd^{2+} concentration was reduced by a factor of two or DLPSH was omitted, no NWs were formed showing that a critical concentration of Cd^{2+} is necessary. NWs appeared when lipid multilayers were prepared by drying a lipid dispersion in 10 mM $CdCl_2$ solution but did not appear when a 5 mM solution was used. A fully hydrated DMPC multilamellar phase comprise about 30 water molecules/lipid molecule [116]. If that would hold also for our case, the critical concentration of $CdCl_2$ for NW crystallization would be about 1M in the interlamellar water film. The solubility of $CdCl_2$ in bulk water is 7.7 M, which indicates that the number of free water molecules in the multilamellar lipid phase is lower than 30 mol/lipid as they are bound to the lipid headgroups.

Growth mechanism:
The synthesis of anisotropic structures requires that the template, here the lipid lamellar phase, restricts or promotes the growth in specific directions. The crystal planes have been subsequently extracted using the SAED pattern recorded from the NWs (Fig. 3.12 b) in combination with the published crystal parameters of $CdCl_2{\cdot}4H_2O$ [117].
Orthorhombic $CdCl_2{\cdot}4H_2O$ consists of [001] molecular chains formed by edge-sharing $[CdCl_4\ (H_2O)_2]^{2-}$ octahedrons (Fig. 3.18a) that define a preferential growth direction along the octahedral chain axis resulting into slightly elongated crystals of $CdCl_2{\cdot}4H_2O$ when grown in aqueous solution [117]. It is remarkable that the growth direction of our NWs is perpendicular to the preferential growth direction of bulk $CdCl_2$ crystals. Online monitoring of NW synthesis indicates that the initiation of growth critically depends on a rate-limiting step: Two sequential phases were observed with the rapid apparition of small nucleation points followed after a certain

time lag by the sudden and continuous, non-synchronous 1D growth of the crystals (Fig. 3.18b). Using fluorescent lipids, a close colocalization of lipids and NWs was observed demonstrating that the lipid membranes are intimately involved in the NW growth (Fig. 3.18c). Taking these observations together, we propose a mechanistic model for the unusual, asymmetric growth of the NWs. $CdCl_2{\cdot}4H_2O$ crystal nuclei grow unperturbed up to a critical size where a collective binding of numerous protonated, positively charged headgroups of the planar lipid membranes to the crystal planes rich in Cl^- (i.e., high negative charge density) becomes favorable; this occurs for all crystal planes except the (100), in which Cl^- ions are shielded by a layer of coordinated water molecules, thus inhibiting growth in these directions.

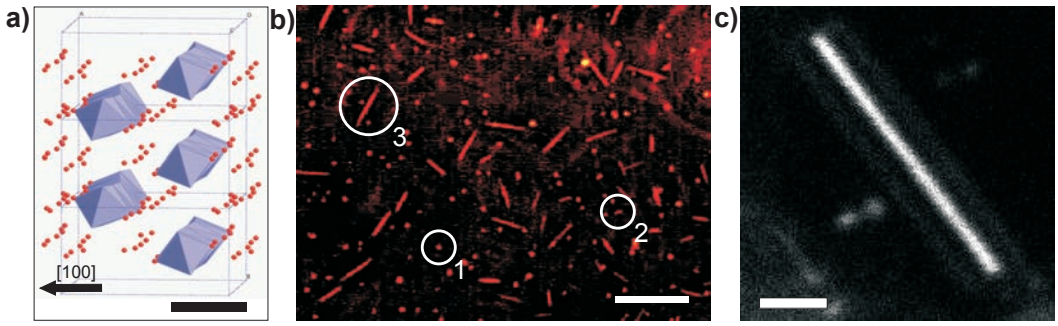

Figure 3.18: Crystal growth in the NWs. *(a) The crystal structure of orthorhombic $CdCl_2{\cdot}4H_2O$ showing the 1D molecular chains formed by edge-sharing $[CdCl_4\ (H_2O)_2]^{2-}$ octahedrons (in blue) and the water molecules (in red). The arrow indicates the [100] growth direction (scale bar = 6 Å). (b) White-light transmission image (false color) of growing NWs. Because the initiation of growth is asynchronous, the various phases of the NW growth are present in a single image. NW growth occurs in two distinct steps: First numerous nucleation points appear (1), after a while some nucleation points grow into small NWs (2) that continuously elongate upon addition of HCl vapor (3) without noticeable change in the diameter (scale bar = 60 μm). (c) Fluorescence confocal image showing colocalization of a NW and rhodamine-labelled lipids (scale bar = 2 μm, excitation = 543 nm, emission = 560 - 610 nm).*

3.3.5 Conclusion

In conclusion, a novel synthetic route for state-of-the-art NWs has been presented based on lipid membranes as an anisotropic template. This allows a straightforward, high-yield production of high aspect ratio monocrystalline NWs at mild conditions that act as nanoscopic optical fibers (Fig. 3.19). The synthesized $CdCl_2{\cdot}4H_2O$ NWs can be furthermore endowed with fluorescent properties by addition of H_2S. The

appearance of highly fluorescent CdS QDs demonstrates that such nanoparticles can be synthesized in the confined interlamellar water film which might open novel synthetic routes for quantum dots. Our fluorescent NWs could find a broad range of applications in optoelectronics, for instance in the development of nanolasers, in complement to CdS NWs [81]. A further speculation is that this novel procedure using lipid membranes as templates might be extended to the synthesis of other materials by exchanging the thiolipid with other lipids having suitable head groups which reversibly bind various ions. The possibility to manipulate the NWs laterally, for instance using laser tweezers encourages the use of these NWs for nanofabrication of devices. In this respect, particularly attractive are the recent developments to form networks of lipid vesicles and lipid nanotubes [118], which might be used as a template to build an array of connecting NWs opening a way to pre-assemble nanocomponents for future optoelectronics.

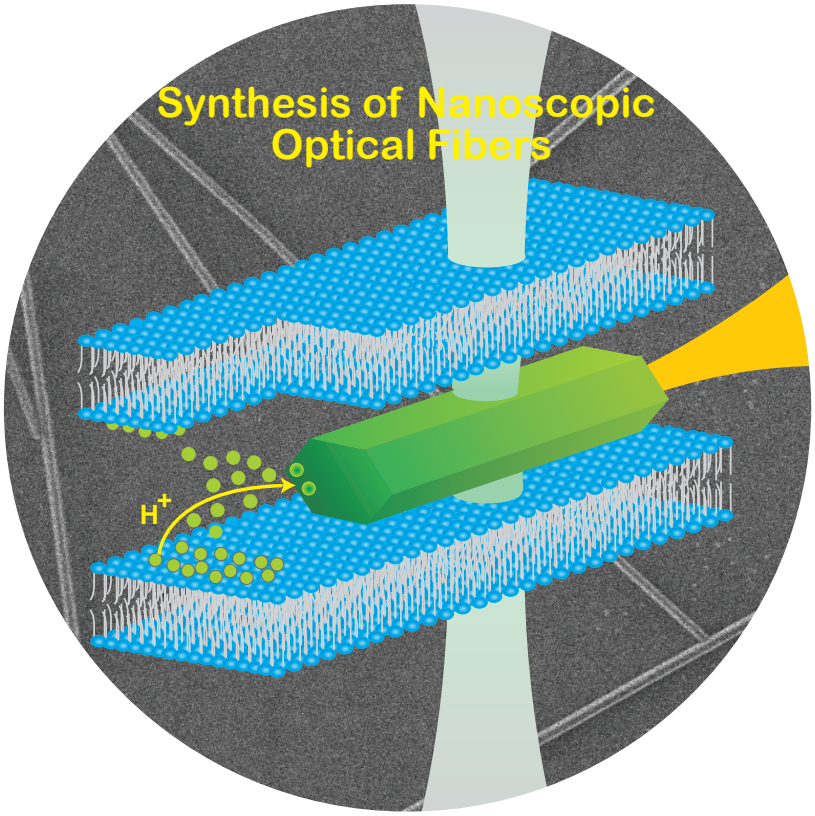

Figure 3.19: Synthesis of nanoscopic optical fibers. *Illustration of the synthesis and optical fiber properties of* $CdCl_2 \cdot 4H_2O$ *NWs (Angew. Chem. Int. Ed., 2005, 44, 4957- 4960).*

Chapter 4

Multifunctional Nanocontainers For Controlled Targeting Live Cells

4.1 Introduction

Nanocrystal based organic-inorganic functional hybrid materials with novel, exceptional properties have been explored in recent years due to their potential applications in nano-biotechnology [4], [119], [8], [120], [121]. Viral assembly of inorganic nanoparticles [122], their polypeptide [123] and ligand-receptor mediated organization [77], protein templated synthesis [124], are a few examples in this direction. Of utmost interest in the context of this chapter are lipid molecules due to their unique capabilities to form a variety of self-organized, supramolecular structures [71], [73], [125]. Though planar and vesicular lipid membranes have been used to compartmentalize and to synthesize nanocrystals in confined volume [78], [126], [64], the enormous possibilities of lipid based, biocompatible nano/microstructures in nanobiotechnology has still to be fully exploited. For example, native and artificial vesicles offer novel possibilities to investigate (bio)chemical reactions and cellular signal transduction processes at nanometer and attoliter scales [127], [70], [108]. Furthermore, the interaction between specially designed lipid vesicles and mammalian cells (adsorption, fusion, endocytosis) [128] has been used to deliver DNA and RNA into cells and has high potential for smart diagnostics, controlled drug delivery and gene transfer [126], [129], [130], [131]. Inorganic nanoparticles could offer novel ways to image native and artificial vesicles and control (bio)chemical reactions therein, if it would be possible to selectively position the particles on or within the vesicles.
In this context, we investigated quantum dots (QDs), inorganic, strongly fluorescent nanoparticles of exceptional photostability, to image cellular processes in vivo [20],

[132]. Notably, coating hydrophobic QDs with phospholipids is a generic method to make them water soluble [133] and biocompatible [134], useful for investigating biochemical reactions in-vitro [135] and when microinjected into live cells [136].
This chapter discusses on an interesting observation of wide-ranging potential in cellular imaging and manipulation: Hydrophobic QDs can be easily incorporated into the bilayer membrane of lipid vesicles. Such lipid/QD hybrid vesicles (HVs) are capable to fuse with live cells, thereby stain the cell's plasma membrane selectively with fluorescent QDs and transfer the vesicle's cargo into the cell.
Though it has already been described in chapter 1, a more precise look into the biological interests of fluorescent QDs as well as the formation and applications of lipid vesicles will be described here as they are the key components in the design and fabrication of HVs, which is the central system under study in this (chapter 4) and the preceding chapter (chapters 5).

4.2 Quantum dots

A quantum dot (QD) is a semiconductor particle that has all three dimensions confined to the 1- to 10-nm length scale [22]. To understand why a semiconductor particle of this size would be interesting from a quantum mechanical point of view, when an electron is promoted to the conduction band from the valence band, a "hole" (a particle with its own charge (+1) and effective mass) will be generated in the valence band. The electron and hole together known as an "exciton". The exciton can be considered a hydrogenlike system, and hence a Bohr approximation of the atom can be used to calculate the spatial separation of the electron-hole pair of the exciton by

$$r = \epsilon h^2/\pi m_r e^2$$

where r is the radius of the sphere (defined by the 3D separation of the electron-hole pair), ϵ is the dielectric constant of the semiconductor, m_r is the reduced mass of the electron-hole pair (exciton), h is Planck's constant, and e is the charge on the electron. For typical semiconductor dielectric constants, the calculation suggests that the exciton diameter is 1-10 nm for most semiconductors. The electronic structure of these quantum dots, then, becomes intermediate between localized bonds and delocalized bands (Fig. 4.1).
Because the physical dimensions of a QD can be smaller than the exciton diameter, the QD is a good example of the "particle-in-a-box" model. The energies of the particle in the box depend on the size of the box. QDs, thus exhibit a size-dependent

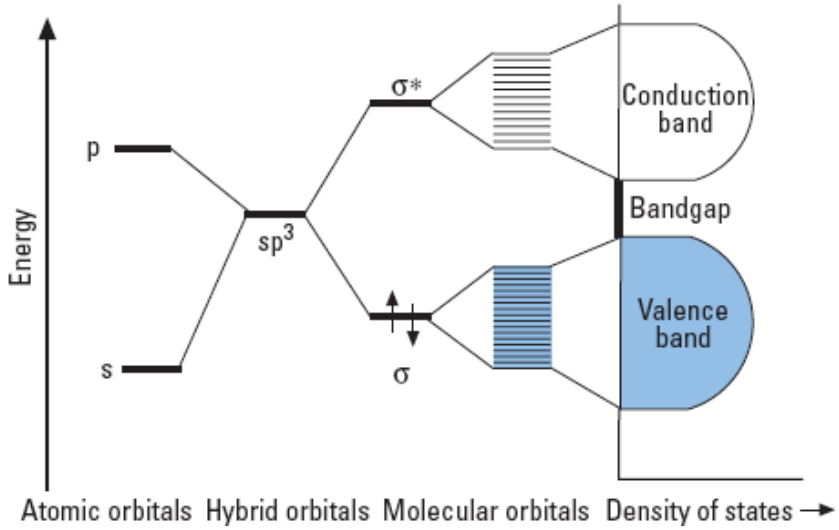

Figure 4.1: Bandgap in a semiconductor. *Comparison of the electronic structure of the atomic orbitals in a silicon atom (left) to that of bulk silicon (right) through that of a silicon cluster molecule (middle) . Atomic orbitals in the atom give rise to bonding and antibonding molecular orbitals (σ, σ^*) in the cluster molecule, which give rise to the filled valence band and empty conduction band in the bulk semiconductor (adapted from [22]).*

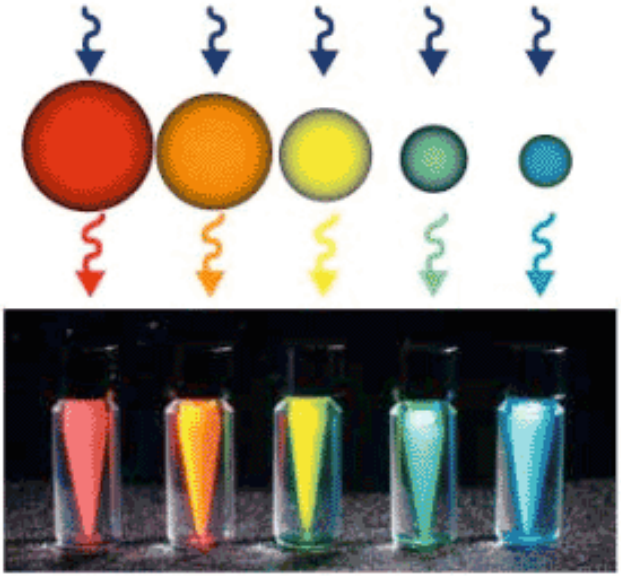

Figure 4.2: Emission from bandgap engineered QDs. *All samples were excited at a single wavelength which resulted in the emission of their respective colors. The colored spheres illustrate the relative sizes of the CdSe quantum dots in the vials (taken from http://probes.invitrogen.com).*

bandgap structure [21]. As the particle size decreases, the absorption onset and thus emission shifts to lower wavelengths (blue shift). Fig. 4.2 shows the tunable emission property of QDs via bandgap engineering, which depends on the crystal size. Surface defects in the crystal structure may create temporary "traps" for the exciton and thus prevent a radiative recombination. The main result of these surface traps are the intermittence in the fluorescence (blinking), which is observed using single-molecule microscopy [137], [77].

Inorganic fluorescent probes having the same surface chemistry with different emission bands ranging from near IR to blue, has thus been emerged. Due to their high photostability and tunable emission properties, QDs became an important tool in the toolbox of many biologists and chemists [20]. Longer-term observation of biological events using a laser scanning confocal microscopy or single-molecule microscopy observations of cellular events are some of the advantages QDs can offer due to their high photostability.

4.2.1 (Bio)chemical modification of QDs

As discussed in 1.4.1, the high quality QDs (from hereon, the term QD is used to represent CdSe QDs) are usually synthesized in organic solvents [30]. Though water soluble QDs have also been synthesized [35], [36], still the most commonly used approach to produce high quality fluorescent QDs is the synthesis in organic solvent using TOPO as a stabilizer [30]. First to make them water soluble, and later to target specific biological locations both in-vitro and in-vivo, various surface modifications on QDs have been established. The first of this kind was introduced by Alivisatos and co-workers [33] through silica coating of the CdSe QD surface. Later, several molecules have ben found useful for a successful transfer of TOPO coated QDs to water, which may allow further bio-functionalization of the QD surface. The common group of molecules that has been used for the surface functionalization of QDs are (i) ligand exchange using water soluble thiol- containing molecules [34] such as oligomeric phosphines, [138], dendrons [139], and peptides [140]: (ii) encapsulation by di/triblock copolymers [141], [142] silica shells [33], phospholipids [135], [136], polymer shells [143], amphiphilic polysacharides [144].

4.2.2 Lipid modification of QDs

Among the possible surface functionalization shown above, coating of QDs using phospholipid molecules stands as a very generic method to make them water soluble and biocompatible due to the simplicity of the reaction procedure. Phospholipid

modified QDs are found useful for investigating biochemical reactions in-vitro [135], and when microinjected into live cells [136]. Additionally, the availability of various types of lipid headgroups that may allow further (bio)chemical conjugation on the surface of the QDs as well as the extreme biocompatibility of phospholipids make this approach more attractive.

In a typical procedure, Geissbuehler et al. [135] developed a general and versatile procedure to make TOPO coated QDs water-soluble, based on the self-assembly of single lipid monolayers, and simultaneously decorate them with a diverse range of multiple functionalities. The lipid coat shields the QDs perfectly from physical and chemical modification. Simple control over the composition of the lipids (for example: by varying the polar head groups of the lipid) used for self-assembly allowed them to tune the physical (electrical charges, structures, entropic shielding) and chemical (reactive group, biological recognition elements) surface properties of the QDs. They have demonstrated that such multifunctionalized lipid-coated QDs can bind different proteins per particle specifically and subsequently position themselves on micropatterned surfaces to form nanometer-sized supramolecular structures of higher complexity.

In a different approach, Dubertret et al. showed that TOPO coated QDs can be further coated with micelle forming lipids [136], which allowed them an efficient phase transfer of QDs from organic solvent to water. They encapsulated individual QDs in phospholipid block-copolymer micelles (micelle composed of a mixture of n-poly(ethylene glycol) phosphatidylethanolamine (PEG-PE) and phosphatidylcholine (PC)) and demonstrated both in vitro and in vivo imaging. Here, PEG-PEs are the micelle-forming hydrophilic polymer-grafted lipids. When conjugated to DNA, the QD-micelles acted as in vitro fluorescent probes to hybridize to specific complementary sequences. Moreover, when injected into Xenopus embryos, the QD-micelles were stable, nontoxic, and slow to photobleach.

4.3 Lipid vesicles

Lipid vesicles, or liposomes, are spherical, closed lipid bilayer structures which entrap part of the solvent, in which they freely float, into their interior. The size of such vesicles ranges from 10 nm to tens of micrometers while keeping the membrane thickness of about 4 nm. They are usually formed from amphiphilic molecules, molecules having hydrophobic and hydrophilic groups. In general, they are not soluble in water, instead form colloidal dispersions. The solubility of such amphiphiles depends on the ordering of lipid molecules: the hydrophilic part (usually the lipid

headgroups) tends to be in contact with water while the hydrophobic part (alkyl chains) tends to be hidden inside the closed structures [72], (see section 1.5). With respect to the size and lamellae, vesicles are classified into large multilamellar vesicles (MLVs: 100 nm -2 μm), giant unilamellar vesicles (GUVs: 10-100 μm), large unilamellar vesicles (LUVs: 100-200 nm) and small unilamellar vesicles (SUVs: 30-100 nm). Phospholipid bilayers are known for their thermotropic phase transition behavior [71] and thus the vesicles formed can be controlled thermally by changing membrane composition. For instance, release of entrapped substances, fusogenic ability, deformability etc. of lipid vesicles can be tailored well. The biological membrane constitutes the fluid lipid bilayers (Fig. 4.3), which is responsible for defining the size and shape of the organelle, act as a permeability barrier and provide stable matrix in which several functional membrane proteins are embedded, showing the biological relevance of bilayer lipid membranes.

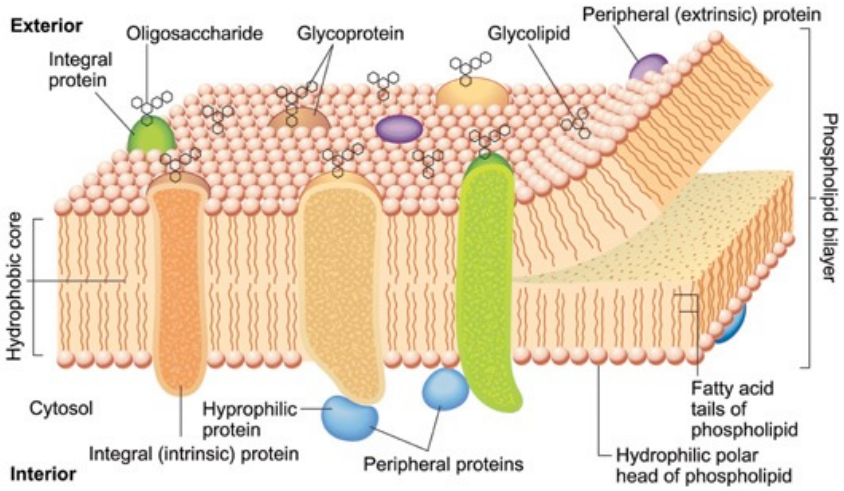

Figure 4.3: The fluid mosaic model of cell membrane. *The biological membrane constitutes the fluid bilayer lipid membrane, which is responsible for defining the size and shape of the organelle, act as a permeability barrier and provide stable matrix in which several functional membrane proteins are embedded.*

As mentioned earlier, the vesicles usually trap the part of the solvent in which it is originally formed. This allows one to entrap certain molecules of interest into the confined, size-tunable inner space of lipid vesicles through prior mixing in the solvent. The closed lipid bilayer shell allows these entrapped molecules to cross different hydrophobic barriers, which otherwise cannot, or to deliver those molecules though other membranes. Fig. 4.4 shows the interaction of different molecules with unilamellar vesicles. The water soluble ones are entrapped, whereas the amphiphilic ones orient into the bilayers, and hydrophobic ones reside in the hydrophobic region

of the bilayer.

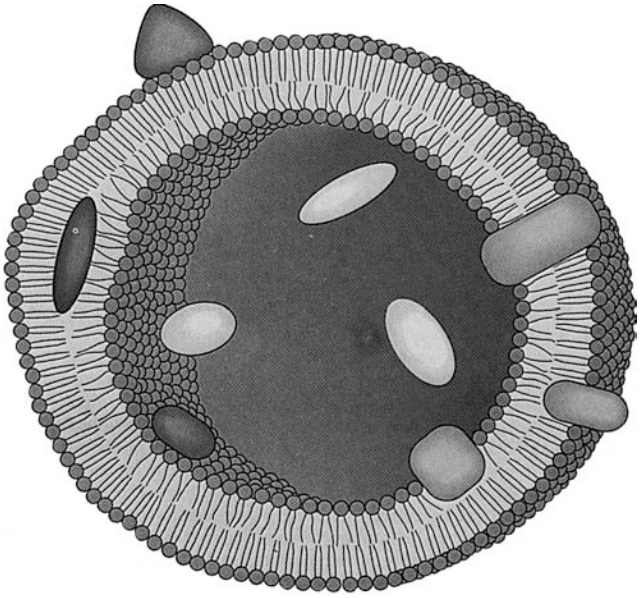

Figure 4.4: Interaction of different molecules with lipid vesicles. *The molecules are entrapped inside or bound to the lipid vesicles depending on their nature of solubility (adapted from [72]).*

4.3.1 General methods of preparation of vesicles

There are many different methods for preparing different sized lipid vesicles. The method of preparation strictly depends on the application. In model membrane studies, often GUVs are used because of the huge size, which offers ease of optical imaging whereas in drug or delivery applications SUVs are most commonly used. The encapsulated volume is much lower in SUVs compared to GUVs. The entrapped volume increases roughly as a cube of the radius. More precisely, with $(r-\delta)^3$, where δ is the membrane thickness. In order to form lipid vesicles, the lipid molecules must be introduced into an aqueous environment from the organic solvent, where they usually available. Though lipid powders are also available, direct dispersion of these powders in water or any other aqueous solvents wouldn't yield lipid vesicles. Following are the most commonly used methods to prepare lipid vesicles.

Hydration of thin lipid film:

In this method, a thin film of lipid is dried in a clean, glass flask from an organic solvent such as chloroform. The film is then dry well to remove any traces of chloroform, which subsequently hydrated using water or other aqueous buffers. This method generally results in the formation of heterogeneous dispersion of all sizes and lamellae of vesicles. Fig. 4.5 shows a schematic representation of the most common thin-film hydration approach to produce different kinds of lipid vesicles. Thin-film hydration when performed through a very slow swelling process is termed in this chapter as classical swelling whereas when performed with agitation is termed as spontaneous swelling.

Figure 4.5: Thin-film hydration approach to produce lipid vesicles. *Schematic representation of MLV preparation (a-c) through agitation of the flask; relatively homogeneous population of unilamellar vesicles can be prepared by following slow swelling process (classical swelling) as shown in (d). This approach would result with a high percentage of GUVs [145]; (e) a dialyzed preparation of (d) will ensure that all non-entrapped molecules are decanted away (adapted from [72]).*

The vesicles thus formed can be further treated mechanically to get more homogeneous vesicle population. For example, extrusion (forcing through filters having defined pores) would result in vesicles with the sizes matching the pore size used. Freeze-thawing is another approach to get more homogeneous and unilamellar vesicles from a heterogeneous dispersion of vesicles. In applications that need SUVs, the most commonly adapted method is sonication of few seconds using a bath or tip sonicator. For the exclusive formation of GUVs, Akashi et al. [145] introduced a

method that works in physiological conditions and with many different lipids. They have produced GUVs in sizes ranging from 25-100 μm.

Though it has been widely used for more than few decades, the exact mechanism of the process of thin-film hydration is not clear. The scheme in Fig. 4.6 shows the possible mechanism in the formation of MLVs. Additionally, the number of lipid molecules in the vesicle structure depends on the level of agitation and on the macroscopic stacking and organization of the crystalline bilayers in the dry lipid film.

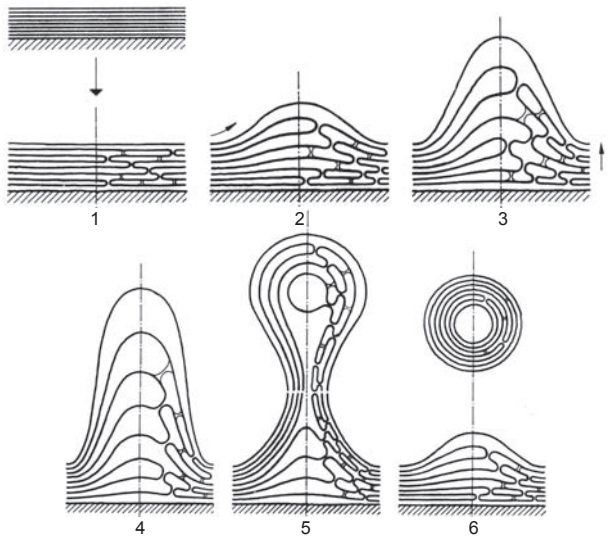

Figure 4.6: Possible mechanism in thin-film hydration method of MLV formation. *Upon hydration, the dry phospholipid film tends to grow via self-connected adjacent bilayers (right hand side of the drawing). The lines indicate phospholipid bilayers and the arrows in 2 and 3 indicates the preferential direction of the migration of the lipid bilayers (adapted from [72]).*

Electroformation:

Though there were methods established for the formation of unilamellar lipid vesicles, the sample heterogeneity is often a problem. Angelova et al. has first introduced the method of electroformation in 1986 to overcome this problem [146] and still remains the only method to produce homogeneous sample of GUVs. It is established that lipid vesicles can be prepared from neutral as well as charged lipids and lipid mixtures by inducing the swelling of lipid films by applying external electric fields while the lipid films are swelled on electrode surfaces in aqueous media. The sizes, lamellariry, and the yields of the resulting unilamellar vesicles can be controlled well by the thickness of the initial lipid film, and the parameters of applied electric field. The electroformation set-up (Fig. 4.7) consists of the electrodes on which the lipid

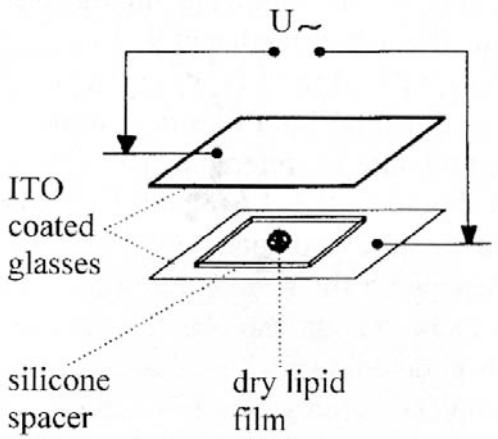

Figure 4.7: Electroformation method to produce unilamellar lipid vesicles. *Two plane parallel transparent electrodes of ITO coated glass plates are connected to an AC/DC source. The lipid film is dried in one of the electrode surface, surrounded by a non-conducting spacer, which is then filled with water [147]).*

film is dried and an external AC/DC supply. The AC supply is a low-frequency generator (0.1-50 Hz at up to 7V). An oscilloscope is also connected to monitor the applied parameters. As mentioned earlier, this method has been proven to be efficient in making homogeneous GUVs from variety of lipid mixtures of different polarity, chain length etc. In a typical protocol, the film dried on one of the ITO coated glass electrodes will be hydrated, preferably at a temperature above the phase transition of the lipid employed, by incubating with an aqueous buffer. An alternating electric field of 1.2 V/10 Hz during the first 2 hours is applied for an effective swelling followed by a lower frequency (2.0 V/4 Hz) for the next 1 hour. The latter step will help the vesicles to become spherical and for an easy detachment from the electrode surface.

Though there had been several speculations on the underlying mechanism of the electroformation of vesicles, the exact mechanism of this event has still not been completely understood. There are many possible mechanisms predicted but here the discussion is limited to the most probable one. As depicted schematically in Fig. 4.8, the predominant mechanism could be the electro-osmotic periodic movement of the water medium at the water-electrode interface. These vibrations are directed perpendicular to the electrode surface (Fig. 4.8a) and thus pulling off the lipid lamellae from the electrode thereby they grow perpendicular to the electrode surface (Fig. 4.8b). The size of this growth increases up to 10- 20 μm and at this stage, two adjacently grown buds start to touch each other (Fig. 4.8c). As the zone of contact increases, and at certain point they fuse together and form a large

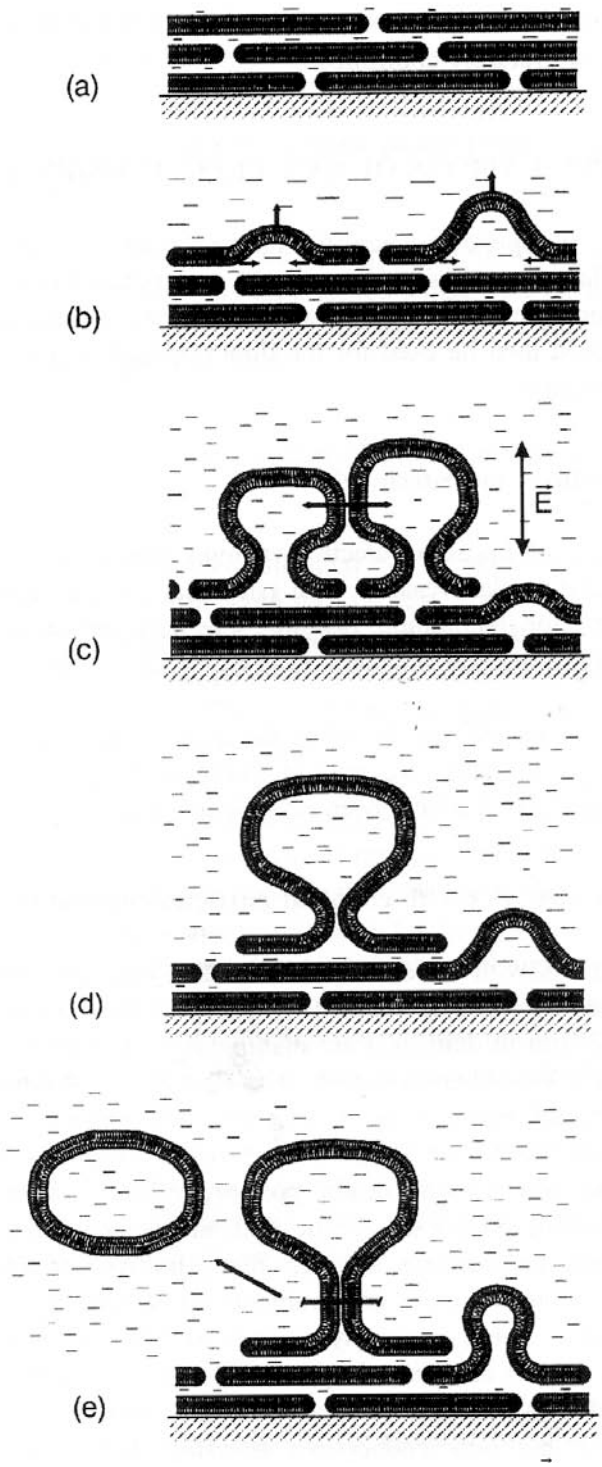

Figure 4.8: Possible mechanism in electroformation method of GUV formation. *Sketch showing vesicle AC electroformation. $\bar{E}$ indicates the direction of the external electric field (adapted from [147]).*

one. (Fig. 4.8d). The resulting large lipid bilayer structure slowly becomes a closed sphere and eventually gets separated from the electrode surface (Fig. 4.8e).
Examples of GUV formation is shown in the confocal fluorescence images (Fig. 4.9, Fig. 4.10). These images are presented only to show that the appearance of vesicles are the same in both cases. The lipids used here is a mixture of DLPC and DPPC, which is known to form vesicles showing phase domains [148], [149]. The images shown here though do not show any phase domains but in the case of Fig. 4.10, the lipids seem to have phase separated before vesicle formation, which resulted in vesicles with two different composition.

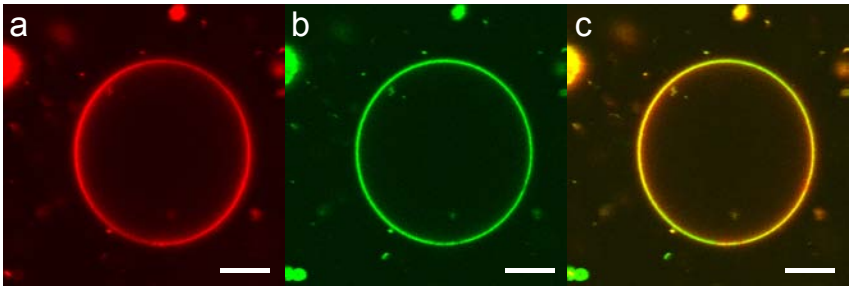

Figure 4.9: Confocal fluorescence images showing GUVs formed using classical swelling. *A 30/70 mixture of DLPC and DPPC were swelled at 65 °C using two different membrane dyes. These two lipids usually phase separate at room temperature as DLPC is in the fluid and DPPC is in the gel phase. Bodipy FL usually prefers DLPC phase than DPPC whereas DiI C_{18} prefers DPPC phase. But in this particular vesicle shown here, both lipids are mixed and hence the fluorescence is colocalized. (a) shows the emission from DiI C_{18} while (b) shows the Bodipy emission. (c) is the overlay of the two (scale bar= 10 μm).*

4.3.2 Applications of vesicles

The most important feature of lipid vesicles is their ability to trap, protect and carry hydrophilic as well as hydrophobic molecules. Their similarity with cell membranes and the possibility to undergo membrane modification to occupy several functional moieties make them a very interesting candidate in diverse areas of fundamental and applied research fields. The scope of this thesis doesn't allow to give a full overview of current applications of lipid vesicles. Instead, the discussion will be limited to the following classes: (i) applications in biophysics/materials science, (ii) applications in chemistry, (iii) applications in pharmacology and medicine, and (iv) applications in diagnostics, food industry and cosmetics.
Biophysicists use planar and spherical bilayer lipid structures as model biomembranes since many vital cell-cell interactions such as adhesion, endo- and exo-cytosis

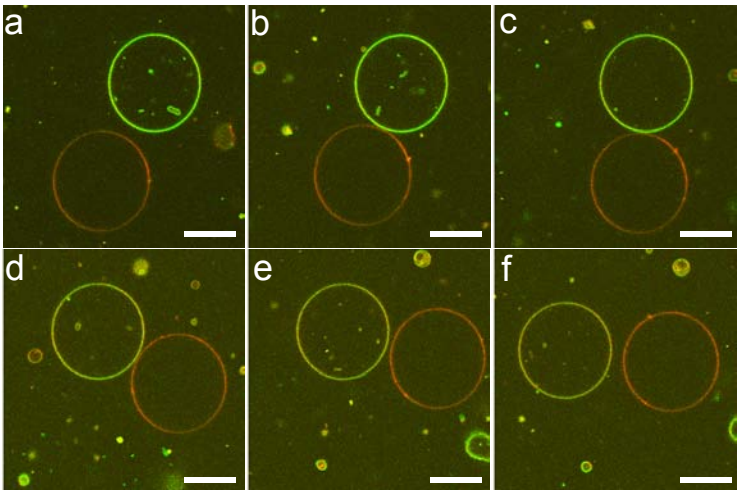

Figure 4.10: Confocal fluorescence images showing GUVs formed using electro-swelling. *A 30/70 mixture of DLPC and DPPC were electro-swelled at 65 ^{o}C using two different membrane dyes as in Fig. 4.9. In this case, the lipids were phase separated and formed individual vesicles bearing more DLPC (green) and more DPPC (red). Moving from (a) through (f): the red vesicle was moving and rolled over the green vesicle without getting fused to each other (scale bar= 10 μm).*

can be studied in-vitro using lipid vesicles. Studies on the aggregation and fusion of lipid vesicles is an important tool to understand certain biological events such as infections, inactivation of viruses and cell transfection events etc. The process of fusion has another important application, which will be discussed later, in understanding and control the drug/gene delivery process and kinetics.

Materials scientists, on the other hand, make use of lipid vesicles and planar lipid bilayers for creating engineered surfaces. The membrane of lipid vesicles with its highly tailorable in terms of charge density, binding specificity etc, and immunoliposomes with attached proteins or antibodies are important tools for making biocompatible surfaces. Such biocompatible surfaces are important in cell-cell and ligand-receptor interaction studies in-vitro.

The interest of lipid vesicles in chemistry is more for practical applications by utilizing mainly the confinement offered by these closed structures. The formation of inorganic nanoparticles inside lipid vesicles and lipid tubules have already been discussed in (1.4.2). The same principle of compartmentalized chemical reactions have been used widely in the filed of biomineralization, which also has been discussed already (1.4.2) and several studies have shown that lipid vesicles are important candidates in achieving such controlled mineralization. Also, encapsulated magnetic

nanoparticles inside lipid vesicles have been found useful in medical applications. The pharmacological as well as medical applications of lipid vesicles are known since many years and the main reason for researchers to choose lipid vesicles for this purpose is nothing but its nontoxicity and biocompatibility. Not all lipid compositions are equally tolerated by the human body, though. Considering for example, the use of lipid vesicles as drug delivery systems: The ability of vesicles to carry cargos in attoliter volumes [127] and release them on request are the two most important properties in this respect. The chemical& mechanical stability of vesicles are equally important for applications as drug carriers in the body. PEG modified vesicles were found to have a higher circulation time than non-modified vesicles. Many studies have been performed or are under development and might produce potential smart drug delivery systems. Another important medical interest of lipid vesicles is their possible use in anticancer therapy through its systematic or sustained release as well as site avoidance and tumor targeting.

Other applications of lipid vesicles are in diagnostics, food industry and in cosmetics. Lipid vesicles loaded with radioactive or magnetic particles are proven to be useful in medical imaging techniques such as radiography and magnetic resonance imaging (MRI). The use of lipid vesicles in food industry is based on their emulsifying properties. The encapsulation capability of vesicles also have serious impact in food industry. For example, in cheese making, encapsulated enzymes can improve the fermentation time by half at present, which have been improved in recent years. Finally, the cosmetic applications: the ability of lipid vesicles to dissolve simultaneously the hydrophobic and hydrophilic substances make it a useful candidate in this particular industry. Vesicles can help to dissolve water insoluble ingredients, can form a viscous matrix and thus introduce a long lasting and unwashable film, can enhance penetration, as well as can humidify the skin.

4.4 Fabrication of lipid/QD hybrid vesicles

Depicted in Fig. 4.11 are the steps involved in the fabrication of the lipid/QD hybrid vesicles (HVs). A solution of TOPO (trioctylphosphine oxide) coated CdSe QDs and lipids in chloroform is dried in a vial to form a multilamellar lipid film, from which by hydration under water vesicles were spontaneously formed. We have tried a wide range of phospholipid molecules (different headgroups, various alkyl chain lengths, etc.) as well as different established methods of formation (classical swelling, electroswelling) of liposomes [145], [146]. More precisely, the HVs were prepared using saturated lipids such as DLPC, DMPC, DPPC and DSPC as well

as unsaturated lipids such as DOPC and DOPG using classical and electro swelling. We found that the formation of the HVs is not limited to any particular class of lipid and/or method of formation. HVs with sizes ranging from 50 nm to few tens of micrometers can be produced in a controlled manner.

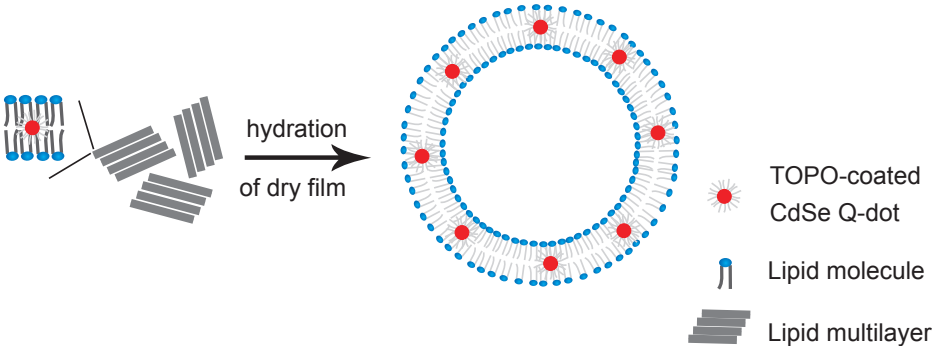

Figure 4.11: Steps involved in the formation of lipid/QD hybrid vesicles. *Chloroform solutions of lipid molecules and QDs are mixed, dried and then hydrated using water, which resulted in the formation of lipid/QD HVs. Depending on the method of vesicle formation adopted, small, large and giant vesicles with uni or multi lamallarity can be prepared.*

Experimental part:
Lipids used:

- ▷ 1,2-Dimyristoyl-sn-glycero-3-phosphatidylcholine (DMPC)
- ▷ 1,2-Dioleoyl-3-trimethylammonium-propane (chloride salt) (DOTAP)
- ▷ 1,2-Distearoyl-sn-glycero-3-phosphatidylethanolamine-N-[biotinyl (polyethyleneglycol)2000] (ammonium salt) (DSPE-PEG2000-biotin)
- ▷ 1,2-Dipalmitoyl-sn-glycero-3-phosphatidylethanolamine-N-[methoxy (polyethyleneglycol)2000] (ammonium salt) (DPPE-PEG2000)
  (All lipids used were from Avanti Polar Lipids)

Preparation of Hybrid Vesicles (HVs):
(1) Classical Swelling: Chloroform solutions of DMPC (1.5 mM, 100 μL), DSPE-PEG2000-biotin (0.6 mM, 5 μL) and CdSe/TOPO QDs (5 μM, 10 μL) were mixed and dried in vacuum for 4 h in a teflon chamber. The film was then hydrated overnight at 37 ^{o}C by incubating with 0.1 M sucrose.
(2) Electroswelling: Chloroform solutions of DMPC (1.5 mM, 100 μL), DSPE-PEG2000-biotin (0.6 mM, 5 μL) and CdSe/TOPO QDs (5 μM, 10 μL) were mixed

and dried in vacuum for 4 h on an ITO (Indium Tin Oxide) coated glass slide (Sigma). The film was then hydrated at 37 ^{o}C by incubating with 0.1 M sucrose and applying an alternating electric field of 1.2 V/10 Hz during the first 2 h for an effective swelling and then 2.0 V/4 Hz for the next hour for an easy detachment of the formed vesicles.

Cryo-electron microscopy (Cryo-TEM):

Samples for Cryo-TEM were prepared as described elsewhere [150] using 4 μL of classically swelled HVs, which then sonified in a bath sonifier for 10 seconds for making small (50-200 nm) HVs. The images were recorded at -172 ^{o}C using a CCD camera equipped in a Philips CM12 electron microscope operated at 80 kV. The cryo-TEM images performed using different concentrations of 3 nm CdSe QD solutions to a fixed concentration of DMPC (Fig. 4.12b&c) show that stable HVs are formed at all the concentrations. The bilayer membrane is clearly visible in (a) and (c). The cryo-TEM images doesn't clearly show the QDs in the HV membranes could be due to the extremely low concentration of QDs used as well as the resolution limit of this method. The fluorescence microscopic images of giant uni and multi lamellar HVs (Fig. 4.13) also provide evidence that HVs were formed, which carry fluorescent QDs in the bilayer membrane.

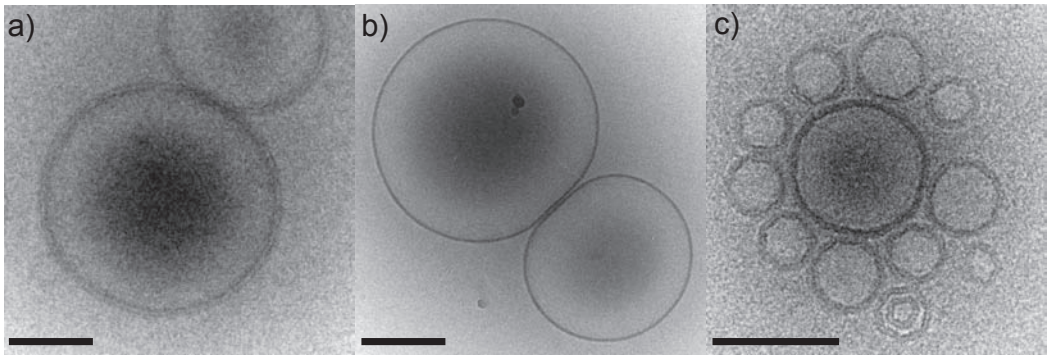

Figure 4.12: Cryo-TEM images of small. unilamellar lipid/QD hybrid vesicles. *(a) Pure DMPC vesicles, (b) HVs made of DMPC with 5 μM QD solution, and (c) HVs made of DMPC with 25 μM QD solution (scale bars=100 nm).*

4.4.1 Membrane imaging

For the ease of observation by confocal microscopy, we have first fabricated giant vesicles (1 - 50 μm) by classical swelling. Biotinylated HVs in 0.1 M sucrose were incubated on a glass coverslip, which was pre-treated with 0.1 mg/mL avidin, in 0.1

M glucose. The glucose solution was used to keep the osmotic pressure balanced while allowing quick settling of sucrose filled HVs. Fig. 4.13a-c shows representative confocal cross-sections of vesicles (formed via classical swelling) appearing as clear and sharp fluorescent circular perimeters. These images are comparable with those known to result from vesicles stained with fluorescent organic dyes [145], and shown for comparison as inset of figure 1c. This demonstrates that the hydrophobic QDs must be integrated in or attached to the lipid bilayer of the HV. A high yield of giant unilamellar vesicles was obtained along with some mutilamellar ones, as is usually the case with this approach. Electroswelling [146], in turn, produced more homogeneous unilamellar structures (Fig. 4.13d).

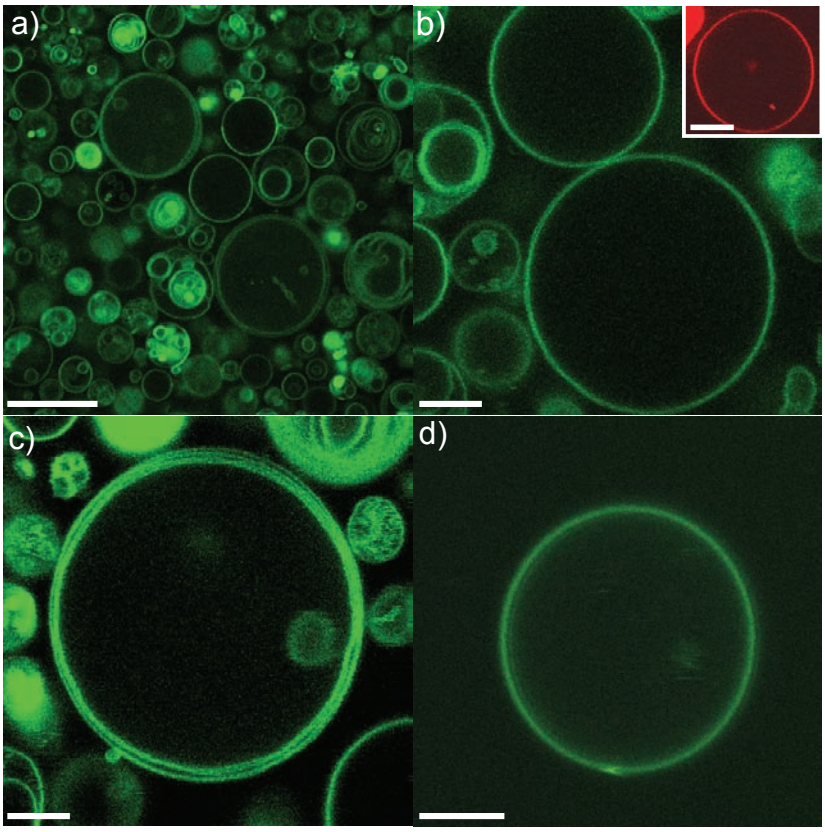

Figure 4.13: Confocal fluorescence cross-section image of HVs made of DMPC. *(a) Population of fluorescent HVs in a typical classically swelled sample (scale bar=20 μm), (b) close-up view of two adjacent unilamellar HVs. The inset shows an image of vesicles stained with rhodamine labeled lipids (scale bars=10 μm), and (c) a multilamellar HV (scale bar=10 μm). A representative HV formed via electroswelling (d) that resulted more homogeneous, unilamellar structures (scale bar=10 μm).*

Fig. 4.14 shows the absorption and the emission spectrum of the hydrophobic QDs

employed in the production of the hybrid vesicles. TOPO stabilized CdSe QDs were synthesized as published elsewhere [17] and isolated in toluene. For the HV preparation, the QDs in toluene was transferred into chloroform through solvent exchange. The spectral properties (position of maxima, narrow emission spectrum) indicate a uniform size of about 3 nm of the CdSe QD core [30]; including the hydrophobic coating, our TOPO/QDs have a size of about 5 nm.

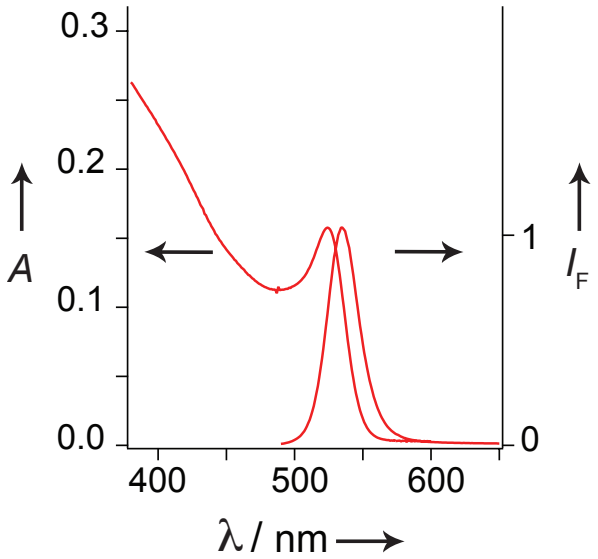

Figure 4.14: Typical absorption/emission spectra of the CdSe QDs used in the preparation of HVs. *The spectra were recorded in toluene solution. The X- axis shows the absorption/emission wavelengths scanned in nm and the Y- axes indicating the absorptivity (left) and fluorescence intensity (right) in arbitrary units. The narrow emission spectrum indicates uniform size (ca 3 nm) of the QDs.*

Current limitations due to photobleaching of organic membrane dyes in acquiring high-resolution images, thin z-sectioning for eventual 3D- reconstruction and longer-term in-situ observations could be solved by using our hybrid vesicles. Though core-shell QDs [151] offer higher photostability compared to core-only QDs, confocal imaging under maximum laser output conditions were performed uninterruptedly for hours using our TOPO coated QDs. The imaging of vesicles, planar lipid bilayers, as well as lipid monolayers at the air-water interface can thus be performed for hours, which is of interest for studying phase diagrams and phase separation phenomena in lipid mixtures [149], [148] [152], [153], [154].

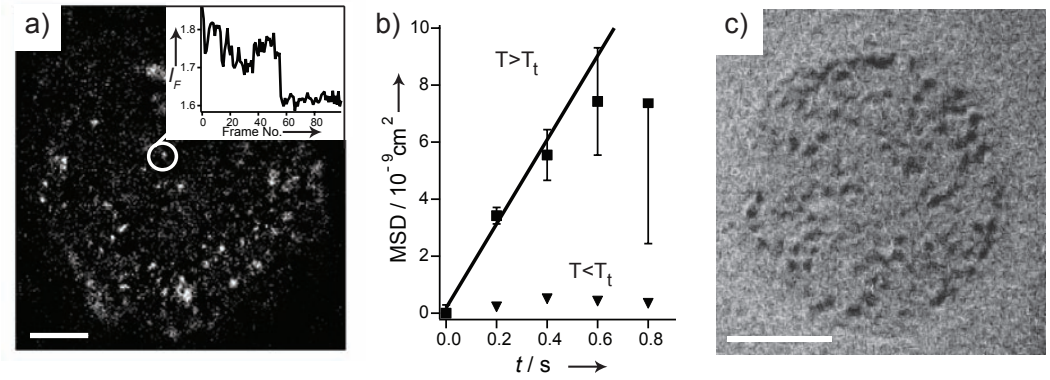

Figure 4.15: Imaging single QDs in the bilayer of an immobilized giant vesicle. *(a) The fluorescence micrograph shows a representative image of single QDs in the planar bilayer region attached to the glass surface at 5 ^{o} C (scale bar= 10 μm). The inset shows a photo-bleaching profile of a single QD. (b) Calculated MSD values (mean of 3 experiments) of the trajectory of single QDs diffusing in a lipid bilayer are plotted as a function of time at 30 ^{o}C for a fluid lipid bilayer (top) and at 5 ^{o}C for an ordered lipid bilayer (bottom). From the MSD values, it is obvious that QDs are immobile in the ordered lipid bilayer. The diffusion coefficient of QDs in the fluid lipid bilayer is calculated from the corresponding slope. (c) Cryo-TEM image of a collapsed HV at twice higher QD concentration than used for confocal microscopic images shown in figure Fig. 4.12c. The ca 3 nm sized QDs (dark spots) are randomly distributed in the vesicle's lipid bilayer (scale bar= 25 nm).*

4.4.2 Diffusion of QDs in the supported hybrid bilayer membrane

Calorimetric measurements revealed the ordered-fluid phase transition temperature (T_t) of the HVs at 23.5 ^{o}C, which is nearly identical as for pure DMPC bilayers [71]. This is actually not surprising considering that the lipid/QD molar ratio of our vesicles is 3000. Furthermore, we studied the lateral diffusion of QDs in the lipid bilayer above and below T_t of giant vesicles of DMPC immobilized on a glass plate. The HVs for the single molecule imaging were prepared as described above using 0.05 μM QD solution (see the experimental part of section 4.4). The immobilization on a glass coverslip was performed as described above (4.4.1).

Fig. 4.15 depicts fluorescence microscopic images of single QDs obtained from the planar membrane region of an immobilized vesicle that is in contact with the glass support. We have observed substantially different diffusion of single QDs within the membrane below and above the T_t of the lipid bilayer. Fig. 4.15a shows single QDs observed at 5 ^{o}C ($<T_t$) with the inset of a single-step photobleaching profile of an

individual QD, proving the spots as single QDs. The single molecule experiments were performed on a modified epiluminescence wide-field microscope (Axiovert 100 TV, Zeiss). Circularly polarized light of 488 nm of an Ar^+ laser (Innova Sabre, Coherent) was directed by a dichroic mirror (Q495LP, Chroma) into a microscope objective (C-Apochromat 63x, 1.2 NA, W Korr, Zeiss) to illuminate a 35 μm diameter region of the sample. The sample temperature was controlled using a thermostat attached to the sample stage.

Trajectories of individual QDs were constructed using a custom developed single-particle tracking algorithm [155]. Mean-square displacements (MSDs) were obtained from the cumulative distributions of square displacements of 80 particles at different delay times assuming a two-component model above the lipid phase transition temperature, and a one-component model below. From the mean square displacements (MSD) of the diffusing single QDs in the bilayer membrane we calculated the lateral diffusion coefficient D as shown in Fig. 4.15b. In the fluid lipid bilayer at 30 ^{o}C, the lateral diffusion of the QDs ($D = 0.3 \cdot 10^{-8}$ cm^2/s) is about 10 times slower than that of a lipid molecule ($D = 4 \cdot 10^{-8}$ cm^2/s) [148]; this reduced diffusion could be due to the larger size of the QDs compared to lipid molecules. The actual diffusion coefficient might be slightly larger because of a systematic underestimation of fast particles by the single particle-tracking algorithm [155]. In the fluid membrane phase, 75% of the tracked particles follow the diffusion profile whereas 25% are less mobile. The tracked single QDs in the ordered bilayer state ($T<T_t$) are nearly immobile as revealed by the negligibly small MSD values. It is important to mention here that the switching of the diffusion properties of the QDs occurs exactly at 23.5 ^{o}C, which is identical to the phase transition temperature observed in the calorimetric measurements. These observations show that the QDs are tightly associated to the lipid membrane because otherwise there would be little or no effect with respect to the membrane state.

It has been suggested that hydrophobic QDs could be incorporated into lipid bilayers and thereby achieve efficient phase transfer from organic to aqueous medium [133] and study membrane association by FRET in-vitro [134]. In spite of these experimental approaches, predicting the exact location of the QDs relative to a lipid bilayer remains a difficult task, where artefacts and over interpretations have to be carefully avoided. For all applications discussed in this chapter, it is sufficient to know that the QDs are stably associated with the bilayer, irrespective of whether they are fully or only partially inserted in the lipid bilayer.

4.4.3 Controlled targeting live cells

The interactions of the fluorescent HVs with living cells have been tested for two different lipid compositions.

Experimental part:

Cell Culture: Adherent human embryonic kidney cells (HEK293) were cultured in Dulbecco's Modified Eagle Medium (D-MEM) (Gibco, Invitrogen, USA) supplemented with 2.2% fetal calf serum (Gibco, Invitrogen, USA), in a humidified 5% CO_2 atmosphere at 37 ^{o}C. Cells were split in regular intervals. For confocal microscopy, HEK293 cells were seeded into 6-well plates TPP (Trasadingen, Switzerland) containing 25 mm diameter glass coverslips (Assistent, Germany), in 2 ml culture medium containing 2.2 % fetal calf serum. The cells were grown for 24 h at 37 ^{o}C, were then washed with phosphate buffered saline (PBS) and used for further experiments.

Cells/Construct I HVs: Chloroform solutions of DMPC (1.5 mM, 75 μL), DOTAP (1.5 mM, 25 μL) and CdSe/TOPO QDs (5 μM, 10 μL) were mixed and dried in vacuum for 4 h and the film was then hydrated at 40 ^{o}C in PBS under vigorous mixing. The solution was then sonified in a bath sonifier for 10 seconds. 10 μL of this solution of small (20 - 100 nm) HVs were added to the cells suspended in 500 μL PBS.

Cells/Construct II HVs: Chloroform solutions of DMPC (1.5 mM, 75 μL), DOTAP (1.5 mM, 25 μL), DPPE-PEG2000-PE (0.6 mM, 5 μL) and CdSe/TOPO QDs (5 μM, 10 μL) were mixed and dried in vacuum for 4 h and the film was then hydrated at 40 ^{o}C in PBS under vigorous mixing and the solution was then sonified in a bath sonifier for 10 s. 10 μL of this solution of small (20 - 100 nm) HVs were added to the cells suspended in 500 μL PBS.

The cryo-TEM image (Fig. 4.16) shows that the construct II form stable, closed nanocontainer HVs. At higher concentrations, PEG lipids predominantly form micelles. In our case, it is explicitly clear that the constructs used for different targeting to live cells form closed, spherical vesicles. TEM images of construct I vesicles (not shown) are very similar in shape.

Construct I HVs are designed for transfer into the cell (Fig. 4.17b). The bilayer of small (20-100 nm; characterized by electron microscopy, similar as in Fig. 4.16, HVs consists 25% of a positively charged lipid (DOTAP), which is known to enhance the cellular internalization [156], [157], and 75% DMPC. Lipid/QD hybrid structures were found inside the cytosol within seconds after incubation with cells (Fig. 4.17a).

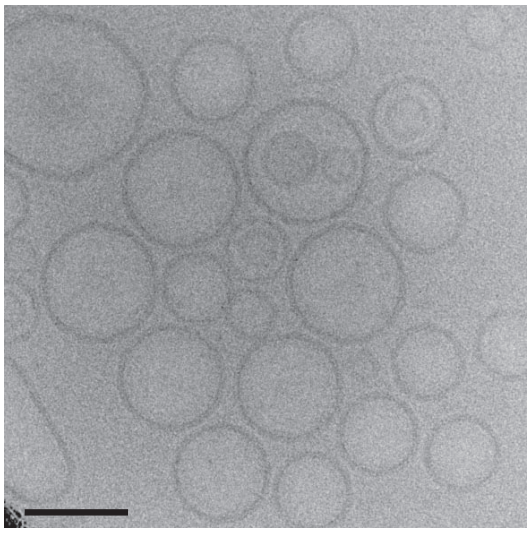

Figure 4.16: Cryo-TEM image indicating formation of Construct II HVs. *This image shows that the construct II HVs that has been used to fuse with live cells are nanocontainers that can potentially carry any water soluble molecules in it (scale bar = 100 nm).*

This efficient uptake might allow further targeting of lipid/QDs to specific locations inside live cells through prior decoration of the hybrid vesicle surface with specific receptors [158], [159]. Despite the universal use of cationic lipids in DNA transfection experiments [156], the exact mechanism of this event is still not clear [160], [161].

Construct II HVs have been designed to fuse with the plasma membrane of a live cell (Fig. 4.18b). This process is usually very difficult to achieve at room temperature [162], [163], [131]. As in the preceeding experiment, small (20-100 nm, Fig. 4.16) HVs are used which now comprise 25% of a positively charged lipid (DOTAP), 0.5% DPPE-PEG-2000 and 74.5% DMPC. Fig. 4.18a shows a confocal image of live cells that have been incubated with construct II vesicles. Interestingly in this case the cell membrane is selectively labeled and no fluorescence has been observed in the cytosol even after 1 hr of incubation. The mechanism is difficult to understand but we speculate that the membrane incorporated PEG-molecules act as a transient-barrier [164], [165] between the cationic liposomal and anionic cellular membranes, thus preventing them from getting internalized. At this distance (nm range), the collective process of electrostatic attraction (due to positively charged lipids) and membrane vulnerability (due to PE lipids and QDs) triggers the fusion between the membranes.

The appearance of QD fluorescence in the cellular membrane (Fig. 4.18a) could be either due to stable adhesion of intact vesicles on the surface of the plasma membrane

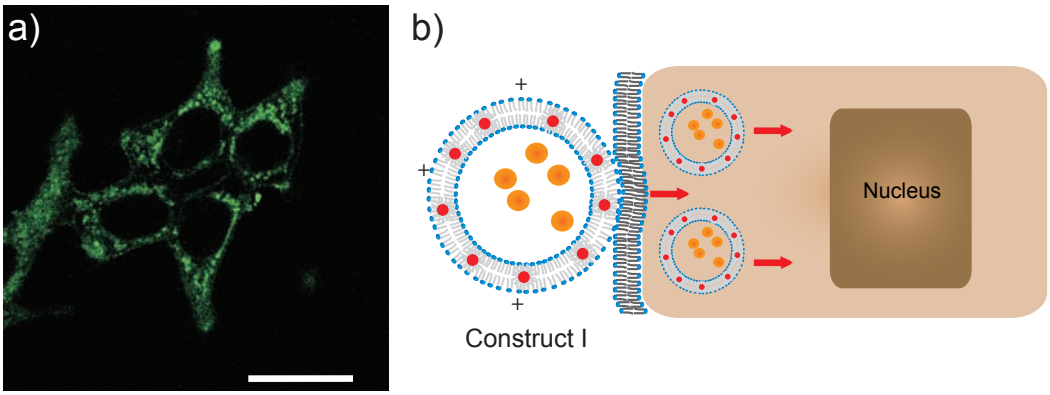

Figure 4.17: Interaction of construct I HVs with HEK293 cells. *Confocal micrographs of HEK293 cells 30 s after addition of vesicles: (a) construct I vesicles are totally internalized into the cells, and (b) shows a schematic representation of the possible event (scale bar = 10μm).*

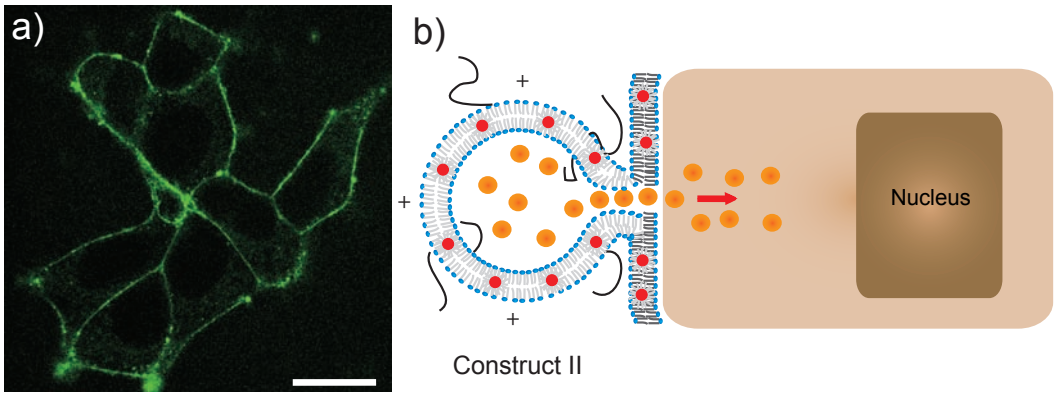

Figure 4.18: Interaction of construct II HVs with HEK293 cells. *Confocal micrographs of HEK293 cells 30 s after addition of vesicles: (a) construct II vesicles selectively labeled the cell membrane without internalization into cytoplasm, and (b) shows a schematic representation of the possible event (scale bar = 10μm).*

or due to fusion between the bilayer of HVs and the plasma membrane resulting in integration of the QDs into the cell membrane. For better understanding of the exact event, the HVs were used as nanocontainers filled with aqueous $CaCl_2$ and incubated with cells, which were loaded with Fluo-3 (a fluorescence indicator to measure Ca^{2+} ion concentration in the cytoplasm).

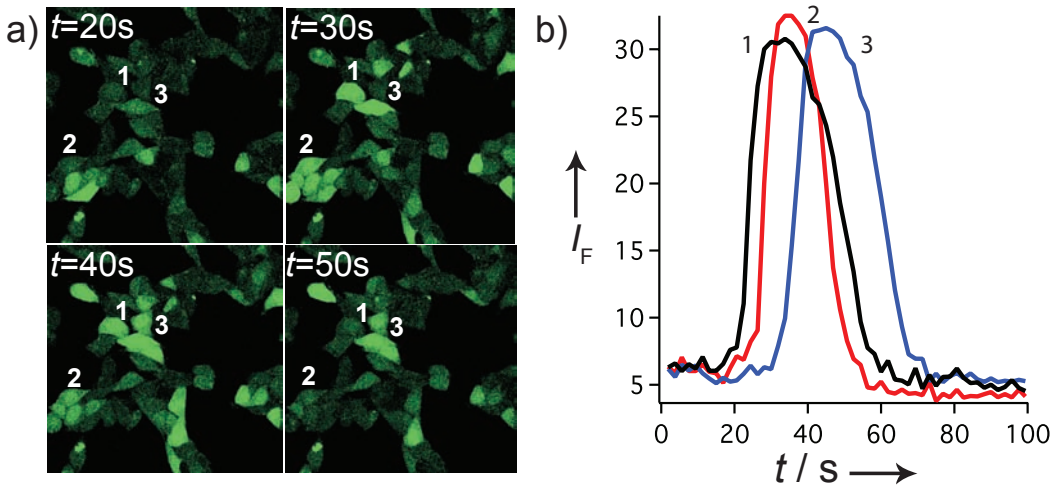

Figure 4.19: Ca imaging using $CaCl_2$ encapsulated construct II HVs on HEK293 cells. *Series of confocal images (a) (recorded at 300 milliseconds scan rate showing the fluorescence intensity response of Fluo-3 inside HEK293 cells at different times after fusion with construct II vesicles loaded with 1 mM $CaCl_2$. (b) The transient Fluo-3 fluorescence signals of a few representative cells are depicted (numbers correspond to numbered cells in (a)).*

In a typical experiment for intracellular Ca^{2+} signaling tests, HEK293 cells were grown on sterile microscope coverslips as described above. 24 h after seeding at 37 ^oC in D-MEM medium containing 2.2 % fetal calf serum, cells were loaded with Fluo-3 dye (Molecular Probes, Invitrogen, USA) by incubating in serum-free D-MEM medium containing Fluo-3 for 30 min at 37 ^oC. Thereafter Fluo-3 containing medium was replaced by D-MEM medium supplemented with 10% fetal calf serum and incubated for 30 min at 37 ^oC. Subsequently, dye-loaded cells were washed with PBS and subjected to Ca^{2+} imaging. Construct II vesicles were prepared as explained above in 1 mM $CaCl_2$/PBS. 10 μL of a solution of such small (20 - 100 nm) vesicles loaded with $CaCl_2$ were applied to the cells suspended in 500 μL PBS. After a certain time lag the cells responded by a transient intracellular Ca^{2+} ion concentration increase (Fig. 4.19) followed by selective labeling of the plasma membrane (similar as in Fig. 4.18a for an experiment without intracellular Fluo-3). The intracellular Ca^{2+} concentration increase is transient because the Ca^{2+} vesicle cargo

released into the living cells becomes accommodated in the endoplasmic reticulum by the cellular machinery. The following control experiments were performed to prove the fusion capability of the hybrid nanocontainers: (1) When adding 1 mM $CaCl_2$/PBS without vesicles to the external medium of cells loaded with Fluo-3, the cells did not give an intracellular Ca^{2+} response. (2) Addition of HVs without $CaCl_2$ cargo to Fluo-3 loaded cells did also not induce an intracellular Ca^{2+} response. This shows that the Ca^{2+} ions were not generated inside the cells through any kind of activation of intracellular Ca^{2+} ion stores upon the vesicle interactions with the cellular membrane surface, but was delivered into the cell from the nanocontainers via fusion.

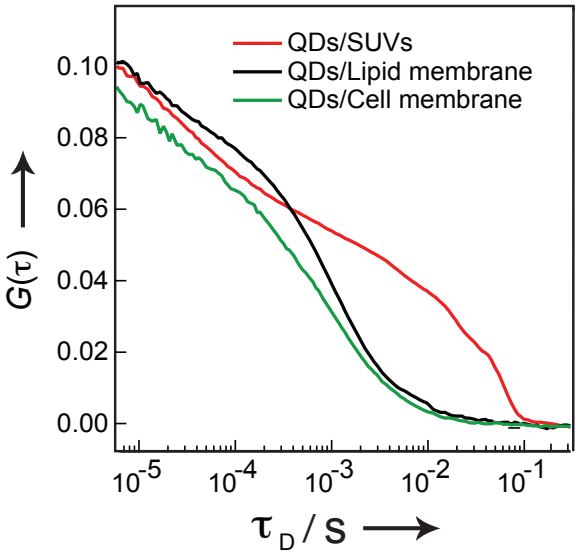

Figure 4.20: FCS experiments on HV membrane and HV fused cell membrane. *FCS autocorrelation curves showing diffusion times of QDs in different environments. Diffusion times of QDs in the cell plasma membrane observed after the fusion of HVs with the cell (green) is nearly identical with that in the lipid bilayer of an immobilized giant HV (black). The red curve shows the diffusion of small (20-100 nm) HVs (construct II) in solution.*

Fluorescence correlation spectroscopy (FCS) measurements have been performed on the plasma membrane of live cells after incubating them with construct II vesicles in order to exclude any possibility that nanocontainers are simply adsorbed on the cell membrane e.g. via electrostatic interaction. The samples were excited at 488 nm with an argon ion laser (3 kW/cm^2), and its fluorescence was detected through a pinhole (70 μm diameter) and a 505 nm long-pass filter. The excitation intensity was adjusted to maximize the detected counts per particle. For each series of FCS measurements, a standard calibration was performed using Rhodamine 6G in PBS

solution at pH 7.4 [166]. Fig. 4.20 shows the measured auto-correlation functions (ACFs). The ACFs of QDs in the plasma membrane (green) and in the lipid bilayer of immobilized micrometer-sized vesicles (black) are very similar, whereas the ACF of a solution of small unilamellar vesicles show much slower diffusion (red). This demonstrates that the QDs reside within the plasma membrane of the cell and gives additional proof that the observed cell membrane labeling and subsequent Ca^{2+} influx is due to fusion between vesicle bilayer and cell membrane. Using this approach, one can potentially carry any water-soluble material that can be enclosed inside the nanocontainers and deliver them into the live cells.

4.4.4 Discussion

Using QDs in biological cells always pose concerns about potential cytotoxicity. It has been found that unmodified TOPO coated QDs are toxic to live cells [167] probably by releasing Cd^{2+} ions into the cell due to poor surface coverage. Proper surface coating of QDs seems to avoid direct contact of the QD core to cells [167]. However, in our experiments the QD/vesicles did not show any cytotoxic effects even after 3 hours of incubation with live cells. This indicates, but of course does not prove, that our QDs are well embedded in the membrane rather than at the membrane-water interfacial region. The in-vivo experiments reported elsewhere using lipid-coated QDs [136] also did not show any cytotoxic effects in embryonic cells, suggesting lipid coating is an effective way to make QDs biocompatible.

Our results imply that cell and lipid membranes, and certainly also the walls of polymeric vesicles [168], [169] can integrate any kind of hydrophobic nanoparticles whose size matches the membrane thickness. The incorporation of, for instance, nanometer-sized magnetic [170], [171], [172], or metallic particles [173], [174] into the membranes will transform the properties of the cells or vesicles accordingly and open novel possibilities to manipulate them as individuals or in ensemble with widerranging applications for nanoscale reactors [118], [127], [70], [108], cellular targeting [175], targeted drug delivery, [176], [177] contrast agents [178], [179], [180] etc. The collective magnetic properties offered by the supramolecular membrane systems will add complementary advantages compared to individual biopolymer-modified, large magnetic nanoparticles [47]. Another interesting field of investigation in the present context are Au nanoparticles; they are known for their thermal response to radio and photo irradiations, which presently receives great attraction in photo/radiotherapy as magnetic particles in hyperthermia aided diagnostics and treatment [174].

The facile, controlled targeting achieved with the HVs is extremely interesting as

the diverse lipid chemistry could lead to novel in-vivo and in-vitro applications. For instance, prior incorporation of specific ligands in the membrane of construct I HVs (Fig. 4.17) and subsequent targeting to living cells could help in transporting them into the respective cellular locations, which upon selection of appropriate nanocrystal, can be used to control, to kill or to cure specific locations inside the cells. The construct II HVs (Fig. 4.18) on the other hand, could be interesting to label cellular membranes specifically with other kinds of nanocrystals viz, metallic or magnetic, depending on the application. The fusion properties of construct II HVs can be extremely useful to transport many non-membrane crossing molecules or drugs into the cells.

4.4.5 Perspectives

Looking at the results presented in this chapter, one could think of a potential multi-stimulus-responsive drug delivery system. For instance, the design and construction of a 3-in-1 optical/magnetic/thermal responsive hybrid nanocontainers (Fig. 4.21) can be done through simple mixing of respective nanocrystals at the initial preparation step. Thus many permutations are possible with this smart organic/inorganic hybrid nanocontainers. Furthermore, extension of spherical constructs into tubular hybrid nanocontainers using tubule forming lipid molecules, a potential multi-stimulus-responsive cargo system with zero-order kinetics [181], [182] could be fabricated, which may find interesting applications in sustainable drug-delivery.
In short, we have described the fabrication of highly controllable organic/inorganic hybrid vesicles where nanometer-sized particles are confined to 4 nm thick membranes. The tunable size, switchable physical properties, response to multiple external stimuli and above all the controlled cell fusion capacity make them very promising tools in nanobiotechnology.

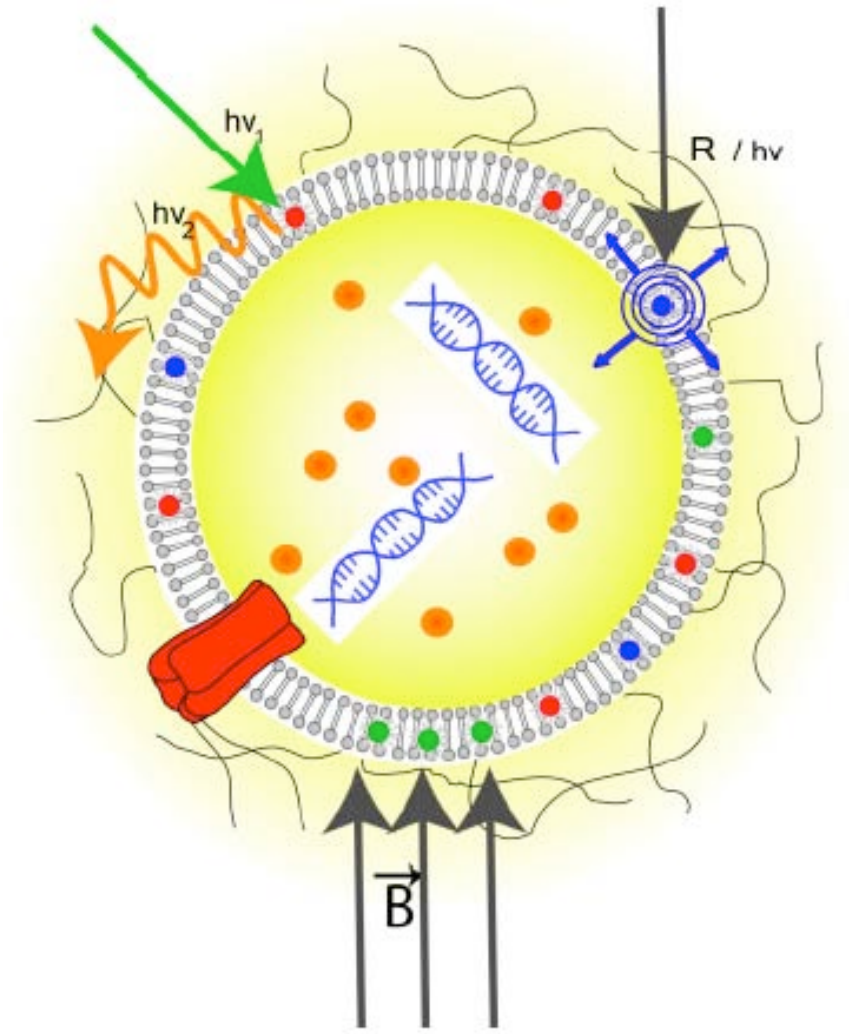

Figure 4.21: Potential 3-in-1 multi-stimulus responsive cargo system. *Envisioning a potential multi-stimulus responsive system for controlled live cell targeting applications. The hydrophobic nanocrystals dissolved in the membrane are: fluorescent QDs (red), metallic nanocrystals (blue) and magnetic nanocrystals (green) (Angew.Chem. Int. Ed., 2006 (in press)).*

Chapter 5

"Lipid Chemistry"- Based Organization of Quantum Dots

5.1 Introduction

Self-assembly of nanocrystalline materials has great potential in future nanodevice construction as the interaction between such assembled components can result remarkable properties [183] due to tailorable interparticle separation. As a consequence, new tools for the synthesis, modification, assembly and characterization has been established by several research groups in the last decade. Non-covalent interactions such as DNA-based reversible organization of Au nanocrystals into macroscopic aggregates [184], [185], polymer- mediated assembly of nanoparticles [186], virus based organization of quantum dots [122], ligand-receptor mediated organization [77], light driven assembly of nanoparticles [187] etc show the diverse approaches that have been used so far to make such functional assemblies. Nanocrystal superlattices [31], [188] based on covalent interactions [189], [190] have also been ascertained by different researchers using the well-established self-assembly technique to form layer-by-layer engineered surfaces [191]. The primitive building blocks in all these approaches are monolayer protected nanocrystals, which can be produced from a wide variety of materials depending upon specific applications. It has already been shown in the previous chapter (Chapter 4) that hydrophobic QDs can be arranged in the bilayer membrane of phospholipids and the resulting hybrid nanocontainers have been found useful for biological applications in-vivo and in-vitro [192]. This chapter, on the other hand, describes an easy and versatile method for the surface modification of TOPO coated CdSe QDs [20], [135] using nonbilayer forming lipid molecules [72], which upon applying conventional lipid chemistry, has been reversibly organized into microscopic fluorescent structures.

5.2 Self- assembly of nanocrystals

The assembly of nanocrystals into mesoscale architectures [184], [186] has widespread interests as molecules enable greater ability of control than atoms when used as building blocks for new materials [183]. Two research groups in parallel have published their findings regarding DNA assembly of nanocrystals in the same issue of Nature/382, 1996 [184], [185]. The DNA-based rational assembly of Au NPs showed first time evidence that NPs could be organized reversibly [184] into macroscopic aggregates. The reversible assembly in this case has been achieved through heating above the dissociation temperature of the DNA duplex that hold the NPs together. Also, assembly of semiconducting QDs using selected peptide [123] and engineered virus molecules [122] have been found useful in achieving controlled assembly of nanocrystals in extended length scales. As shown by Boal et al. [186], the shape and size controlled organization of nanoparticles (Fig. 5.1) by making use of binding complementarity of certain polymers is remarkable due to the fact that unlike what have been published before, they could achieve defined shapes to the resulting NP aggregates as can be seen in Fig. 5.1b. Recently, thermodynamically driven self-assembly of CdSe/ZnS QDs into fluorescent dendrites has been published [193], which may find interesting applications in artificial light-harvesting and light-emitting systems.

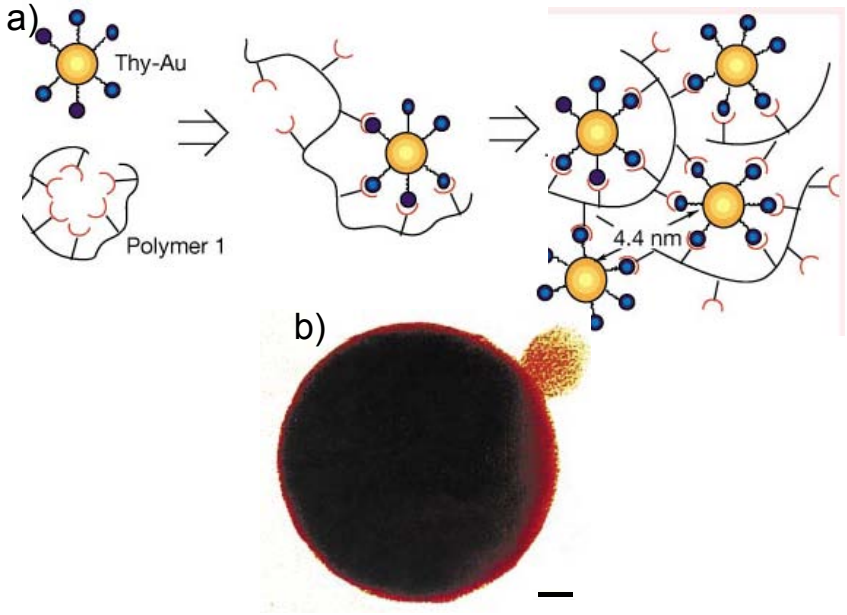

Figure 5.1: Schematic of the polymer-mediated organization of NPs. *Polymer binding technique has been used for the self-assembly of nanoparticles as shown in the scheme (a) and a representative TEM image showing a spherical, assembled Au NPs (scale bar= 50 nm).*

5.3 Nanocrystal superlattices

The self-organization of CdSe QDs into three-dimensional semiconductor QD superlattices has been demonstrated by Murray et al.. in 1995 [31]. The size and spacing of the QDs within the superlattice are controlled with near atomic precision. Later in 1998, J. R. Heath and colleagues showed that Ag NPs ca. 2-5 nm can be successfully organized into 3D superlattices with an impressive interparticle separation of around 5 Å [188]. This has been achieved through compression of a monolayer of hydrophobic Ag NPs, stabilized using thioalkanes of different chain lengths, from an average separation between the surfaces of the metal cores 12 Å (Fig. 5.2b). The linear and nonlinear optical properties evidenced the interparticle coupling phenomena. Another layer-by-layer assembly approach from C. N. R. Rao and his co-workers [189] showed the flexibility of such constructs though his demonstrated fabrication of hetero superlattice structures of metal-metal and metal-semiconductor by using dithiols as cross-linkers (Fig. 5.2a).

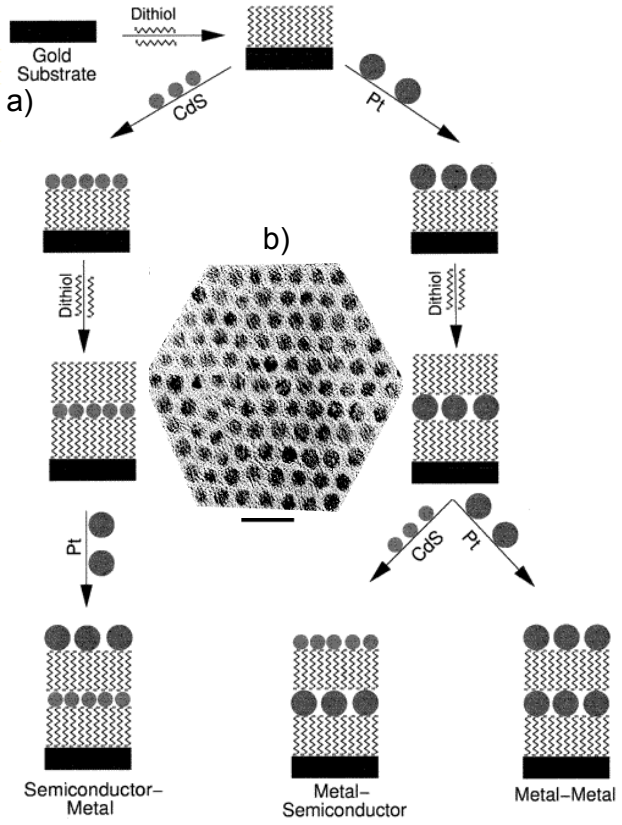

Figure 5.2: Nanoparticle superlattices. *a) Illustration showing a layer-by-layer approach to form superlattice structures from different NPs ([189]). b) TEM image of LB film of decanethiol-capped Ag NPs separated by 12 Å (scale bar= 10 nm) [188].*

5.4 Properties and applications

The fabrication of self-ordered superlattices of controlled size and shape is expected to have important applications in constructing nanodevices. Application of 1D and 2D superlattices of small metal NPs in nanoelectronic devices (single electron transistor, nanowiring), application of 2D superlattices of ferromagnetic FePt and CoPt NPs in nanomagnetic devices (ultra-high density magnetic recording media) and application of 3D superlattices of Ag and Cu nanoparticles in nanooptical devices (optical switch) are some of the applications that have been ascertained. The physical properties of NP assemblies are predominated by particle size, interparticle spacing, and the symmetry of ordering, of which the first two parameters can be easily controlled. The combination of the chemistry of novel, controllable organic bridging molecules with the nanocrystal colloidal chemistry will result new functional meso-assemblies that will contribute to the generation of future nanodevices with low-cost and low-energy consumption.

5.5 "Lipid chemistry"- based organization of QDs

The chemistry of lipids has been studied well in the last few decades due to its importance in fundamental and applied scientific research [71], [72], [73]. It has already been discussed in this thesis (see section 1.5) the unique thermotropic and lyotropic properties of phospholipids as well as the shapes of resulting structures when dispersed in aqueous solution (Fig. 1.9). So far, we have utilized the bilayer forming phospholipids for the fabrication of novel functional nano/mico structures as presented in chapters 3 & 4. It has been already shown [135] that lipid molecules could be used for coating hydrophobic QDs and thereby making them water soluble as well as multifunctional for use in-vitro. Lipid molecules are known for their ability to form molecularly ordered phases depending on the packing geometry, concentration and pH conditions [73]. Here, we have exploited the ordering property of phospholipids by selectively choosing specific lipid molecules that form nonbilayer lipid phases [72] that could produce novel QD based functional assemblies in a controlled way via careful tuning of the above mentioned properties. Fig. 5.3 shows the scheme of the experimental approach we have used to make the QDs charged and render them water soluble. The lipid used in this study to form lipid coated QDs (QD/lipids) (see Fig. 5.3) is 1,2-dipalmitoyl-sn-glycero-3-phosphatidic acid (DPPA). DPPA predominantly forms hexagonal phases (see Fig. 1.10 of 1.5.2) [72], [194] upon addition of Ca^{2+} or at a pH below 6 in water. We have made use of this particular

property of DPPA in the present study to form mesoscale self-assemblies of QD based structures both in solution and in confined systems.

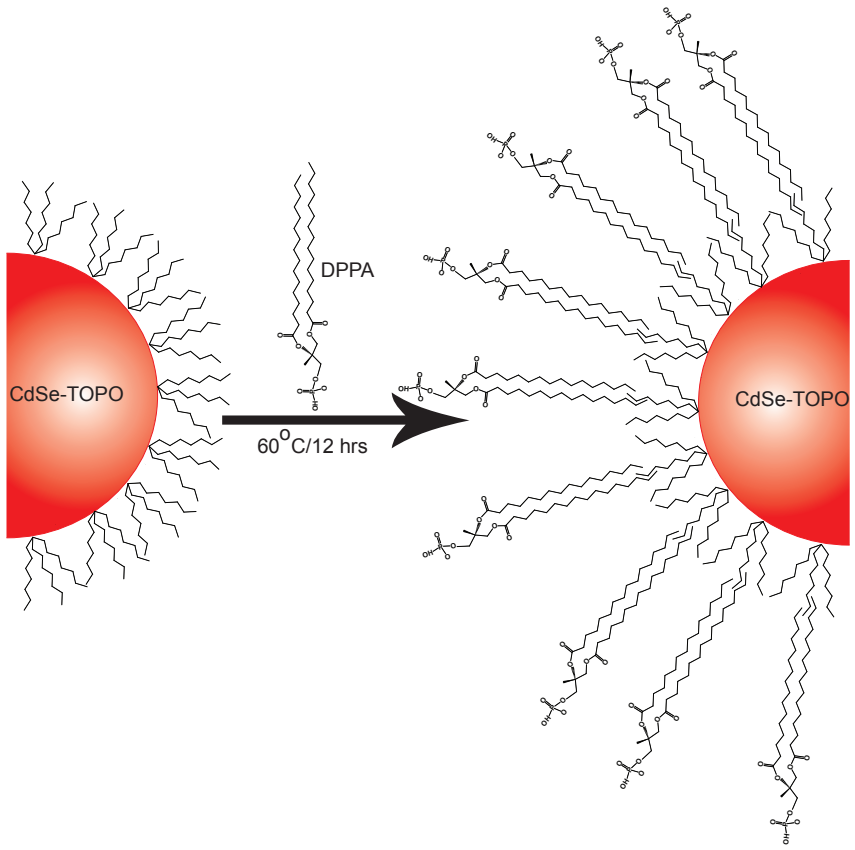

Figure 5.3: Scheme of the surface modification of QDs. *Chloroform solutions of TOPO-coated CdSe QDs and DPPA were mixed, dried and hydrated at 60 ^0C for 12 hours resulting formation of water soluble QDs coated with a monolayer of DPPA.*

Experimental Part:

Lipids used:

- ▷ 1,2-Dimyristoyl-sn-glycero-3-phosphatidylcholine (DMPC)
- ▷ 1,2-Dipalmitoyl-sn-glycero-3-phosphatidic acid (DPPA),
- ▷ 1,2-Distearoyl-sn-glycero-3-phosphatidylethanolamine-N-[biotinyl (polyethyleneglycol)2000] (ammonium salt) (DSPE-PEG2000-biotin)
  (DMPC and DPPA were from Fluka whereas DSPE-PEG2000-biotin was from Avanti Polar Lipids)

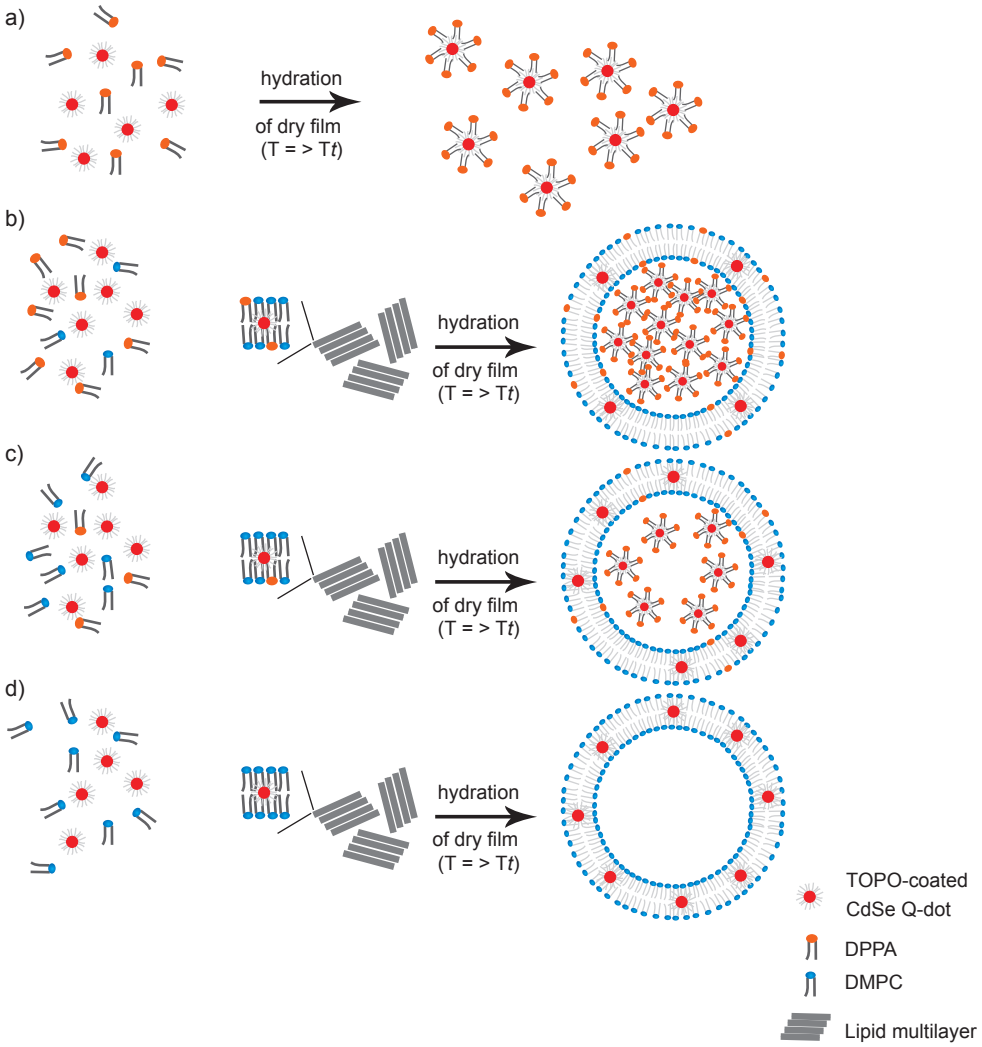

Figure 5.4: Steps involved in the formation of QD/lipids in solution and in vesicles. *(a) 100 % DPPA: Chloroform solutions of TOPO-coated CdSe QDs and DPPA were mixed, dried and hydrated at 60 ^0C for 12 hours resulting formation of water soluble QDs coated with a monolayer of DPPA, (b) 70 % DPPA and 30% DMPC: Chloroform solutions of TOPO-coated CdSe QDs, DMPC and DPPA were mixed, dried and hydrated (through electroswelling) at 60 ^0C resulting formation of QD/lipids encapsulated vesicles, (c) 30 % DPPA and 70% DMPC: Chloroform solutions of TOPO-coated CdSe QDs, DMPC and DPPA were mixed, dried and hydrated (through electroswelling) at 60 ^0C resulting formation of QD/lipids encapsulated vesicles with more QDs arranged in the DMPC bilayer, and (d) Chloroform solutions of DMPC and TOPO-coated CdSe QDs are mixed, dried and then hydrated (through electroswelling) using water, which resulted in the formation of lipid/QD HVs.*

Preparation of QD/lipids:

Chloroform solutions of DPPA (1.5 mM, 100 μL) and CdSe/TOPO QDs (5 μM, 10 μL) were mixed and dried in vacuum for 4 h in a round-bottom flask. The film was then hydrated overnight at 60 ^{o}C by incubating with 1mL, 0.1 M sucrose or nanopure water (Fig. 5.4a). The fluorescent solution obtained were characterized using confocal, FCS as well as fluorescent spectroscopic techniques.

Directed self-sssembly of QD/lipids in solution:

500 μL solution of QD/lipids were incubated with 100 μL solution of 10 mM $CaCl_2$. The pH of the solution was dropped from 7.0 to 3.0 upon addition of $CaCl_2$. The QD/lipids were self-assembled to form asymmetric, microscopic aggregates as observed using confocal microscopy SAXS as well as electron microscopy. The asymmetric assembly of QD/lipids were also observed when the pH was reduced to 3.0 using 20 μL 1M HCl.

In-situ encapsulation of QD/lipids inside spherical vesicles and their confined self-assembly:

Chloroform solutions of DMPC (1.5 mM, 30 μL), DPPA (1.5 mM, 70 μL), DSPE-PEG2000-biotin (0.6 mM, 5 μL) and CdSe/TOPO QDs (5 μM, 10 μL) were mixed and dried in vacuum for 4 h on an ITO (Indium Tin Oxide) coated glass slide (Sigma). The DSPE-PEG2000-biotin was used for immobilization of vesicles for imaging on the confocal microscope. The film was then hydrated at 60 ^{o}C by incubating with 0.1 M sucrose and applying an alternating electric field of 1.2 V/10 Hz during the first 2 h for an effective swelling and then 2.0 V/4 Hz for the next hour for an easy detachment of the formed vesicles (Fig. 5.4 b& c). The fluorescently filled vesicles thus obtained were characterized using FCS, confocal microscopy and electron microscopy. Addition of 100 μL solution of 10 mM $CaCl_2$ lead to the self-assembly of QD/lipids into microscopic aggregates inside the vesicles. They have been characterized using confocal microscopy and electron microscopy.

5.5.1 Characterization

Confocal Fluorescence Microscopy:

The confocal microscopic observations were performed on a Confocor-3 microscope (LSM 510, Zeiss; excitation = 488 nm, emission = 505 - 550 nm). (Fig. 5.5a-c show representative confocal images obtained from typical preparation of QD/lipids. As depicted in Fig. 5.5a, the QD/lipids formed a highly fluorescent solution without any detectable microscopic structures. This clearly shows that DPPA alone do not form giant vesicles in the presence of hydrophobic QDs (see also Fig. 5.4a). The fact

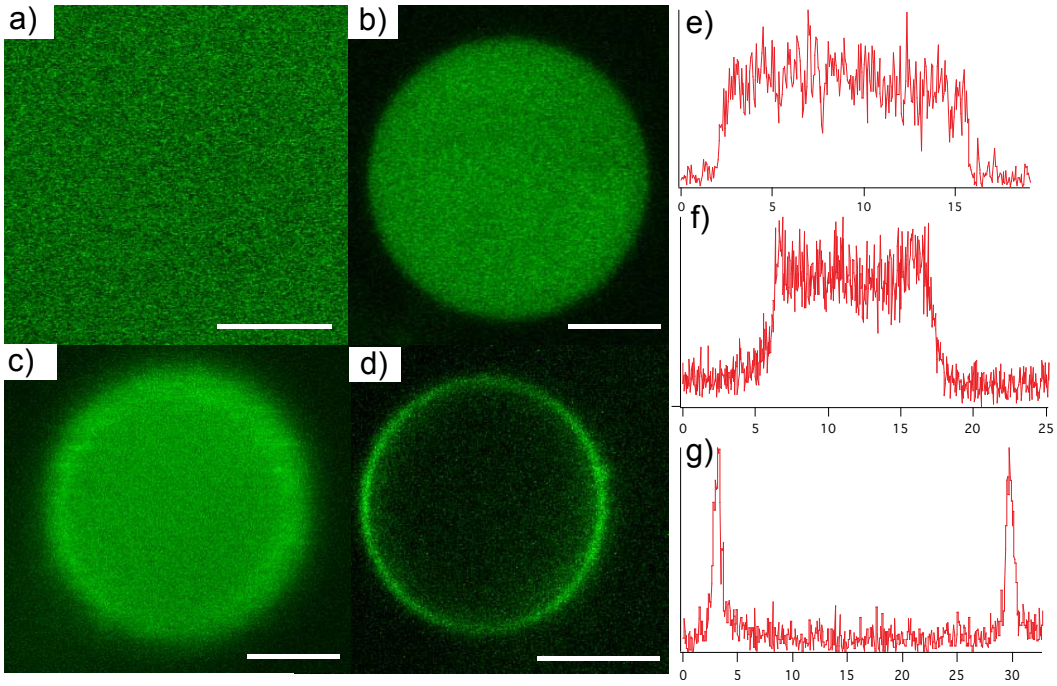

Figure 5.5: Confocal fluorescence micrographs showing QD/lipids. *(a) QD/lipids formed from 100% DPPA (scale bar=10 μm). Representative confocal cross-section images of in-situ formed QD/lipids inside DMPC vesicle at a lipid mixture of (b) 70:30 DPPA:DMPC (scale bar=5 μm), and (c) 30:70 DPPA:DMPC (scale bar=5 μm). (d) For comparison, a representative confocal cross-section image of a QD labeled hybrid vesicle formed from 100 % DMPC is shown (scale bar=10 μm). All the confocal micrographs were obtained at room temperature in 0.1 M glucose at pH 7. The intensity profiles of the cross-sections are shown in (e-g), where (e) corresponds to (b), (f) corresponds to (c) and (g) corresponds to (d).*

that the solution is highly fluorescent underlines the formation of QD/lipids from the TOPO-coated hydrophobic CdSe QDs.

We have extended the formation of QD/lipids into a confined system as can be seen in Fig. 5.5 b-c. When 30 % DMPC was added into the reaction mixture (DMPC is known to form lipid vesicles in water), formation of giant vesicles encapsulated with in-situ formed QD/lipids were observed (see also Fig. 5.4b). Biotinylated vesicles containing QD/lipids in 0.1 M sucrose were incubated on a glass coverslip, which was pre-treated with 0.1 mg/mL avidin, in 0.1 M glucose. The glucose solution was used to keep the osmotic pressure balanced while allowing quick settling of vesicles. In this image the vesicle bilayer is completely invisible owing to the fact that most of the QDs used in the reaction mixture contributed in the formation of small QD/lipids

structures which are contained inside of a giant vesicle. The fluorescence intensity profile of this image (Fig. 5.5 e) shows that the fluorescence is constant throughout. Increasing the ratio of DMPC in the reaction mixture resulted with vesicles as shown in Fig. 5.5 c-d. A lipid mixture containing 70% DMPC and 30% DPPA resulted with vesicles as shown in Fig. 5.5 c where the bilayer membrane is clearly visible compared to Fig. 5.5 b. The fluorescence intensity profile of this image (Fig. 5.5 f) shows that the fluorescence signal is higher at the bilayer membrane than the interior of the vesicle. This is due to the high ratio of DMPC in the reaction mixture that is responsible for the formation of vesicles (see also Fig. 5.4c). Fig. 5.5 d and the corresponding intensity profile shown in Fig. 5.5 g shows a typical empty HV formed under similar conditions, which further confirms that the fluorescent material observed in Fig. 5.5 a-c are lipid modified QDs.

Fluorescence Correlation Spectroscopy:

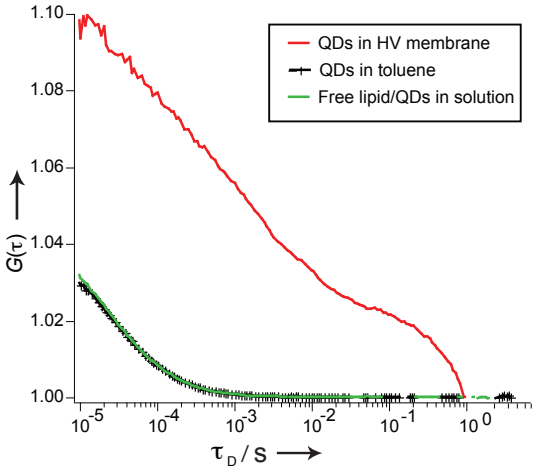

Figure 5.6: FCS curves of QD/lipids. *FCS autocorrelation curves of a free solution of QD/lipids formed from 100% DPPA (green) that has same diffusion as free CdSe QDs in toluene (black scattered lines). This indicates that the QDs in the former case have only very slight surface modification; i.e., a monolayer of DPPA molecules around the TOPO coating of the QDs. The autocorrelation curve obtained from similar QDs in the bilayer membrane of HVs (red) is shown for comparison.*

Further confirmation about the difference in the organization of QDs with DPPA (charged) and DMPC (neutral) lipids has been obtained from fluorescence correlation spectroscopy (FCS). The samples were excited at 488 nm with an argon ion laser (3 kW/cm^2), and its fluorescence was detected through a pinhole (70 μm diameter) and a 505 nm long-pass filter. The excitation intensity was adjusted to maximize the detected counts per particle. For each series of FCS measurements, a

standard calibration was performed using Rhodamine 6G in PBS solution at pH 7.4 ([166]). Fig. 5.6 shows the measured auto-correlation functions (ACFs). The ACF of the QD/lipids showed entirely different diffusion compared to the QDs in the HVs of DMPC. QD/lipids diffuse very fast as free QDs in toluene compared to their diffusion when organized inside HV membrane. The speed of QD/lipids were two times slower than conventional organic dyes usually observed in FCS experiments. These findings give additional proof that the fluorescent solution of QD/lipids do not contain any small vesicles but lipid coated individual QDs.

5.5.2 Directed self-assembly of QD/lipids

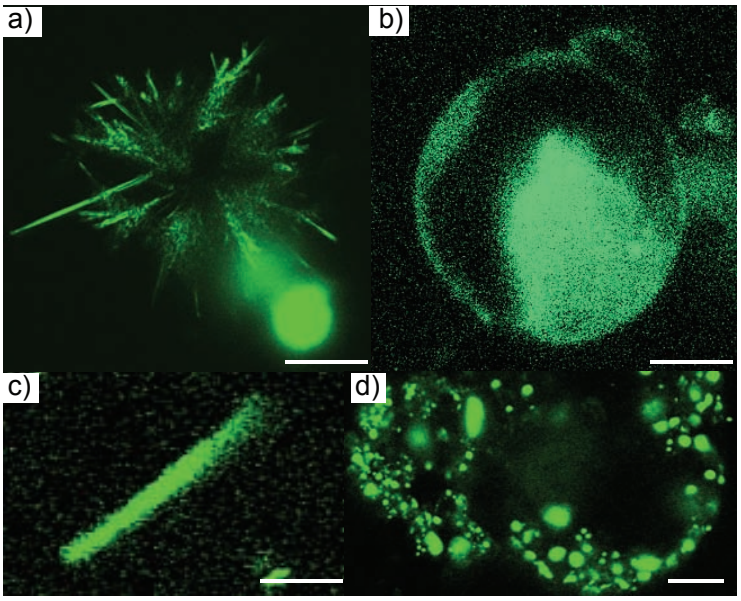

Figure 5.7: Confocal fluorescence micrographs showing self-assembled QD/lipids structures. *Addition of 100 μL, 10 mM $CaCl_2$ into (a) QD/lipids in solution (as in Fig. 5.5 a) resulted in asymmetrically organized fluorescent structures (scale bar=10 μm) and (b) into in-situ formed QD/lipids enclosed in a 70:30 DPPA:DMPC (scale bar=10 μm) vesicle as in Fig. 5.5 b. The effect of pH is illustrated in the following figures (c-d). Addition of 20 μL, 1 M HCl into 500 μL solution of QD/lipids resulted with two different kinds of assembled structures (scale bars=5 μm (c) and 10 μm (d)).*

Addition of Ca^{2+} ions to QD/lipids have resulted aggregation of material (Fig. 5.7) along with a sudden disappearance of background fluorescence was observed using confocal microscopy. The aggregation was observed in solution as well as in confined volumes inside vesicles. Fig. 5.7 a shows long, asymmetric structures of QD/lipids that has maximum optically resolvable diameters of 200 nm. This means that the

actual diameter of these structures could be any number below 200 nm. The pH of the solution after addition of $CaCl_2$ was 4. Similar asymmetric structures were observed when the pH of the solution was brought from 7 to 3 in the absence of Ca^{2+} ions. As can be seen in Fig. 5.7 c, addition of 20 μL, 1 M HCl into 500 μL solution of QD/lipids has predominantly resulted in aggregation of material into a rod-like structure. But in this case, the rod-like structures were not as extended as in the case with Ca^{2+} ions (Fig. 5.7 a). Fig. 5.7 d shows another area of the same sample that shows random aggregation of QD/lipids.

Transmission electron micrographs (TEM) of non-aggregated QD/lipids are shown in Fig. 5.8 a&b which resembles typical TEM images of surfactant coated individual QDs. This further proves the formation of individually coated QDs when DPPA is used in the reaction medium. The directed self-assembly observed in confocal microscopy also is further proved by TEM image shown in Fig. 5.8 c.

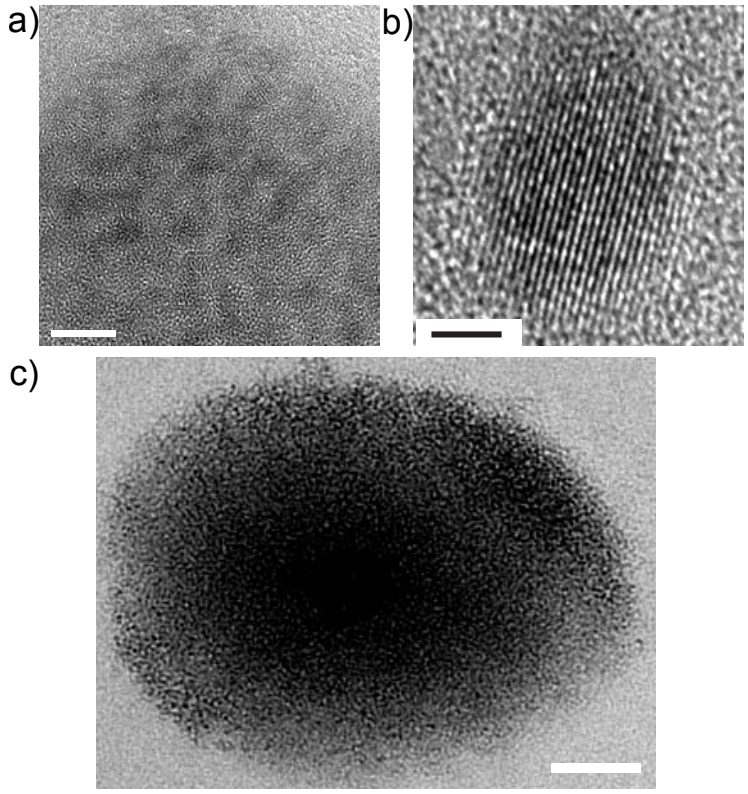

Figure 5.8: Transmission electron micrographs showing self-assembled QD/lipids structures. *(a) QD/lipids show individual QDs as observed using CdSe-TOPO QDs (scale bar=5 nm). (b) shows a high resolution image of an individual QD/lipid (scale bar=3 nm). (c) Addition of 100 μL, 10 mM $CaCl_2$ into QD/lipids in solution resulted in asymmetrically organized structures (scale bar=100 nm).*

Extending the directed aggregation of QD/lipids in bulk volumes to nano/femtoliter volumes inside vesicles of DMPC has shown interesting effects. As depicted in Fig. 5.7 b, a precipitation of fluorescent mass was observed upon addition of 100 μL, 10 mM $CaCl_2$ solution into immobilized giant vesicles that has been formed with in-situ encapsulation of QD/lipids. The vesicles were suspended in 300 μL glucose solution. The vesicles used in this experiment were produced from 70:30 DPPA:DMPC mixture and thus having encapsulated QD/lipids as seen in Fig. 5.5 b. Unlike PC membranes, vesicular bilayers containing PA are more prone to Ca^{2+} ion permeability [195]. In the case of Fig. 5.5 b, though majority of DPPA lipids would contribute to the surface modification of QDs to result QD/lipids, a few percentage might be ordered in the bilayer along with DMPC that is responsible for the vesicle formation. The permeability of Ca^{2+} ion would otherwise not happen. For the ease of illustration, we have used giant vesicular structures, but the same could be tried at vesicles as small as 25 nm carrying attoliter volumes inside, which allow one to carry out sensing of tiny amounts of ion influx.

5.5.3 Discussion

The surface modification of TOPO coated CdSe QDs was achieved using a negatively charged phospholipid, DPPA. This approach not only gives an easy phase transfer into water but also several other possibilities by exploiting the phosphatidic acid moiety around the QDs.

A naturally arising question at this point is why do charged DPPA induce the formation of QD/lipids (Fig. 5.3) and DMPC and other neutral lipids form bilayer HVs (Fig. 4.11) when phospholipids interact with hydrophobic QDs? Our hypothesis to this question is the following: due to energetic reasons, DPPA molecules prefer to arrange themselves around QDs as it would reduce the repulsion between the negatively charged headgroups compared to when they arranged in a vesicle bilayer. The latter indeed need more closer molecular packing compared to the formation of QD/lipids. This together with the intrinsic nature of PA lipids to form nonbilayer structures results in the formation of QD/lipids.

Firstly, the directed assembly of QD/lipids opens an additional route to obtain reversible mesoscale ordering of tiny particles in complementary to already established DNA, polymer etc based organization. The multiple stimuli (i.e., Ca^{2+} ions and pH) used for the assembly gives more control over the system. The method illustrated here could be extended to other kinds of particles such as metallic and magnetic nanocrystals. As has already been discussed earlier, the construction of nanocrystal

based functional devices requires components that are handy and manipulable. Our approach provides an easy and reversible method that will contribute in producing such building blocks from different kinds of hydrophobic nanocrystals.

Secondly, the effect of Ca^{2+} ions observed inside lipid vesicles is remarkable in several aspects. From the biological point of view, the ion permeability across cellular membranes is a very important property to study as it controls many vital processes in living beings. Biophysicists thus study the ion permeability across lipid bilayers in model membrane systems. Extending the precipitation carried out in Fig. 5.7 b into small size vesicles ca 25 nm, it could be used as a Ca^{2+} ion sensor at attoliter volumes. It also demonstrates that precipitation can be performed and observed in these attoliter sized vesicle.

The mechanism of the assembly of QD/lipids could at least be the followings: (1) The Ca^{2+} ions act as bridging agents between the negatively charged QD/lipids and thus enabling ordering of QD/lipids as observed in the case of random assembly (Fig. 5.9 a). (2) DPPA are known to form hexagonal phases in the presence of Ca^{2+} ions as well as at acidic pHs [72], [194]. The observation of extended rod-like structures could be due to the formation of hexagonal I phases of DPPA, which additionally couple together using Ca^{2+} ions resulting micrometer long structures (Fig. 5.9 b). The reason why we believe that the formed hexagonal phases are hexagonal I than hexagonal II is the following: resulting QD/lipids are completely soluble in water which imposes formation of hexagonal I phase as otherwise would not be able to solubilize the hydrophobic QDs (see Fig. 1.10 of 1.5.2). We speculate that the organization observed inside vesicles also follows a similar mechanisms. In order to discriminate the exact mechanism happening both inside vesicles and in free solution, more careful studies such as freeze-fracture EM as well as small angle x-ray scattering etc are needed.

Lastly, it is important to note here that along with all the possibilities mentioned above, one should consider the novelty of the basic lipid/QD moiety that we produced. It can be considered as a fluorescently labeled lipid. Only difference compared to commercially available fluorescent lipids is that here we have multiple DPPA molecules around single QD. Also, fluorescently labeled lipids are very limited in terms of available headgroups. Considering the biological relevance of phosphatidic acids [196], [197], [198], our QD/lipids offer many possibilities to the researchers working in this field. So far, almost all studies were restricted to use spectroscopic techniques as illustrated by the published works in this field. Our QD/lipids would definitely offer the use of fluorescence microscopy for both in-vitro and in-vivo studies. For example, lysophosphatidic acid induced neuronal shape changes [198], phos-

phatidic acid mediated inhibition of insulin receptors [197], effect of phosphatidic acid on recombinant protein production observed in CHO cell-lines [196]etc could potentially profit from highly fluorescent DPPA structures. Being considered "seeing is believing" and the growing importance of fluorescence microscopy as an important tool in biological studies, researchers could definitely profit from our QD/lipids.

5.5.4 Perspectives

In short, we have developed an easy and versatile method to make water soluble, functional lipid coated QDs. They were found useful in making self-assembled mesoscopic structures that can be controlled by multiple stimuli such as ionization and pH. Indeed, detailed studies on the organizational properties need to be performed in order to draw a better conclusion of the observations discussed in this chapter. However, the easy experimental approach and possibility of multiple stimuli to induce assembly of QDs into mesoscale aggregates seem to be very promising. The method could be extended to any kind of hydrophobic nanocrystals depending on the application. The designed QD/lipids will be equally useful for many researchers working in chemical, cellular as well as biophysical areas.

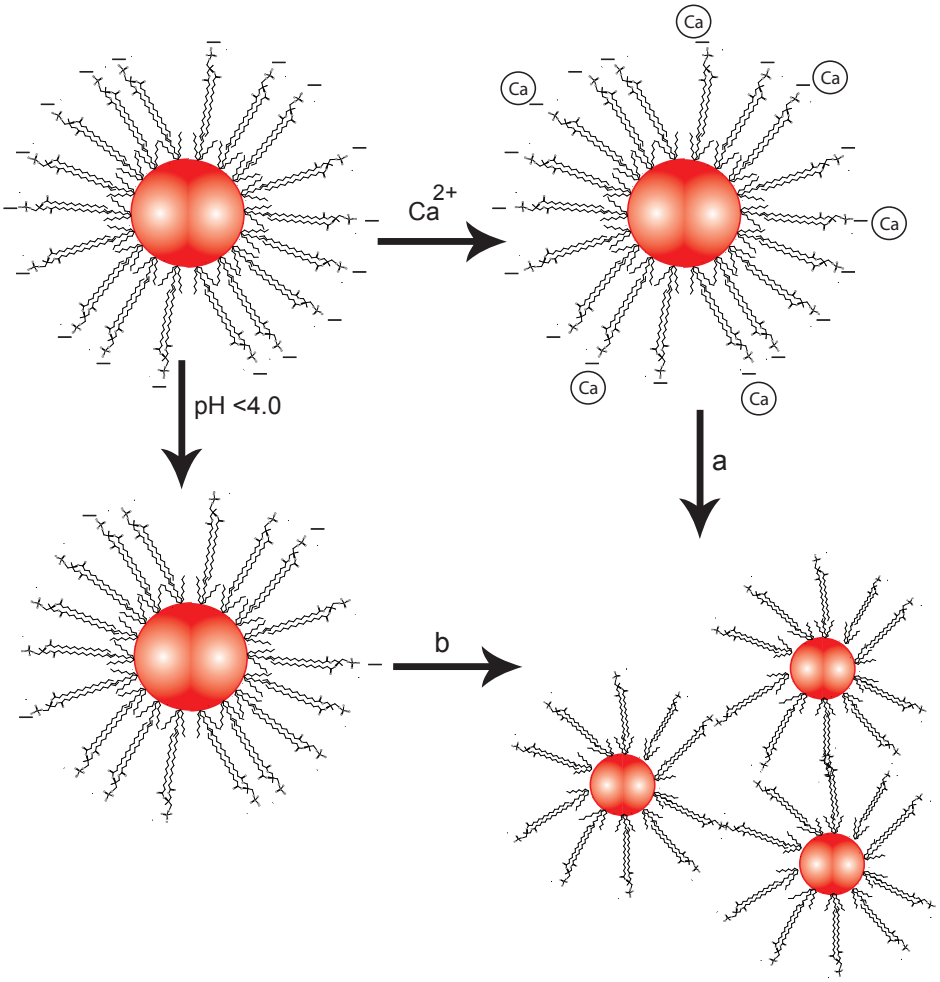

Figure 5.9: Illustration of possible mechanisms of the directed self-assembly of QD/lipids. *The negatively charged QD/lipids were either assembled upon addition of Ca^{2+} ions (to the right through a) or formed hexagonal phase directed assembly upon reduction of the solution pH (down through b).*

Chapter 6

Conclusion

This thesis demonstrates the enormous possibilities of phospholipid membranes in the development of novel functional nanomaterials:

The template directed synthesis of nanoscopic optical fibers achieved during this thesis work provides an easy, room temperature synthetic route to produce novel, single crystal, high aspect ratio nanowires. Though many other (bio)chemical molecules and structures have been used as templates for the synthesis of 1D nanostructures, our approach shows, for the first time, that such high aspect ratio functional nanostructures could be produced at room temperature. The combination of optical and electron microscopy techniques provided us a powerful approach to understand the growth mechanism and properties of the resulting nanofibers.

The fabrication of hybrid vesicles based on phospholipids and semiconductor QDs has created novel micro/nano structures that have been found useful in many cellular applications in-vivo and in-vitro. The successful incorporation of QDs in the bilayer membrane of phospholipids resulted a multifunctional nanocontainer that can be modified for specific applications. The two different constructs fabricated from such hybrid vesicles showed extreme control over cellular targeting as described in chapter 4. The possibility of using other kinds of nanocrystals individually or as ensembles in single nanocontainers would find several interesting applications in nanobiotechnology.

The directed self-assembly of fluorescent QDs discussed in chapter 5 shows another example of using conventional lipid-chemistry in the development of handy functional materials from tiny building blocks such as nanocrystals. The multi-stimulus that has been used to induce the assembly of QDs in bulk solution as well as in confined volumes make our approach more attractive in terms of controllability.

Taken together, this thesis work shows that the rich variability of the lipid hydrocarbon chains that results in numerous lyotropic and thermotropic phases and lipid polar headgroups that bind selectively and reversibly certain cations if tuned

well could be used for the fabrication of novel, functional materials that will find enormous applications in future optoelectronic, biomedical, nanobiotechnology applications.

The use of lipid structures for the creation of functional nanocrystals is gaining much interest due to the extreme biocompatibility and tailorable surface functionalities that enables their use in several biological applications in-vivo and in-vitro.

Abbreviations

AFM	atomic force microscopy
Au	gold
CCD	charge coupled device
$CdCl_2$	cadmium chloride
CdS	cadmium sulfide
CdSe	cadmium selenide
CNT	carbon nanotube
Cryo-TEM	cryogenic transmission electron microscopy
DLPC	1,2-dilauroyl-sn-glycero-3-phosphocholine
DLPSH	1,2-dilauroyl-sn-glycero-3-phosphothioethanol
DMPC	1,2-dimyristoyl-sn-glycero-3-phosphocholine
DOPC	1,2-dioleoyl-sn-glycero-3-phosphocholine
DOPG	1,2-dioleoyl-sn-glycero-3-phosphoglycerol
DOTAP	1,2-dioleoyl-3-trimethylammonium-propane (chloride salt)
DPPA	1,2-dipalmitoyl-sn-glycero-3-phosphatidic acid
DPPC	1,2-dipalmitoyl-sn-glycero-3-phosphocholine
DSPC	1,2-distearoyl-sn-glycero-3-phosphocholine
ED	electron diffraction
FCS	fluorescence correlation spectroscopy
FRET	fluorescence resonance energy transfer
GUV	giant unilamellar vesicle
HEK	human embryo kidney
HV	hybrid vesicle
LSM	laser scanning confocal microscopy
LUV	large unilamellar vesicle
MLV	multilamellar vesicle
MRI	medical resonance imaging
NP	naoparticle
NW	nanowire
PA	phosphatidicacid

PBS	phosphate buffered saline
PC	phosphatidylcholine
PE	phosphatidylethanolamine
PEG	polyethylene glycol
PEG-biotin	1,2-distearoyl-sn-glycero-3-phosphatidylethanolamine-N-[biotinyl (polyethyleneglycol)2000] (ammonium salt) or DSPE-PEG2000-biotin
PEG-PE	1,2-dipalmitoyl-sn-glycero-3-phosphatidylethanolamine-N-[methoxy (polyethyleneglycol)2000] (ammonium salt) or DPPE-PEG2000
PS	phosphatidylserine
QDs	quantum dots
SEM	scanning electron microscopy
STM	scanning tunneling microscopy
SUV	small unilamellar vesicle
TEM	transmission electron microscopy
TOPO	trioctylphosphinoxide

Bibliography

[1] B. Bhushan. *Handbook of Nanotechnology*, volume 1 of *Springer Handbook of Nanotechnology*. Springer-Verlag, Heidelberg, 2004.

[2] C. M. Niemeyer. Nanoparticles, proteins, and nucleic acids: Biotechnology meets materials science. *Angew. Chem. Int. Ed.*, 40(22):4128, 2001.

[3] E. Katz and I. Willner. Integrated nanoparticle-biomolecule hybrid systems: Synthesis, properties, and applications. *Angew. Chem. Int. Ed.*, 43(45):6042, 2004.

[4] S. Mann. *Biomemetic Materials Chemistry*. VCH, New York, 1996.

[5] J. Aizenberg, A. J. Black, and G. M. Whitesides. Control of crystal nucleation by patterned self-assembled monolayers. *Nature*, 398(6727):495, 1999.

[6] Y. J. Han and J. Aizenberg. Face-selective nucleation of calcite on self-assembled monolayers of alkanethiols: Effect of the parity of the alkyl chain. *Angew. Chem. Int. Ed.*, 42(31):3668, 2003.

[7] J. Aizenberg. A bio-inspired approach to controlled crystallization at the nanoscale. *Bell Labs Technical Journal*, 10(3):129, 2005.

[8] T. Douglas. A bright bio-inspired future. *Science*, 299(5610):1192, 2003.

[9] H. Colfen and S. Mann. Higher-order organization by mesoscale self-assembly and transformation of hybrid nanostructures. *Angew. Chem. Int. Ed.*, 42(21):2350, 2003.

[10] S. Slomkowski. Hybrid polymeric materials for medical applications. *Polimery*, 51(2):87, 2006.

[11] Y. W. Wang, C. T. Yen, and W. C. Chen. Photosensitive polyimide/silica hybrid optical materials: Synthesis, properties, and patterning. *Polymer*, 46(18):6959, 2005.

[12] T. Pellegrino, S. Kudera, T. Liedl, A. M. Javier, L. Manna, and W. J. Parak. On the development of colloidal nanoparticles towards multifunctional structures and their possible use for biological applications. *Small*, 1(1):48, 2005.

[13] H. Colfen and S. H. Yu. Biomimetic mineralization/synthesis of mesoscale order in hybrid inorganic - organic materials via nanoparticle self-assembly. *MRS Bull.*, 30(10):727, 2005.

[14] M. Iijima, T. Watabe, S. Ishii, A. Koshio, T. Yamaguchi, S. Bandow, S. Iijima, K. Suzuki, and Y. Maruyama. Fabrication and STM-characterization of novel hybrid materials of DNA/carbon nanotube. *Chem. Phys. Lett.*, 414(4-6):520, 2005.

[15] E. Katz and I. Willner. Biomolecule-functionalized carbon nanotubes: Applications in nanobioelectronics. *ChemPhysChem*, 5(8):1085, 2004.

[16] C. Sanchez, B. Lebeau, F. Chaput, and J. P. Boilot. Optical properties of functional hybrid organic-inorganic nanocomposites. *Adv. Mater.*, 15(23):1969, 2003.

[17] X. G. Peng, L. Manna, W. D. Yang, J. Wickham, E. Scher, A. Kadavanich, and A. P. Alivisatos. Shape control of CdSe nanocrystals. *Nature*, 404(6773):59, 2000.

[18] C. B. Murray, C. R. Kagan, and M. G. Bawendi. Synthesis and characterization of monodisperse nanocrystals and close-packed nanocrystal assemblies. *Annu. Rev. Mater. Sci.*, 30:545, 2000.

[19] S. M. Lee, S. N. Cho, and J. Cheon. Anisotropic shape control of colloidal inorganic nanocrystals. *Adv. Mater.*, 15(5):441, 2003.

[20] X. Michalet, F. F. Pinaud, L. A. Bentolila, J. M. Tsay, S. Doose, J. J. Li, G. Sundaresan, A. M. Wu, S. S. Gambhir, and S. Weiss. Quantum dots for live cells, in vivo imaging, and diagnostics. *Science*, 307(5709):538, 2005.

[21] A. P. Alivisatos. Semiconductor clusters, nanocrystals, and quantum dots. *Science*, 271(5251):933, 1996.

[22] C. J. Murphy and J. L. Coffer. Quantum dots: A primer. *Appl. Spectr.*, 56(1):16A, 2002.

[23] M. Faraday. The Bakerian Lecture: Experimental relations of Gold (and other metals) to light. *Phil. Trans. Roy. Soc.*, 147:145, 1857.

[24] M. Brust, M. Walker, D. Bethell, D. J. Schiffrin, and R. Whyman. Synthesis of thiol-derivatized gold nanoparticles in a 2-phase liquid-liquid system. *J. Chem. Soc. Chem. Commun.*, (7):801, 1994.

[25] K. V. Sarathy, G. U. Kulkarni, and C. N. R. Rao. A novel method of preparing thiol-derivatised nanoparticles of gold, platinum and silver forming superstructures. *Chem. Commun.*, (6):537, 1997.

[26] A. Schroedter and H. Weller. Ligand design and bioconjugation of colloidal gold nanoparticles. *Angew. Chem. Int. Ed.*, 41(17):3218, 2002.

[27] G. Schmid, M. Baumle, M. Geerkens, I. Helm, C. Osemann, and T. Sawitowski. Current and future applications of nanoclusters. *Chem. Soc. Rev.*, 28(3):179, 1999.

[28] L. Spanhel, M. Haase, H. Weller, and A. Henglein. Photochemistry of colloidal semiconductors.20. Surface modification and stability of strong luminescing CdS particles. *J. Am. Chem. Soc.*, 109(19):5649, 1987.

[29] L. Brus. Electronic wave-functions in semiconductor clusters - experiment and theory. *J. Phys. Chem.*, 90(12):2555, 1986.

[30] C. B. Murray, D. J. Norris, and M. G. Bawendi. Synthesis and characterization of nearly monodisperse CdE (E = S, Se, Te) semiconductor nanocrystallites. *J. Am. Chem. Soc.*, 115(19):8706, 1993.

[31] C. B. Murray, C. R. Kagan, and M. G. Bawendi. Self-organization of CdSe nanocrystallites into 3-dimensional quantum-dot superlattices. *Science*, 270(5240):1335, 1995.

[32] M. Nirmal, C. B. Murray, and M. G. Bawendi. Fluorescence-line narrowing in CdSe quantum dots - surface localization of the photogenerated exciton. *Phys. Rev. B*, 50(4):2293, 1994.

[33] M. Bruchez, M. Moronne, P. Gin, S. Weiss, and A. P. Alivisatos. Semiconductor nanocrystals as fluorescent biological labels. *Science*, 281(5385):2013, 1998.

[34] W. C. W. Chan and S. M. Nie. Quantum dot bioconjugates for ultrasensitive nonisotopic detection. *Science*, 281(5385):2016, 1998.

[35] H. Weller. Colloidal semiconductor Q-Particles - chemistry in the transition region between solid-state and molecules. *Angew. Chem. Int. Ed.*, 32(1):41, 1993.

[36] N. Gaponik, D. V. Talapin, A. L. Rogach, K. Hoppe, E. V. Shevchenko, A. Kornowski, A. Eychmuller, and H. Weller. Thiol-capping of CdTe nanocrystals: An alternative to organometallic synthetic routes. *J. Phys. Chem. B*, 106(29):7177, 2002.

[37] R. H. Kodama. Magnetic nanoparticles. *J. Magn. Magn. Mater.*, 200(1-3):359, 1999.

[38] A. C. Nunes and Z. C. Yu. Size and quality dispersion of a single preparation of colloidal magnetic particles. *J. Magn. Magn. Mater.*, 78(2):241, 1989.

[39] X. K. Zhao, S. Q. Xu, and J. H. Fendler. Ultrasmall magnetic particles in Langmuir-Blodgett-films. *J. Phys. Chem.*, 94(6):2573, 1990.

[40] II Yaacob, A. C. Nunes, A. Bose, and D. O. Shah. Synthesis and characterization of magnetic nanoparticles in spontaneously generated vesicles. *J. Colloid Interface Sci.*, 168(2):289, 1994.

[41] II Yaacob, A. C. Nunes, and A. Bose. Magnetic nanoparticles produced in spontaneous cationic-anionic vesicles - room-temperature synthesis and characterization. *J. Colloid Interface Sci.*, 171(1):73, 1995.

[42] S. V. Sonti and A. Bose. Cell-separation using Protein-A-coated magnetic nanoclusters. *J. Colloid Interface Sci.*, 170(2):575, 1995.

[43] J. Ugelstad, A. Berge, T. Ellingsen, O. Aune, L. Kilaas, T. N. Nilsen, R. Schmid, P. Stenstad, S. Funderud, G. Kvalheim, K. Nustad, T. Lea, F. Vartdal, and H. Danielsen. Monosized magnetic particles and their use in selective cell-separation. *Makromolekulare Chemie-Macromolecular Symposia*, 17:177, 1988.

[44] M. Lewin, N. Carlesso, C. H. Tung, X. W. Tang, D. Cory, D. T. Scadden, and R. Weissleder. Tat peptide-derivatized magnetic nanoparticles allow in vivo tracking and recovery of progenitor cells. *Nature Biotechnol.*, 18(4):410, 2000.

[45] Q. A. Pankhurst, J. Connolly, S. K. Jones, and J. Dobson. Applications of magnetic nanoparticles in biomedicine. *J. Phy. D-Appl. Phys.*, 36(13):R167, 2003.

[46] T. Osaka, T. Matsunaga, T. Nakanishi, A. Arakaki, D. Niwa, and H. Iida. Synthesis of magnetic nanoparticles and their application to bioassays. *Anal. Bioanal. Chem.*, 384(3):593, 2006.

[47] A. Ito, M. Shinkai, H. Honda, and T. Kobayashi. Medical application of functionalized magnetic nanoparticles. *J. Biosci. Bioeng.*, 100(1):1, 2005.

[48] R. Weissleder, K. Kelly, E. Y. Sun, T. Shtatland, and L. Josephson. Cell-specific targeting of nanoparticles by multivalent attachment of small molecules. *Nature Biotechnol.*, 23(11):1418, 2005.

[49] A. Ito, M. Shinkai, H. Honda, and T. Kobayashi. Heat-inducible TNF-alpha gene therapy combined with hyperthermia using magnetic nanoparticles as a novel tumor-targeted therapy. *Cancer Gene Therapy*, 8(9):649, 2001.

[50] C. R. Martin. Nanomaterials - a membrane-based synthetic approach. *Science*, 266(5193):1961, 1994.

[51] K. L. Hobbs, P. R. Larson, G. D. Lian, J. C. Keay, and M. B. Johnson. Fabrication of nanoring arrays by sputter redeposition using porous alumina templates. *Nano Lett.*, 4(1):167, 2004.

[52] J. H. Zhan, X. G. Yang, D. W. Wang, S. D. Li, Y. Xie, Y. Xia, and Y. Qian. Polymer-controlled growth of CdS nanowires. *Adv. Mater.*, 12(18):1348, 2000.

[53] H. J. Liang, T. E. Angelini, J. Ho, P. V. Braun, and G. C. L. Wong. Molecular imprinting of biomineralized cds nanostructures: Crystallographic control using self-assembled dna-membrane templates. *J. Am. Chem. Soc.*, 125(39):11786, 2003.

[54] C. B. Mao, D. J. Solis, B. D. Reiss, S. T. Kottmann, R. Y. Sweeney, A. Hayhurst, G. Georgiou, B. Iverson, and A. M. Belcher. Virus-based toolkit for the directed synthesis of magnetic and semiconducting nanowires. *Science*, 303(5655):213, 2004.

[55] G. R. Patzke, F. Krumeich, and R. Nesper. Oxidic nanotubes and nanorods - anisotropic modules for a future nanotechnology. *Angew. Chem. Int. Ed.*, 41(14):2446, 2002.

[56] F. Favier, E. C. Walter, M. P. Zach, T. Benter, and R. M. Penner. Hydrogen sensors and switches from electrodeposited palladium mesowire arrays. *Science*, 293(5538):2227, 2001.

[57] C. J. Barrelet, Y. Wu, D. C. Bell, and C. M. Lieber. Synthesis of CdS and ZnS nanowires using single-source molecular precursors. *J. Am. Chem. Soc.*, 125(38):11498, 2003.

[58] D. A. Bazylinski, A. J. Garrattreed, and R. B. Frankel. Electron-microscopic studies of magnetosomes in magnetotactic bacteria. *Micr. Res. Tech.*, 27(5):389, 1994.

[59] J. H. Fendler. *Membrane-Mimetic Approach to Advanced Materials*, volume 113 of *Advances in Polymer Science*. Springer-Verlag, Berlin-Heidelberg, 1994.

[60] I. F. Williams, K. G. McCullagh, and I. A. Silver. The distribution of Type-I and Type-III collagen and fibronectin in the healing equine tendon. *Conn. Tiss. Res.*, 12(3-4):211, 1984.

[61] M. P. Pileni. The role of soft colloidal templates in controlling the size and shape of inorganic nanocrystals. *Nature Mater.*, 2(3):145, 2003.

[62] M. P. Pileni. Reverse micelles as microreactors. *J. Phys. Chem.*, 97(27):6961, 1993.

[63] J. H. Fendler and F. C. Meldrum. The colloid-chemical approach to nanostructured materials. *Adv. Mater.*, 7(7):607, 1995.

[64] S. Mann, J. P. Hannington, and R. J. P. Williams. Phospholipid-vesicles as a model system for biomineralization. *Nature*, 324(6097):565, 1986.

[65] D. Bruhwiler and G. Calzaferri. Molecular sieves as host materials for supramolecular organization. *Micropor. Mesopor. Mater.*, 72(1-3):1, 2004.

[66] F. C. Meldrum, V. J. Wade, D. L. Nimmo, B. R. Heywood, and S. Mann. Synthesis of inorganic nanophase materials in supramolecular protein cages. *Nature*, 349(6311):684, 1991.

[67] M. Antonietti, M. Breulmann, C. G. Goltner, H. Colfen, K. K. W. Wong, D. Walsh, and S. Mann. Inorganic/organic mesostructures with complex architectures: Precipitation of calcium phosphate in the presence of double-hydrophilic block copolymers. *Chem. Eur. J.*, 4(12):2493, 1998.

[68] Y. C. Tian and J. H. Fendler. Langmuir-Blodgett film formation from fluorescence-activated, surfactant-capped, size-selected cds nanoparticles spread on water surfaces. *Chem. Mater.*, 8(4):969, 1996.

[69] J. H. Fendler. Nanoparticles at air/water interfaces. *Curr. Opin. Coll. Inter. Sci.*, 1(2):202, 1996.

[70] P. Y. Bolinger, D. Stamou, and H. Vogel. Integrated nanoreactor systems: Triggering the release and mixing of compounds inside single vesicles. *J. Am. Chem. Soc.*, 126(28):8594, 2004.

[71] D. Marsh G. Cevc. *Phospholipid Bilayers: Physical Principles and Models.* Wiley Interscience, New York, 1987.

[72] D. D. Lasic. *Liposomes- from Physics to Applications.* Elsevier Science B.V, Netherlands, 1993.

[73] R. B. Gennis. *Biomembranes: Molecular Structure and Function.* Springer-Verlag, New York, 1989.

[74] X. S. Xie and J. K. Trautman. Optical studies of single molecules at room temperature. *Annu. Rev. Phys. Chem.*, 49:441, 1998.

[75] S. Weiss. Fluorescence spectroscopy of single biomolecules. *Science*, 283(5408):1676, 1999.

[76] M. Dahan, S. Levi, C. Luccardini, P. Rostaing, B. Riveau, and A. Triller. Diffusion dynamics of glycine receptors revealed by single-quantum dot tracking. *Science*, 302(5644):442, 2003.

[77] M. Baumle, D. Stamou, J. M. Segura, R. Hovius, and H. Vogel. Highly fluorescent streptavidin-coated CdSe nanoparticles: Preparation in water, characterization, and micropatterning. *Langmuir*, 20(10):3828, 2004.

[78] G. Gopalakrishnan, J. M. Segura, D. Stamou, U. Gaillard, M. Gjoni, R. Hovius, K. J. Schenk, P. A. Stadelmann, and H. Vogel. Synthesis of nanoscopic optical fibers using lipid membranes as templates. *Angew. Chem. Int. Ed.*, 44(31):4957, 2005.

[79] D. Magde, W. W. Webb, and E. Elson. Thermodynamic fluctuations in a reacting system - measurement by fluorescence correlation spectroscopy. *Phys. Rev. Lett.*, 29(11):705, 1972.

[80] A. Ashkin, J. M. Dziedzic, J. E. Bjorkholm, and S. Chu. Observation of a single-beam gradient force optical trap for dielectric particles. *Opt. Lett.*, 11(5):288, 1986.

[81] X. F. Duan, Y. Huang, R. Agarwal, and C. M. Lieber. Single-nanowire electrically driven lasers. *Nature*, 421(6920):241, 2003.

[82] Q. Wu, Z. Hu, X. Z. Wang, Y. N. Lu, X. Chen, H. Xu, and Y. Chen. Synthesis and characterization of faceted hexagonal aluminum nitride nanotubes. *J. Am. Chem. Soc.*, 125(34):10176, 2003.

[83] J. F. Wang, M. S. Gudiksen, X. F. Duan, Y. Cui, and C. M. Lieber. Highly polarized photoluminescence and photodetection from single indium phosphide nanowires. *Science*, 293(5534):1455, 2001.

[84] H. Kind, H. Q. Yan, B. Messer, M. Law, and P. D. Yang. Nanowire ultraviolet photodetectors and optical switches. *Adv. Mater.*, 14(2):158, 2002.

[85] Z. M. Li, J. P. Zhai, H. J. Liu, I. L. Li, C. T. Chan, P. Sheng, and Z. K. Tang. Synthesis of 4 angstrom single-walled carbon nanotubes in catalytic Si-substituted AlPO4-5 molecular sieves. *Appl. Phys. Lett.*, 85(7):1253, 2004.

[86] S. Hoeppener, R. Maoz, S. R. Cohen, L. F. Chi, H. Fuchs, and J. Sagiv. Metal nanoparticles, nanowires, and contact electrodes self-assembled on patterned monolayer templates - a bottom-up chemical approach. *Adv. Mater.*, 14(15):1036, 2002.

[87] L. M. Dai. Advanced syntheses and microfabrications of conjugated polymers, C-60-containing polymers and carbon nanotubes for optoelectronic applications. *Polym. Adv. Tech.*, 10(7):357, 1999.

[88] B. Q. Wei, R. Vajtai, Y. Jung, J. Ward, R. Zhang, G. Ramanath, and P. M. Ajayan. Organized assembly of carbon nanotubes - cunning refinements help to customize the architecture of nanotube structures. *Nature*, 416(6880):495, 2002.

[89] M. Li, H. Schnablegger, and S. Mann. Coupled synthesis and self-assembly of nanoparticles to give structures with controlled organization. *Nature*, 402(6760):393, 1999.

[90] J. T. Hu, T. W. Odom, and C. M. Lieber. Chemistry and physics in one dimension: Synthesis and properties of nanowires and nanotubes. *Acc. Chem. Res.*, 32(5):435, 1999.

[91] Y Ding and Z. L. Wang. Structure analysis of nanowires and nanobelts by transmission electron microscopy. *J. Phys. Chem. B*, 108(33):12280, 2004.

[92] P. Yang Y. Sun Y. Wu B. Mayers B. Gates Y. Yin F. Kim H. Yan Y. Xia. One-dimensional nanostructures: Synthesis, characterization, and applications. *Adv. Mater.*, 15(5):353, 2003.

[93] C. G. Wu and T. Bein. Conducting carbon wires in ordered, nanometer-sized channels. *Science*, 266(5187):1013, 1994.

[94] L.M. Huang, H. T. Wang, Z. B. Wang, A. Mitra, K. N. Bozhilov, and Y. S. Yan. Nanowire arrays electrodeposited from liquid crystalline phases. *Adv. Mater.*, 14(1):61, 2002.

[95] P. Buffat and J. P. Borel. Size effect on melting temperature of gold particles. *Phys. Rev. A*, 13(6):2287, 1976.

[96] Y. Wu and P. Yang. Melting and welding semiconductor nanowires in nanotubes. *Adv. Mater.*, 13(7):520, 2001.

[97] G. Rubio-Bollinger, S. R. Bahn, N. Agrait, K. W. Jacobsen, and S. Vieira. Mechanical properties and formation mechanisms of a wire of single gold atoms. *Phys. Rev. Lett.*, 8702(2), 2001. 026101.

[98] Z. B. Zhang, X. Z. Sun, M. S. Dresselhaus, J. Y. Ying, and J. Heremans. Electronic transport properties of single-crystal bismuth nanowire arrays. *Phys. Rev. B*, 61(7):4850, 2000.

[99] S. H. Choi, K. L. Wang, M. S. Leung, G. W. Stupian, N. Presser, B. A. Morgan, R. E. Robertson, M. Abraham, E. E. King, M. B. Tueling, S. W. Chung, J. R. Heath, S. L. Cho, and J. B. Ketterson. Fabrication of bismuth nanowires with a silver nanocrystal shadowmask. *J. Vac. Sci. Tech. A- Vac. Surf. Films*, 18(4):1326, 2000. Part 1.

[100] A. I. Yanson, G. R. Bollinger, H. E. van den Brom, N. Agrait, and J. M. van Ruitenbeek. Formation and manipulation of a metallic wire of single gold atoms. *Nature*, 395(6704):783, 1998.

[101] Y. Huang, X. F. Duan, Q. Q. Wei, and C. M. Lieber. Directed assembly of one-dimensional nanostructures into functional networks. *Science*, 291(5504):630, 2001.

[102] J. D. Holmes, K. P. Johnston, R. C. Doty, and B. A. Korgel. Control of thickness and orientation of solution-grown silicon nanowires. *Science*, 287(5457):1471, 2000.

[103] M. V. Wolkin, J. Jorne, P. M. Fauchet, G. Allan, and C. Delerue. Electronic states and luminescence in porous silicon quantum dots: The role of oxygen. *Phys. Rev. Lett.*, 82(1):197, 1999.

[104] M. H. Huang, S. Mao, H. Feick, H. Q. Yan, Y. Y. Wu, H. Kind, E. Weber, R. Russo, and P. D. Yang. Room-temperature ultraviolet nanowire nanolasers. *Science*, 292(5523):1897, 2001.

[105] M. Law, D. J. Sirbuly, J. C. Johnson, J. Goldberger, R. J. Saykally, and P. D. Yang. Nanoribbon waveguides for subwavelength photonics integration. *Science*, 305(5688):1269, 2004.

[106] J. C. Johnson, H. Q. Yan, R. D. Schaller, P. B. Petersen, P. D. Yang, and R. J. Saykally. Near-field imaging of nonlinear optical mixing in single zinc oxide nanowires. *Nano Lett.*, 2(4):279, 2002.

[107] Y. Cui, Q. Q. Wei, H. K. Park, and C. M. Lieber. Nanowire nanosensors for highly sensitive and selective detection of biological and chemical species. *Science*, 293(5533):1289, 2001.

[108] D. Stamou, C. Duschl, E. Delamarche, and H. Vogel. Self-assembled microarrays of attoliter molecular vessels. *Angew. Chem. Int. Ed.*, 42(45):5580, 2003.

[109] D. M. Bagnall, B. Ullrich, H. Sakai, and Y. Segawa. Micro-cavity lasing of optically excited CdS thin films at room temperature. *J. Cryst. Growth*, 214:1015, 2000.

[110] N. Chestnoy, T. D. Harris, R. Hull, and L. E. Brus. Luminescence and photophysics of CdS semiconductor clusters - the nature of the emitting electronic state. *J. Phys. Chem.*, 90(15):3393, 1986.

[111] M. Green, R. Taylor, and G. Wakefield. The synthesis of luminescent adenosine triphosphate passivated cadmium sulfide nanoparticles. *J. Mater. Chem.*, 13(8):1859, 2003.

[112] T. Vossmeyer, L. Katsikas, M. Giersig, I. G. Popovic, K. Diesner, A. Chemseddine, A. Eychmuller, and H. Weller. CdS nanoclusters - synthesis, characterization, size-dependent oscillator strength, temperature shift of the excitonic-transition energy, and reversible absorbency shift. *J. Phys. Chem.*, 98(31):7665, 1994.

[113] A. L. Rogach, A. Kornowski, M. Y. Gao, A. Eychmuller, and H. Weller. Synthesis and characterization of a size series of extremely small thiol-stabilized CdSe nanocrystals. *J. Phys. Chem. B*, 103(16):3065, 1999.

[114] K. Svoboda and S. M. Block. Biological applications of optical forces. *Annu. Rev. Biophys. Biomol. Str.*, 23:247, 1994.

[115] L. Girault, A. Boudou, and E. J. Dufourc. Cd-113-, P-31-NMR and fluorescence polarization studies of cadmium(II) interactions with phospholipids in model membranes. *Biochim. Biophys. Acta- Biomembranes*, 1414(1-2):140, 1998.

[116] M. J. Janiak, D. M. Small, and G. G. Shipley. Nature of thermal pre-transition of synthetic phospholipids - dimyristoyllecithin and dipalmitoyllecithin. *Biochemistry*, 15(21):4575, 1976.

[117] H. Leligny and J. C. Monier. Structure of Cadmium dichloride tetrahydrate. *Act. Cryst. Sect. B-Struct. Sci.*, 35(MAR):569, 1979.

[118] M. Karlsson, M. Davidson, R. Karlsson, A. Karlsson, J. Bergenholtz, Z. Konkoli, A. Jesorka, T. Lobovkina, J. Hurtig, M. Voinova, and O. Orwar. Biomimetic nanoscale reactors and networks. *Annu. Rev. Phys. Chem.*, 55:613, 2004.

[119] J. Aizenberg, A. Tkachenko, S. Weiner, L. Addadi, and G. Hendler. Calcitic microlenses as part of the photoreceptor system in brittlestars. *Nature*, 412(6849):819, 2001.

[120] B. I. Ipe and C. M. Niemeyer. Nanohybrids composed of quantum dots and cytochrome P450 as photocatalysts. *Angew. Chem. Int. Ed.*, 45(3):504, 2006.

[121] C. M. Niemeyer. Functional hybrid devices of proteins and inorganic nanoparticles. *Angew. Chem. Int. Ed.*, 42(47):5796, 2003.

[122] S. W. Lee, C. B. Mao, C. E. Flynn, and A. M. Belcher. Ordering of quantum dots using genetically engineered viruses. *Science*, 296(5569):892, 2002.

[123] S. R. Whaley, D. S. English, E. L. Hu, P. F. Barbara, and A. M. Belcher. Selection of peptides with semiconductor binding specificity for directed nanocrystal assembly. *Nature*, 405(6787):665, 2000.

[124] T. Douglas and M. Young. Host-guest encapsulation of materials by assembled virus protein cages. *Nature*, 393(6681):152, 1998.

[125] O.G. Mouritsen. *Life as a Matter of Fat. The Emerging Science of Lipidomics.* Springer Verlag, Heidelberg, 2005.

[126] J. H. Collier and P. B. Messersmith. Phospholipid strategies in biomineralization and biomaterials research. *Annu. Rev. Mater. Res.*, 31:237, 2001.

[127] H. Pick, E. L. Schmid, A. P. Tairi, E. Ilegems, R. Hovius, and H. Vogel. Investigating cellular signaling reactions in single attoliter vesicles. *J. Am. Chem. Soc.*, 127(9):2908, 2005.

[128] R. E. Pagano and J. N. Weinstein. Interactions of liposomes with mammaliancells. *Annu. Rev. Biophys. Bioeng.*, 7:435, 1978.

[129] G. Gregoriadis. Engineering liposomes for drug delivery: Progress and problems. *Trends. Biotech.*, 13(12):527, 1995.

[130] V. P. Torchilin and T. S. Levchenko. TAT-liposomes: A novel intracellular drug carrier. *Curr. Prot. Pept. Sci.*, 4(2):133, 2003.

[131] J. Kunisawa, T. Masuda, K. Katayama, T. Yoshikawa, Y. Tsutsumi, M. Akashi, T. Mayumi, and S. Nakagawa. Fusogenic liposome delivers encapsulated nanoparticles for cytosolic controlled gene release. *J. Contr. Rel.*, 105(3):344, 2005.

[132] X. H. Gao, L. L. Yang, J. A. Petros, F. F. Marshal, J. W. Simons, and S. M. Nie. In vivo molecular and cellular imaging with quantum dots. *Curr. Opin. Biotech.*, 16(1):63, 2005.

[133] L. Y. Feng, X. G. Kong, K. F. Chao, Y. J. Sun, Q. H. Zeng, and Y. L. Zhang. Efficient phase transfer of hydrophobic CdSe quantum dots: From nonpolar organic solvent to biocompatible water buffer. *Mater. Chem. Phys.*, 93(2-3):310, 2005.

[134] J. A. Kloepfer, N. Cohen, and J. L. Nadeau. FRET between CdSe quantum dots in lipid vesicles and water- and lipid-soluble dyes. *Journal Of Physical Chemistry B*, 108(44):17042, 2004.

[135] I. Geissbuehler, R. Hovius, K. L. Martinez, M. Adrian, K. R. Thampi, and H. Vogel. Lipid-coated nanocrystals as multifunctionalized luminescent scaffolds for supramolecular biological assemblies. *Angew. Chem. Int. Ed.*, 44(9):1388, 2005.

[136] B. Dubertret, P. Skourides, D. J. Norris, V. Noireaux, A. H. Brivanlou, and A. Libchaber. In vivo imaging of quantum dots encapsulated in phospholipid micelles. *Science*, 298(5599):1759, 2002.

[137] M. Nirmal, B. O. Dabbousi, M. G. Bawendi, J. J. Macklin, J. K. Trautman, T. D. Harris, and L. E. Brus. Fluorescence intermittency in single cadmium selenide nanocrystals. *Nature*, 383(6603):802, 1996.

[138] S. Kim and M. G. Bawendi. Oligomeric ligands for luminescent and stable nanocrystal quantum dots. *J. Am. Chem. Soc.*, 125(48):14652, 2003.

[139] W. Z. Guo, J. J. Li, Y. A. Wang, and X. G. Peng. Conjugation chemistry and bioapplications of semiconductor box nanocrystals prepared via dendrimer bridging. *Chem. Mater.*, 15(16):3125, 2003.

[140] F. Pinaud, D. King, H. P. Moore, and S. Weiss. Bioactivation and cell targeting of semiconductor CdSe/ZnS nanocrystals with phytochelatin-related peptides. *J. Am. Chem. Soc.*, 126(19):6115, 2004.

[141] X. Y. Wu, H. J. Liu, J. Q. Liu, K. N. Haley, J. A. Treadway, J. P. Larson, N. F. Ge, F. Peale, and M. P. Bruchez. Immunofluorescent labeling of cancer marker her2 and other cellular targets with semiconductor quantum dots. *Nature Biotechnol.*, 21(1):41, 2003.

[142] X. H. Gao, Y. Y. Cui, R. M. Levenson, L. W. K. Chung, and S. M. Nie. In vivo cancer targeting and imaging with semiconductor quantum dots. *Nature Biotechnol.*, 22(8):969, 2004.

[143] T. Pellegrino, L. Manna, S. Kudera, T. Liedl, D. Koktysh, A. L. Rogach, S. Keller, J. Radler, G. Natile, and W. J. Parak. Hydrophobic nanocrystals coated with an amphiphilic polymer shell: A general route to water soluble nanocrystals. *Nano Lett.*, 4(4):703, 2004.

[144] F. Osaki, T. Kanamori, S. Sando, T. Sera, and Y. Aoyama. A quantum dot conjugated sugar ball and its cellular uptake on the size effects of endocytosis in the subviral region. *J. Am. Chem. Soc.*, 126(21):6520, 2004.

[145] K. Akashi, H. Miyata, H. Itoh, and K. Kinosita. Preparation of giant liposomes in physiological conditions and their characterization under an optical microscope. *Biophys. J.*, 71(6):3242, 1996.

[146] M. I. Angelova and D. S. Dimitrov. Liposome electroformation. *Faraday Discussions*, (81):303, 1986.

[147] P. L. Luisi. *Giant Vesicles*, volume 6 of *Perspectives in Supramolecular Chemistry*. Wiley-VCH, Weinheim, Germany, 1999.

[148] A. E. Hac, H. M. Seeger, M. Fidorra, and T. Heimburg. Diffusion in two-component lipid membranes - a fluorescence correlation spectroscopy and Monte Carlo simulation study. *Biophys. J.*, 88(1):317, 2005.

[149] J. Korlach, P. Schwille, W. W. Webb, and G. W. Feigenson. Characterization of lipid bilayer phases by confocal microscopy and fluorescence correlation spectroscopy. *Proc. Natl. Acad. Sci. U.S.A*, 96(15):8461, 1999.

[150] J. Dubochet, M. Adrian, J. J. Chang, J. C. Homo, J. Lepault, A. W. McDowall, and P. Schultz. Cryo-electron microscopy of vitrified specimens. *Quart. Rev. Biophys.*, 21(2):129, 1988.

[151] B. O. Dabbousi, J. RodriguezViejo, F. V. Mikulec, J. R. Heine, H. Mattoussi, R. Ober, K. F. Jensen, and M. G. Bawendi. (CdSe)ZnS core-shell quantum dots: Synthesis and characterization of a size series of highly luminescent nanocrystallites. *J. Phys. Chem. B*, 101(46):9463, 1997.

[152] H. Mohwald. Phospholipid and phospholipid-protein monolayers at the air/water interface. *Annu. Rev. Phys. Chem.*, 41:441, 1990.

[153] H. M. McConnell. Structures and transitions in lipid monolayers at the air-water-interface. *Annu. Rev. Phys. Chem.*, 42:171, 1991.

[154] H. M. McConnell and M. Vrljic. Liquid-liquid immiscibility in membranes. *Annu. Rev. Biophys. Biomol. Str.*, 32:469, 2003.

[155] P. H. M. Lommerse, K. Vastenhoud, E. Snaar-Jagalska, H. P. Spaink, and T. Schmidt. Single-molecule studies show that H-Ras activation modulates its membrane diffusion. *Biophys. J.*, 86(1):602A, 2004. Part 2 Suppl. S.

[156] P. L. Felgner, T. R. Gadek, M. Holm, R. Roman, H. W. Chan, M. Wenz, J. P. Northrop, G. M. Ringold, and M. Danielsen. Lipofection - a highly efficient, lipid-mediated DNA-transfection procedure. *Proc. Natl. Acad. Sci. U.S.A*, 84(21):7413, 1987.

[157] I. Wrobel and D. Collins. Fusion of cationic liposomes with mammalian-cells occurs after endocytosis. *Biochim. Biophys. Acta- Biomembranes*, 1235(2):296, 1995.

[158] K. S. Kawamura, M. Sung, E. Bolewska-Pedyczak, and J. Gariepy. Probing the impact of valency on the routing of arginine-rich peptides into eukaryotic cells. *Biochemistry*, 45(4):1116, 2006.

[159] S. Balayssac, F. Burlina, O. Convert, G. Bolbach, G. Chassaing, and O. Lequin. Comparison of penetratin and other homeodomain-derived cell-penetrating peptides: Interaction in a membrane-mimicking environment and cellular uptake efficiency. *Biochemistry*, 45(5):1408, 2006.

[160] S. Berezhna, S. Schaefer, R. Heintzmann, M. Jahnz, G. Boese, A. Deniz, and P. Schwille. New effects in polynucleotide release from cationic lipid carriers revealed by confocal imaging, fluorescence cross-correlation spectroscopy and single particle tracking. *Biochim. Biophys. Acta- Biomembranes*, 1669(2):193, 2005.

[161] A. L. Bailey and P. R. Cullis. Membrane fusion with cationic liposomes: Effects of target membrane lipid composition. *Biochemistry*, 36(7):1628, 1997.

[162] E. H. Chen and E. N. Olson. Unveiling the mechanisms of cell-cell fusion. *Science*, 308(5720):369, 2005.

[163] S. J. Scales, M. F. A. Finley, and R. H. Scheller. Cell biology - fusion without SNAREs? *Science*, 294(5544):1015, 2001.

[164] B. R. Lentz. Polymer-induced membrane-fusion - potential mechanism and relation to cell-fusion events. *Chem. Phys. Lipids*, 73(1-2):91, 1994.

[165] S. W. Hui, T. L. Kuhl, Y. Q. Guo, and J. Israelachvili. Use of poly(ethylene glycol) to control cell aggregation and fusion. *Coll. Surf. B-Bioint.*, 14(1-4):213, 1999.

[166] R. Rigler, U. Mets, J. Widengren, and P. Kask. Fluorescence correlation spectroscopy with high count rate and low-background - analysis of translational diffusion. *Eur. Biophys. J. Biophys. Lett.*, 22(3):169, 1993.

[167] A. M. Derfus, W. C. W. Chan, and S. N. Bhatia. Probing the cytotoxicity of semiconductor quantum dots. *Nano Letters*, 4(1):11, 2004.

[168] P. Rigler and W. Meier. Encapsulation of fluorescent molecules by functionalized polymeric nanocontainers: Investigation by confocal fluorescence imaging and fluorescence correlation spectroscopy. *J. Am. Chem. Soc.*, 128(1):367, 2006.

[169] D. E. Discher and A. Eisenberg. Polymer vesicles. *Science*, 297(5583):967, 2002.

[170] S. B. Lecommandoux, O. Sandre, F. Checot, J. Rodriguez-Hernandez, and R. Perzynski. Magnetic nanocomposite micelles and vesicles. *Adv. Mater.*, 17(6):712, 2005.

[171] H. W. Duan, D. A. Wang, D. G. Kurth, and H. Mohwald. Directing self-assembly of nanoparticles at water/oil interfaces. *Angew. Chem. Int. Ed.*, 43(42):5639, 2004.

[172] J. Park, K. J. An, Y. S. Hwang, J. G. Park, H. J. Noh, J. Y. Kim, J. H. Park, N. M. Hwang, and T. Hyeon. Ultra-large-scale syntheses of monodisperse nanocrystals. *Nature Mater.*, 3(12):891, 2004.

[173] C. Burda, X. B. Chen, R. Narayanan, and M. A. El-Sayed. Chemistry and properties of nanocrystals of different shapes. *Chem. Rev.*, 105(4):1025, 2005.

[174] P. Gangopadhyay, S. Gallet, E. Franz, A. Persoons, and T. Verbiest. Novel superparamagnetic core(shell) nanoparticles for magnetic targeted drug delivery and hyperthermia treatment. *IEEE Trans. Magn.*, 41(10):4194, 2005.

[175] K. C. Crowder, M. S. Hughes, J. N. Marsh, A. M. Barbieri, R. W. Fuhrhop, G. M. Lanza, and S. A. Wickline. Sonic activation of molecularly-targeted nanoparticles accelerates transmembrane lipid delivery to cancer cells through contact-mediated mechanisms: Implications for enhanced local drug delivery. *Ultras. Med. Biol.*, 31(12):1693, 2005.

[176] T. M. Allen and P. R. Cullis. Drug delivery systems: Entering the mainstream. *Science*, 303(5665):1818, 2004.

[177] P. Broz, S. M. Benito, C. Saw, P. Burger, H. Heider, M. Pfisterer, S. Marsch, W. Meier, and P. Hunziker. Cell targeting by a generic receptor-targeted polymer nanocontainer platform. *J. Contr. Rel.*, 102(2):475, 2005.

[178] W. J. M. Mulder, G. J. Strijkers, G. A. F. van Tilborg, A. W. Griffioen, and K. Nicolay. Lipid-based nanoparticles for contrast-enhanced MRI and molecular imaging. *NMR. Biomed.*, 19(1):142, 2006.

[179] G. J. Strijkers, W. J. M. Mulder, R. B. van Heeswijk, P. M. Frederik, P. Bomans, Pcmm Magusin, and K. Nicolay. Relaxivity of liposomal paramagnetic MRI contrast agents. *Magn. Res. Mater. Phys. Biol. Med.*, 18(4):186, 2005.

[180] M. S. Martina, J. P. Fortin, C. Menager, O. Clement, G. Barratt, C. Grabielle-Madelmont, F. Gazeau, V. Cabuil, and S. Lesieur. Generation of superparamagnetic liposomes revealed as highly efficient MRI contrast agents for in vivo imaging. *J. Am. Chem. Soc.*, 127(30):10676, 2005.

[181] M. S. Spector, J. V. Selinger, and J. M. Schnur. Thermodynamics of phospholipid tubules in alcohol/water solutions. *J. Am. Chem. Soc.*, 119(36):8533, 1997.

[182] M. S. Spector, J. V. Selinger, A. Singh, J. M. Rodriguez, R. R. Price, and J. M. Schnur. Controlling the morphology of chiral lipid tubules. *Langmuir*, 14(13):3493, 1998.

[183] A. P. Alivisatos, P. F. Barbara, A. W. Castleman, J. Chang, D. A. Dixon, M. L. Klein, G. L. McLendon, J. S. Miller, M. A. Ratner, P. J. Rossky, S. I. Stupp, and M. E. Thompson. From molecules to materials: Current trends and future directions. *Adv. Mater.*, 10(16):1297, 1998.

[184] C. A. Mirkin, R. L. Letsinger, R. C. Mucic, and J. J. Storhoff. A DNA-based method for rationally assembling nanoparticles into macroscopic materials. *Nature*, 382(6592):607, 1996.

[185] A. P. Alivisatos, K. P. Johnsson, X. G. Peng, T. E. Wilson, C. J. Loweth, M. P. Bruchez, and P. G. Schultz. Organization of 'nanocrystal molecules' using dna. *Nature*, 382(6592):609, 1996.

[186] A. K. Boal, F. Ilhan, J. E. DeRouchey, T. Thurn-Albrecht, T. P. Russell, and V. M. Rotello. Self-assembly of nanoparticles into structured spherical and network aggregates. *Nature*, 404(6779):746, 2000.

[187] T. Vossmeyer, E. DeIonno, and J. R. Heath. Light-directed assembly of nanoparticles. *Angew. Chem. Int. Ed. In English*, 36(10):1080, 1997.

[188] C. P. Collier, T. Vossmeyer, and J. R. Heath. Nanocrystal superlattices. *Annu. Rev. Phys. Chem.*, 49:371, 1998.

[189] K. V. Sarathy, P. J. Thomas, G. U. Kulkarni, and C. N. R. Rao. Superlattices of metal and metal-semiconductor quantum dots obtained by layer-by-layer deposition of nanoparticle arrays. *J. Phys. Chem. B*, 103(3):399, 1999.

[190] S. Pethkar, M. Aslam, I. S. Mulla, P. Ganeshan, and K. Vijayamohanan. Preparation and characterisation of silver quantum dot superlattice using self-assembled monolayers of pentanedithiol. *J. Mater. Chem.*, 11(6):1710, 2001.

[191] L. H. Dubois and R. G. Nuzzo. Synthesis, structure, and properties of model organic-surfaces. *Annu. Rev. Phys. Chem.*, 43:437, 1992.

[192] G. Gopalakrishnan, C. Danelon, P. Izewska, M. Prummer, P. Y. Bolinger, I. Geissbuehler, D. Demurtas, J. Dubochet, and H. Vogel. Multifunctional lipid/quantum-dot hybrid nanocontainers for controlled targeting live cells. *Angew. Chem. Int. Ed.*, page in press, 2006.

[193] A Sukhanova, A. V Baranov, T. S. Perova, H. M. Jacques, and C. H. Nabiev. Controlled self-assembly of nanocrystals into polycrystalline fluorescent dendrites with energy-transfer properties. *Angew. Chem. Int. Ed.*, 45(13):2048, 2006.

[194] K. Harlos and H. Eibl. Hexagonal phases in phospholipids with saturated-chains - phosphatidylethanolamines and phosphatidic acids. *Biochemistry*, 20(10):2888, 1981.

[195] E. B. Smaal, T. K. Sixma, J. G. Mandersloot, and J. Degier. Differences in permeability of dioleoylphosphatidylcholine model membranes containing saturated or unsaturated phosphatidic acids. *Bioelectrochemistry and Bioenergetics*, 15(2):167, 1986.

[196] K. Sakai, T. Matsunaga, C. Hayashi, H. Yamaji, and H. Fukuda. Effects of phosphatidic acid on recombinant protein production by chinese hamster ovary cells in serum-free culture. *Biochem. Eng. J.*, 10(2):85, 2002.

[197] R. S. Arnold and A. C. Newton. Inhibition of the insulin receptor tyrosine kinase by phosphatidic acid. *J. Cell. Biochem.*, 62(4):516, 1996.

[198] K. Jalink, T. Eichholtz, F. R. PoSTMa, E. J. Vancorven, and W. H. Moolenaar. Lysophosphatidic acid induces neuronal shape changes via a novel, receptor-mediated signaling pathway - similarity to thrombin action. *Cell Gr. Differ.*, 4(4):247, 1993.

Acknowledgements

I am indebted to all who encouraged me to produce this thesis at the Laboratory of Physical Chemistry of Polymers and Membranes (LCPPM):
First I would like to thank Prof. Horst Vogel who has encouraged and supported me, by means of money and space, to achieve this thesis work. His excellent supervision and guidance made me motivated, without which this thesis work would not have been possible.
My sincere thanks to Dr. Vijayamohanan K. Pillai (Scientist, NCL, Pune, India), who introduced me into the world of nanotechnology during my masters thesis in his laboratory.
I also want to thank in particular Dr. K. Ravindranathan Thampi (LPI, EPFL) with whom I collaborated in the first year of my research life at EPFL and Dr. Arunan Chandravarkar (LCBP, EPFL) for their helps, especially during my first days in Lausanne:
Dr. Monika Baümule, my former office-mate, for her sincere help in the first years which is unforgettable.
Dr. Samuel Terrattaz, my office-mate, for his all-time support in every aspects of my stay at EPFL: both personal and academic.
Dr. Dimitrios Stamou, former group member, for his sincere friendship during my life in Lausanne as well as for his helps at work.
Dr. Ruud Hovius for helping by transmitting his deep-knowledge of every corners of LCPPM.
Dr. Jean-Manuel Segura and Dr. Michael Prummer for their helps in the single-molecule imaging experiments.
Dr. Christophe Danelon for introducing me to the immobilization of model membrane system and for general discussions on biophysics.
Paulina Izewska for introducing me to the live-cell cultures and treatments, which in fact has opened new possibilities to pursue during the last year of this thesis work.
Pierre-Yves Bolinger for his helps with FCS experiments.
Isabelle Geissbühler for synthesizing CdSe particles.
Dr. Wolf-Peter Ulrich for various helps during my stay at LCPPM.

Mme. Tabet, the secretary for administrative affairs, for her all-time help during my stay at LCPPM.
Prof. Pierre A. Stadelmann and Dr. Cédric Gaillard (CIME, EPFL) for their dedicated help with electron microscopy experiments and analysis.
Dr. Kurt J. Schenk (LCR, EPFL) for his help in solving several crystallographic question marks.
Davide Demurtas and Prof. Jacques Dubochet, UNIL for their help with Cryo-TEM imaging.
I am grateful to all members of LCPPM, who helped me one way or the other, especially to my former and current office-mates Joerg and Pedro.
I am specially grateful to Mme. Piccolo, who was the "maman du jour" of my son during his 4-18 months age and the regular conversations with her helped me a lot in improving my spoken french. The love and friendship of the whole Piccolo family is unforgettable.
Thanks to the éducatrices of "La Croquignole", the garderie where my son spends his day time.
I am also grateful to Raji, Sibi, Reshmi, Anil, Thomaskutty and other friends and well-wishers for making my stay in Lausanne a great, unforgettable time.
Sibi's role deserves special acknowledgment as his helps whenever I was lost with 'LaTex' while writing this thesis will always be etched in my mind.
Finally, I thank my greater family including parents, brother, sisters and lalettan (my brother-in-law), Sobha (my wife) and Yadu (my lovely son) for supporting me during this thesis period. Sobha and Yadu ought to have special thanks for their immense understanding and tolerance.

CV

Date and place of birth: 20, May 1976 in Kerala, Indian nationality

Languages

English: Fluent
French: Speak/read with moderate proficiency and write with basic competence
Hindi: Speak with basic proficiency and read/write with high competence
Malayalam: Mother tongue

Education

Since 2001 Swiss Federal Institute of Technology Lausanne, Switzerland
Doctorate: **"Lipid Membranes for the Fabrication of Functional Micro/Nano Structures"**
with Prof. Horst Vogel

1997 - 2000 Mahathma Gandhi University, Kottayam, Kerala, India
Master of Science (M.Sc.): Chemistry **"Synthesis and functionalization of hydrophobic nanoclusters"**
with Dr. K. Vijayamohanan, NCL, Pune

1993 - 1997 Mahathma Gandhi University, Kottayam, Kerala, India
Bachelor of Science (B.Sc.): Chemistry (Studied at Catholicate College, Pathanamthitta, Kerala, India)

1991 - 1993 University of Kerala, Trivandrum, Kerala, India
Pre-Degree Course: Science, Literature (Studied at S.D College, Alleppey, Kerala, India)

1988 - 1991 High School studies in Govt. Higher Secondary School, K.S. Puram, Karunagappally, Kerala, India

1981 - 1988 Primary School studies in Govt. Higher Secondary School, K.S. Puram, Karunagappally, Kerala, India

Professional Experience

Since 2001 Swiss Federal Institute of Technology Lausanne, Switzerland
Assistant Doctorant
Synthesis and characterization of fluorescent nanocystals and their bio-modification

2000 - 2001 Cochin University of Science and Technology, Cochin, Kerala, India
Junior Research Scholar with Dr. N. C. Kumar, Dept. of Chemical Oceanography
Chemical speciation and modeling of mangrove eco-systems on Kerala coast

1999 - 2000 National Chemical Laboratory, Pune, India
Masters Project Fellow- with Dr. Vijayamohanan K. Pillai, Physical & Materials Chemistry Division
Synthesis and characterization of metal nanoclusters

Teaching Experience

Supervised chemistry students in physical chemistry laboratory (EPFL, CH)	2 years
Supervised forensic science students in organic chemistry laboratory (EPFL, CH)	1 year
Physical chemistry lectures to the M.Sc. Hydrochemistry students (CUSAT, IN)	1 year
Chemistry lectures to pre-university and university students (Private Institutes, IN)	3 years

Publications/Conferences

2006 Multifunctional Lipid/Quantum-Dots Hybrid Nanocontainers for Controlled Targeting Live Cells
Publication: **Angew. Chem. Int. Ed., 2006, 45, in press**

2005 Synthesis of Nanoscopic Optical Fibers using Lipid Membranes as Templates
Publication: **Angew. Chem. Int. Ed., 2005, 44, 4957- 4960 (with Cover Page, 31/2005, 4815)**

2005 Gordon Research Conference on "Clusters, Nanocrystals and Nanostructures - Connecticut College, NL, USA
Poster: **Synthesis of Nanoscopic Optical Fibers using Lipid Membranes as Templates**

2005 Final Symposium of Swiss National Science Foundation's NRP 47 "Supramolecular Functional Materials Murten, Switzerland
Poster: **Lipid Membrane Templated Synthesis of Nano Optical Fibers**

2002 Formation of Cu and Cu_2O nanoparticles by variation of the surface ligand: Preparation, structure, and insulating-to-metallic transition
Publication: **J. Colloid. Interfaces Sci., 2002, 255, 79-90**